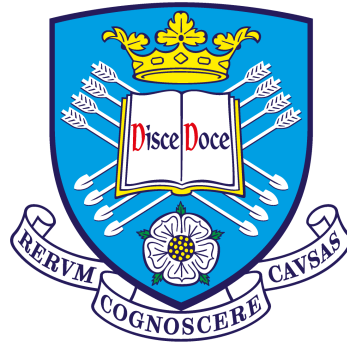


Additive Manufacturing of Carbon Fibre Reinforced Polymer Composites



Büşra Karaş

Department of Mechanical Engineering
The University of Sheffield

This dissertation is submitted for the degree of
Doctor of Philosophy

May 2022

Declaration

I hereby declare that except where specific reference is made to the work of others, the contents of this dissertation are original and have not been submitted in whole or in part for consideration for any other degree or qualification in this, or any other university. This dissertation is my own work and contains nothing which is the outcome of work done in collaboration with others, except as specified in the text and Acknowledgements. This dissertation contains fewer than 65,000 words including appendices, bibliography, footnotes, tables and equations and has fewer than 150 figures.

Büşra Karaş
May 2022

Acknowledgements

First and foremost, I would like to express my sincere gratitude to my supervisor Dr. Kamran Mumtaz for his continuous motivation and guidance throughout my research. His innovative ideas and feedback have been crucial in this entire process.

A big thank you to The Turkish Ministry of Education for funding this PhD and giving me the opportunity to do this project.

I would like to extend my deepest gratitude to Dr. Patrick J. Smith who has been an incredible mentor in inkjet printing, to Prof. Patrick Fairclough and Dr. Simon Hayes for their invaluable feedback and their expertise in composites. Many thanks to the Royal Exchange people, especially my colleagues Pablo, Kübra, Mohammed, and Halil who have been always open to exchanging ideas and very resourceful.

I am also grateful to my teaching coordinator, Martyn Aspinall, from the Advanced Manufacturing Technology in Multidisciplinary Engineering Education team for all the Graduate Teaching Assistant experiences in Engineering Applications and his patience in 'teaching me how to teach'. To Joanna Bates, who also supported me with the resources, I had the most fun teaching in Materials Lab. It was a great pleasure to work with them in The Diamond.

To my very supportive family, a huge thanks to my relatives who did not hesitate for a second when I needed guarantors. I am grateful for my mum who was always there whenever I needed support (I do not think she predicted that I would end up being a researcher abroad when she was preparing 'extra homework' for little me to solve endless math questions), and to my dad who taught me how to be curious and never give up, thank you for fuelling up my love for books. To my sister Şule, you are the reminder of all the things more important than work in this life.

Sheffield has been a great place to meet amazing people. To my Turkish family here, thank you for making this city a home to me, especially Fidan and Meltem.

I am incredibly lucky to be surrounded by amazing f.r.i.e.n.d.s. To Vimanyu, who was literally in front of my desk whenever I needed help, I am grateful for all the professional guidance and unconditional bro-ship. To Cindy, thank you for being my sister and my coach. Even if Sheffield was rainy, all the breakfasts have been sunny with you. To Özgün, for all the fun ranting sessions and good quality music. To Karl, for showing me that one can be so savage yet extremely kind and good-hearted. Finally, to Răzvanel, thank you for teaching me to chase the life I desire. You are my support system who makes me smile every day.

Abstract

Additive manufacturing (AM) of carbon fibre reinforced thermoplastic composites can offer advantages over traditional carbon fibre manufacture through improved design freedom and reduction in production time and cost. However state-of-the-art fused deposition modelling (FDM) approaches for the production of carbon fibre composites, generally possess high porosity compared to conventionally manufactured advanced composites. On the other hand, the addition of fibre to the polymer powder bed fusion processes such as selective laser sintering (SLS) creates drawbacks such as poor fibre distribution in the powder feedstock, high porosity and low strength in the final parts. The reason for low-performance composites in AM processes is the lack of heat and pressure application. The traditional manufacturing processes for advanced composites improve the consolidation of the layers with autoclave machines or hot press processes, whereas in AM processes, compaction is not ideal to sustain the complexity of final geometry.

In this study, the development of a novel alternative to the current composite AM based on sheet lamination, named composite fibre additive manufacturing (CFAM), is presented with the aim of reducing component porosity. This approach involves selectively inkjet printing a binder and polymer powder onto discontinuous carbon fibre sheets which are then compressed and heated to form net shape components. Using CFAM, complex-shaped discontinuous carbon fibre reinforced nylon composite parts were successfully manufactured for the first time.

First of all the effect of process parameters such as applied pressure level, compaction time, and the volume of printed ink on the mechanical and microstructural properties of final parts was investigated to benchmark the process. Further investigation focused on polymer morphology to understand the effect of crystallinity on the CFAM final part properties. Additionally, a combination of hybrid layers involving continuous and discontinuous carbon fibre was examined with the aim of improving the mechanical properties. Finally, complex-shaped drone frames were manufactured to investigate the dimensional tolerances. The geometric accuracy and the load-carrying performance of the final products produced with the CFAM

and other AM processes are examined and compared.

The results demonstrate a correlation between the amount of pressure applied and the percentage of porosity and fibre volume fraction in the final parts. By providing an optimum level of pressure, the voids which can act as crack propagators, reduce significantly (1.5%). Hence more consolidated parts with relatively higher tensile strength and stiffness were obtained. Interaction between the crystallization process of thermoplastic matrix material in CFAM and resultant part properties was established using a new approach based on elements of DSC analysis, which provides a new level of understanding into the polymer behaviour under the different processing conditions. Finally, the end-use product performance of CFAM was found to be superior compared to the other composite AM techniques. The innovative fabrication process established in this thesis achieved the rapid production of high-performance discontinuous carbon fibre reinforced polymer parts with flexibility in material composition.

Table of contents

List of figures	xiii
List of tables	xvii
Nomenclature	xix
1 Introduction	1
1.1 Motivation	1
1.2 Aim and Objectives	3
1.3 Contribution to Knowledge and Novelty Statement	3
2 Literature Review	5
2.1 Composite Materials	6
2.1.1 Fibre Reinforcement	6
2.1.2 Matrices	9
2.1.3 Metal Matrix Composites	10
2.1.4 Ceramic Matrix Composites	10
2.1.5 Polymer Matrix Composites	11
2.1.6 Carbon Fibre Reinforced Polymer (CFRP) Composites	14
2.2 Conventional Manufacturing Techniques of Fibre Reinforced Composites	15
2.2.1 Filament Winding	16
2.2.2 Automated Tape Lay-up	17
2.2.3 Automated Fibre Placement	18
2.3 Additive Manufacturing Techniques of Fibre Reinforced Composites	20
2.3.1 Powder Bed Fusion AM Processes	22
2.3.2 Stereolithography	23
2.3.3 Fused Deposition Modelling	24
2.3.4 Sheet Lamination	32
2.4 Inkjet Printing	34

2.5	Literature Review Conclusions	40
3	Experimental Methodology	41
3.1	Materials	42
3.2	Development of the Composite Fibre Additive Manufacturing (CFAM) Process	42
3.2.1	Printing Process	45
3.2.2	Deposition of Powder	51
3.2.3	Hot Press Process	52
3.2.4	Sand Blasting Process	55
3.3	Characterisation	56
3.3.1	Differential Scanning Calorimetry (DSC)	56
3.3.2	X-Ray Computed Tomography (CT)	57
3.3.3	Sample Preparation for Optical Microscopy	57
3.3.4	Optical Microscopy	58
3.3.5	Scanning Electron Microscopy	58
3.3.6	Tensile Testing	58
3.3.7	Flexural Testing	59
3.3.8	Short Beam Shear Test	60
4	Optimization of CFAM Process Parameters	61
4.1	Introduction	62
4.2	Design of Experiments	64
4.2.1	Process parameters	64
4.2.2	Taguchi analysis	65
4.3	Results	65
4.3.1	DSC analysis	65
4.3.2	X-ray CT and optical microscopy	67
4.3.3	Mechanical testing	71
4.3.4	Taguchi analysis	75
4.4	Discussion	77
4.4.1	Effect of pressure on porosity and mechanical properties	77
4.4.2	Effect of ink areal density	81
4.4.3	Effect of compaction time	82
4.4.4	Overall analysis of CFAM and comparison with state-of-the-art	83
4.5	Conclusion	85

5	Investigation of Polymer Morphology in CFAM Parts	87
5.1	Introduction	88
5.2	Methodology	89
5.2.1	Experiment I	89
5.2.2	Experiment II	90
5.3	Results and Discussion	92
5.3.1	Effect of process parameters on polymer crystallinity	92
5.3.2	Effect of cooling rate on crystallinity and interlaminar shear strength (ILSS)	96
5.4	Conclusion	98
6	Hybrid Carbon Fibre Reinforced Polymer Composites in CFAM	101
6.1	Introduction	102
6.2	Preliminary Investigation of Continuous Fibre Layers in CFAM	103
6.2.1	Materials and method	103
6.2.2	Characterization	104
6.2.3	Results and discussion	105
6.3	Investigation of Hybrid Carbon Fibre Layers in CFAM	107
6.3.1	Materials and methods	107
6.3.2	Results and discussion	110
6.3.3	Conclusion	115
7	Quality Inspection of Complex-shaped CFAM Parts	117
7.1	Introduction	118
7.2	Methodology	119
7.2.1	Materials and manufacturing	119
7.2.2	3D scanning and measurements	121
7.2.3	Load resistance test	122
7.3	Results and Discussion	123
7.3.1	Tolerance performance analysis	123
7.3.2	Challenges in Manufacturing of CFAM Prototype	128
7.3.3	Load resistance analysis	129
7.4	Conclusion	130
8	Conclusions and Future Work	133
8.1	Conclusions	133
8.2	Future Work	135

References	139
Appendix A Chapter 4 Supporting Information	155
A.1 Tensile test failure in discontinuous CFRP samples	155
A.2 Flexural test failure for three different pressure level in discontinuous CFRP samples	156
Appendix B Chapter 6 Supporting Information	157
B.1 Tensile test failure modes according to ASTM D3039 Standards	157
B.2 Tensile test failure in hybrid samples	158
Appendix C Chapter 7 Supporting Information	159
C.1 Properties of materials used in production of prototypes	160
C.2 Manufacturing of the central plate in drone frame by CFAM	163

List of figures

2.1	Types of fibre reinforced composites	8
2.2	The relationships between groups of engineering materials	9
2.3	The maximum service temperatures of polymers, metals and ceramics	11
2.4	Chain formation of (a) thermoplastics and (b) thermosettings	13
2.5	Thermal analysis of thermoplastics	14
2.6	Filament winding diagram	17
2.7	Automated Tape Lay-up system using filament winding machine	18
2.8	Automated Fibre Placement robot	19
2.9	Local buckling of steered fibres	19
2.10	Schematic of SLS process	22
2.11	Schematic of SL process	24
2.12	Schematic of FDM process	25
2.13	Fibre implementation methods for Fused Deposition Modelling	25
2.14	Mark One Composite 3D Printer and the schematic of the process	27
2.15	Schematic of Laminated Object Manufacturing (LOM)	32
2.16	Deposition of polymer powder in CBAM process	33
2.17	Parts produced by CBAM	34
2.18	(a) Continuous inkjet printing (CIJ), (b) Drop on Demand (DOD) inkjet printing	36
2.19	(a) Piezoelectric DOD, (b) Thermal DOD	37
2.20	Droplet formation process in piezoelectric DOD printhead with the step by step pressure waveform generation	39
3.1	16.95 gsm carbon fibre veil supplied by ACP Composites and properties	42
3.2	Steps of Composite Fibre Additive Manufacturing process	44
3.3	Example of composite component made using CFAM approach; (a) bitmap file for a 2D slice, (b) printed layer before compression, (c) final part with 24 layers (60x60 mm)	45

3.4	JetLab IV piezoelectric DOD inkjet printer by Microfab Inc. and Microfab MJ-A style drop-on-demand single jet dispensing device	46
3.5	Waveform optimization process for HP Instant Ink 67/305 in JetLab IV inkjet printer	48
3.6	Affect of humidity level for evaporation of ink in JetLab IV inkjet printer cabinet	49
3.7	HP Deskjet Plus 4130 drop-on-demand thermal inkjet printer	49
3.8	Jetting station with the sensor used for contact angle measurements	50
3.9	Contact angle measurements (a) Surface treated substrate with 2 hours drying period, (b) Surface treated sample with 12 hours drying period	51
3.10	The amount of powder that is adhered to the printed surface for each printing setting	52
3.11	Hydraulic hot press machine	53
3.12	Hydraulic hot press machine temperature verification with thermocouples	54
3.13	Hydraulic hot press machine temperature verification with thermocouples	54
3.14	Heatmap of a hydraulic hot press machine (a) 120°C, (b) 140°C, (c) 170°C, (d) 190°C	55
3.15	Guyson Euroblast 4 sand blasting machine	56
3.16	Mounted samples to be scanned in X-ray CT system	57
3.17	BS EN ISO 527-4 standards-Type 1B specimen	59
3.18	Zwick Tensometer 2020 Proline with a video extensometer	59
3.19	Standard flexural test specimen and flexural test setup	60
3.20	Standard flexural test specimen and flexural test setup	60
4.1	DSC Analysis of raw CF/Nylon 12 (1.2 mg) specimen	66
4.2	X-ray CT images of different pressure settings; (a) Void content at low pressure level (0.3 MPa) (Set2) – Porosity: 12.09%, (b) Void content at medium pressure level (0.6 MPa) (Set4)– Porosity: 4.19%, (c) Void content at high pressure level (0.9 MPa) (Set9) – Porosity: 1.52% Tensile properties of each experimental set	68
4.3	3D porosity distribution in X-ray CT with the pore segmentation; (a) Set 1, (b) Set 4, (c) Set 6, (d) Set 9	69
4.4	Optical microscopy images; (a) Thresholded stitched images of Set 9 sample (0.9 MPa), (b) Actual stitched images of Set 9 sample (0.9 MPa), (c) Set 9 sample, (d) Set 4 sample, (e) Set 2 sample	70
4.5	SEM images to investigate the voids (a) Set 9 sample top view (b) Set 1 sample top view	71

4.6	Stages of tensile test samples manufacturing (a) carbon fibre sheet after printing and deposition of powder; (b) compressed carbon fibre layers after hot press process; (c) sandblasting process halfway through; (d) final dog bone samples	72
4.7	Stages of flexural test samples manufacturing (a) stacked and aligned carbon fibre sheets after printing and deposition of powder; (b) sandblasting process halfway through; (c) final flexural test samples	72
4.8	(a) Tensile and (b) flexural test results for low, medium and high pressure levels (Set 2, 4 and 9, respectively)	73
4.9	Tensile properties of each experimental set	74
4.10	Flexural properties of each experimental set	74
4.11	Main effects plot for (a) tensile strength and (b) elastic modulus	76
4.12	Relationship between porosity and tensile properties (a), the relationship between fibre volume fraction and tensile properties (b)	78
4.13	X-ray CT images of the sample produced with 1.2 MPa pressure level (a) 2D view top and cross-sectional view, (b) 3D pore formation	79
4.14	Change in tensile strength and stiffness with the increasing pressure from 0.3 MPa to 1.2 MPa	80
4.15	Level of surface coverage for each printing setting (a) low - JetLab IV, (b) medium - HP Deskjet 600 DPI, (c) high - HP Deskjet 1200 DPI	81
4.16	Tensile failures of samples; (a) low, (b) medium (0.3 MPa pressure and 2 hours of compaction time kept constant)	82
4.17	Comparison between Composite Object Manufacturing and other AM parts with continuous and discontinuous fibre	85
5.1	DSC curves of samples from each experimental set (Endo up)	90
5.2	(a) Compression rig, (b) Wera click-torque adjustable torque wrench, (c) pressure sensor	91
5.3	Short beam shear test specimens	91
5.4	(a) DSC curves of samples from each experimental set (Endo up); (b) Melting behaviour of different crystal forms in polymers	92
5.5	Comparison of final part properties; (a) tensile, (b) flexural and (c) porosity, with degree of crystallinity for each experimental condition	94
5.6	Final part properties; (a) tensile, (b) flexural, (c) porosity, as a function of alpha peak height	96
5.7	Force-displacement results from shear test of hot press specimens	98

5.8	Compressive failure occurred during the short beam shear test in a compression rig sample	98
6.1	(a) Printed unidirectional carbon fibre layers, (b) final unidirectional part after sandblasting process	104
6.2	X-ray CT investigation of (a) twill weave and (b) unidirectional carbon fibre parts	105
6.3	Tensile properties of twill, plain and unidirectional CFRP parts	106
6.4	Hybrid laminates manufactured with different compositions and stacking sequences	108
6.5	(a) Hybrid tensile test specimens, (b) end tab preparation	109
6.6	Contact angle measurement for the droplet printed on unidirectional fibre .	110
6.7	X-ray CT imaging of hybrid specimen with 40% UD (a) Top view , (b) cross-sectional view, (c) pore segmentation	111
6.8	Tensile properties of hybrid laminates	112
6.9	Tensile stress-strain graphs of hybrid specimens; (a) 10% continuous, (b) 30% continuous, (c) 40% continuous	113
6.10	Force-displacement curves from shear test of hybrid samples	114
6.11	Shear failure in hybrid composite short beam shear test specimen (50% continuous fibre)	115
7.1	Design of the central PCB plate in drone frame and the inspired application	120
7.2	Einscan 3D scanner set-up	121
7.3	Points of measurements and nominal values for tolerance performance analysis	122
7.4	Four point bending test for load resistance	123
7.5	Tolerance map of the prototypes 2, 3 and 4	125
7.6	Tolerance map of the prototype 5 and CFAM	126
7.7	Tolerance performance of scanned samples	126
7.8	(a) Standard deviations of selected feature dimensions (b) Thickness of each prototype and standard deviations	127
7.9	Geometrical accuracy improvement in CFAM part with better sheet alignment from (a) to (d)	129
7.10	Force-displacement profile and the weights of drone frames	130

List of tables

2.1	Mechanical properties of fibres and bulk materials	7
2.2	Tensile test results of materials printed by Markforged Mark One	28
2.3	Summary of literature review for FDM of continuous fibre composites	30
2.4	Summary of literature review for FDM of discontinuous fibre composites	31
2.5	Comparison of inkjet printing mechanisms	37
4.1	Process parameters with three levels	65
4.2	Taguchi L9 orthogonal array for the design of experiments	66
4.3	Porosity and fibre volume fraction of the samples for each experiment set	67
4.4	ANOVA for tensile strength	76
4.5	ANOVA for flexural strength	76
5.1	Degree of crystallinity for the samples from each experiment set	93
5.2	ANOVA for degree of crystallinity	93
7.1	Types of manufacturing techniques and materials for the drone frames	120
7.2	Maximum deviation for international standard tolerance grades	122
7.3	Mean and standard deviations of general discrepancy for each scanned prototype	124

Nomenclature

Acronyms / Abbreviations

ABS	acrylonitrile butadiene styrene
AFP	Automated Fibre Placement
AM	Additive manufacturing
ANOVA	Analysis of Variance
ATL	Automated tape lay-up
CBAM	Composite based additive manufacturing
CF	Carbon fibre
CFAM	Composite fibre additive manufacturing
CFRP	Carbon fibre reinforced polymer
CIJ	Continuous inkjet
CMC	Ceramic matrix composite
DOC	Degree of Crystallinity
DOD	Drop on demand
DOE	Design of experiments
DSC	Differential scanning calorimetry
FDM	Fused deposition modelling
HSS	High speed sintering

IJP	Inkjet printing
ILSS	Interlaminar shear strength
LOM	Laminated object manufacturing
MMC	Metal matrix composite
PA	Polyamide
PLA	polylactic acid
PMC	Polymer matrix composite
SEM	Scanning electron microscopy
SLA	Stereolithography
SLCOM	Selective lamination composite object manufacturing
SLM	Selective laser melting
SLS	Selective laser sintering
UD	Unidirectional

Chapter 1

Introduction

1.1 Motivation

Composite materials are high performance, lightweight structures, and commonly used in aerospace and automotive industries. By integrating two, or multiple materials to fabricate a composite, unique mechanical properties that are superior can be achieved. As physical and chemical identities of two components in the composite are protected, the combination of such materials can result in distinct properties [1].

A fibre reinforced composite consists of fibres bonded to a matrix with interphases. Polymer, metal or ceramic can be used as a matrix material [2]. Polymer matrix composites have become very common in industry since the use of carbon fibre and glass material has advanced exponentially. While metal and ceramic matrix composites are expensive and difficult to machine, polymer matrix composites are inexpensive, easily accessible, and have unique properties. The service temperature limit in thermosets and thermoplastics is 300 °C lower when it is compared with that of metal and ceramics [3]. Carbon fibre reinforced polymer (CFRP) composites are preferred in industrial applications since they usually give stronger and resilient outcomes [2]. However, manufacturing of carbon fibre with conventional processes is more expensive and labour intensive. While it is tedious to produce the CFRP composites manually, alternative methods which rely on automated machines are unaffordable by manufacturers. New and common conventional manufacturing techniques are filament winding, automated fibre placement and automated tape lay-up. These conventional methods have their own advantages and disadvantages such as void formation, delamination, fibre wrinkles due to poor winding tension, and misalignment in roving [4].

Additive Manufacturing (AM) technology has advanced significantly over the past decades. Complex-shaped parts can be produced, without additional tooling, joining the materials layer by layer. This process is efficient in terms of time, cost and material when compared to conventional manufacturing techniques. The parts can be designed in a flexible way, as opposed to traditional manufacturing techniques, which introduces higher levels of customisability [5].

Recently, considerable literature has grown up around the theme of AM of CFRP composites. The addition of carbon fibre to polymer based AM not only improves mechanical properties, but also enables flexible selection of matrix materials [6]. On the other hand, there are many challenges in this field depending on the chosen AM methodology. High levels of porosity, poor dispersion level of fibres in the feedstock and weak interlaminar bonding due to lack of heat and pressure in the AM are common disadvantages of composite AM [7, 8].

Many researchers have been investigating the influence of process parameters on the final composite parts, as well as developing new kind of composite filaments. Although few studies have been performed to examine the feasibility of the systems using material extrusion technique, less attention has been paid to sheet lamination techniques. It is possible to overcome the disadvantages of extrusion based technique and to reach the performance of conventionally manufactured composites by integrating the AM with heat and pressure application.

This study will investigate a new additive manufacturing system based on sheet lamination technique for CFRP composites, bringing the elements of heat and pressure to the composites AM, to achieve the high performance final product.

1.2 Aim and Objectives

This study aims to develop an efficient additive manufacturing process which is based on sheet lamination technique to produce complex-shaped carbon fibre reinforced polymer parts with high density and strong mechanical properties. The specific objectives are:

1. Develop a good understanding of conventional and currently available additive manufacturing methodologies for fibre reinforced polymer materials
2. Build a sheet lamination process to produce CFRP structures by specifying the pieces of hardware and software of the design
3. Manufacture and characterize the parts to investigate their mechanical and structural properties
4. Optimize the manufacturing process by identifying the process parameters with design of experiments techniques
5. Investigate the effect of fibre types and polymer morphology on the mechanical and microstructural properties of final parts
6. Examine the quality of end-use products by analysing the dimensional accuracy and load resistance capability

1.3 Contribution to Knowledge and Novelty Statement

The use of carbon fibre reinforcements offers high strength to weight ratio for components and an opportunity for additive manufacturing (AM) techniques to manufacture high-performance complex functional parts in an efficient and cost-effective way.

Fused deposition modelling (FDM) is an AM method that can be used for the production of carbon fibre reinforced polymer (CFRP) composites, alongside other AM techniques such as selective laser sintering (SLS) and stereolithography (SLA). However, all of these approaches generate composite components with a high level of porosity. Sheet lamination techniques are a promising alternative to current AM techniques aimed at producing CFRP with high density due to the use of high temperature compaction of layers. However, to date, no independent academic study has investigated sheet lamination and properties of CFRP composites.

In this study, CFRP composite parts are manufactured using a novel custom built system named as Composite Fibre Additive Manufacturing (CFAM). This research is the first comprehensive study to benchmark the performance of the composite parts made by a sheet lamination process with mechanical testing and X-ray tomography, providing novel insights into the additive manufacturing of composites. Components were produced with properties that exceeded those of conventional AM of short fibre reinforced composites. Secondly, this study explores the polymer morphology and provides information concerning the molecular formation of thermoplastics in CFAM. A new approach based on differential scanning calorimetry (DSC) analysis was developed to establish the relationship between the crystallization process and the mechanical properties of the parts. Furthermore, the continuous layers of carbon fibre fabric are introduced to the additive sheet lamination process for the first time. The characterization of the additively manufactured hybrid composite components with a combination of continuous and discontinuous fibres were performed. Finally, a novel case study was carried out to inspect the quality of final products by using a 3D scanner and the PowerInspect software. The tolerances and impact resistance of final parts made by AM processes were compared.

Chapter 2

Literature Review

Summary

This chapter delivers a comprehensive literature review of composites manufacturing. First, a description of composites and their material properties is given. The advantages and disadvantages of different types of matrix materials are discussed. Then, conventional manufacturing techniques are presented to understand the background in composites manufacturing.

This chapter then follows by an introduction of additive manufacturing (AM), and recent advances in AM techniques developed for composites. A survey of carbon fibre composite AM is given, together with the commercial systems and trends towards possible future applications. Then, inkjet printing mechanisms are explained to elaborate on the implementation of the inkjet printing technique to the AM of composites.

Finally, challenges in the field of composite AM and the areas that need attention to improve the quality of final products are addressed. The conclusion of the chapter includes the inferences and research hypothesis.

2.1 Composite Materials

Composite materials are the materials composed of two or more materials which have different mechanical and physical properties to create a totally new material with peerless properties. Matrix and reinforcement, the two constituents of composite materials, are integrated in a way of leveraging on their strengths while avoiding their weaknesses [9]. This process of optimization helps the designer to create tougher and lighter products with the specific requirements of the design without boundaries of selection and manufacturing of traditional materials [10]. Composites are not only artificial; they are also found in nature in the form of bone or wood among others.

2.1.1 Fibre Reinforcement

Fibre reinforced composite materials contain fibres with high mechanical properties, inserted in matrix with definite interfaces. Fibres affect the mechanical properties of composites significantly. It is observed that materials in fibre form show a higher strength and stiffness than those in bulk form, which makes fibrous reinforcement desirable [11].

Carbon, glass and aramid fibres are the most common fibre types that are used in industrial applications [12]. In Table 2.1 the differences between mechanical properties of these popular materials in fibre and bulk forms are listed. Glass fibre, including the types of E-glass and S-glass, is the most popular type of reinforcement in industry due to being cost effective and having high fracture strength and stiffness. Early development of glass fibres also contributed to their widespread popularity [13]. However, glass fibre is not appropriate for high performance applications where high fatigue life or high elastic modulus are a requirement [14]. Aramid fibres, known as the brand name Kevlar, are made of aromatic polyamides and they have high elastic modulus. Their high fatigue damage tolerance enables them to have high tensile strength compared to other fibres after loading. The molecular structure of aramid fibres plays an important role on this unique fatigue mechanism [15]. Since they are considered as high performance fibres with the high temperature and corrosion resistance, they are relatively expensive [16]. Their low compressive strength is another drawback limiting their applications. Natural fibres also emerged as a recent trend since they are environmentally friendly and recyclable. However natural fibres are prone to water absorption due to high amount of cellulose and their mechanical properties are poorer than the other synthetic fibres [17].

Carbon fibres are widely employed since they offer superior mechanical properties with

great thermal resistance, exceeding both glass and aramid fibre properties. Their cost is also much higher compared to other types of fibres, which is a disadvantage for their everyday use. However, they are preferred where the lightweight structures are critical such as in aerospace and automotive fields. Carbon fibre is made of carbonization of a precursor called polyacrylonitrile (PAN) or 'pitch' [18]. This process is followed by graphitization which is a thermal treatment where amorphous carbon is heated for a period of time in order to rearrange the atomic structure. Therefore the transition from amorphous to crystalline structure can be achieved. This thermal treatment and the type of precursor determine the final strength and stiffness of carbon fibres, which is the reason for them to have a range of tensile properties unlike glass fibres [19].

Table 2.1 Mechanical properties of fibres and bulk materials [20]

Materials	Tensile Strength (MPa)	Elastic Modulus (GPa)	Density (g/cm ³)
Bulk 6061T6 Aluminium	310	697	2.71
Bulk SAE 4340 Steel	1034	200	7.83
E-glass fibres	3448	72	2.54
Carbon Fibres (PAN)			
AS-4 (Hercules)	4000	228	1.80
IM-7 (Hercules)	5413	276	1.77
T-300 (Amoco)	3654	231	1.77
Carbon fibres (Pitch)			
P-55 (Amoco)	1724	379	1.99
P-75 (Amoco)	2068	517	1.99
P-100 (Amoco)	2241	690	2.16
Aramid fibres			
Kevlar 29	3792	62	1.44
Kevlar 49	3792	131	1.47
Boron fibres			
Textron	3516	400	2.57
Silicon carbide fibres			
Textron	3448	427	3.04

Different types of fibre placement have been developed for industrial demands. Directions of the fibres are available depending on the application as shown in Figure 2.1. Continuous fiber reinforced laminate (2.1-a) is commonly used in the industries seeking for strong materials. However the delamination between layers can be a disadvantage. On the other hand, delamination problem can be overcome by using woven fibre composites (2.1-b), but mechanical properties of woven fibre composites are generally poorer since the fibre placement is wavy. Thirdly, chopped fiber reinforced composite materials (2.1-c) may have fibers of different lengths randomly distributed in the matrix. They are used widely in mass production due to low cost, but their strength and stiffness are considerably lower than those of continuous fibre reinforced composites. Finally, hybrid composites is a mix of chopped and continuous fibres (2.1-d) [20].

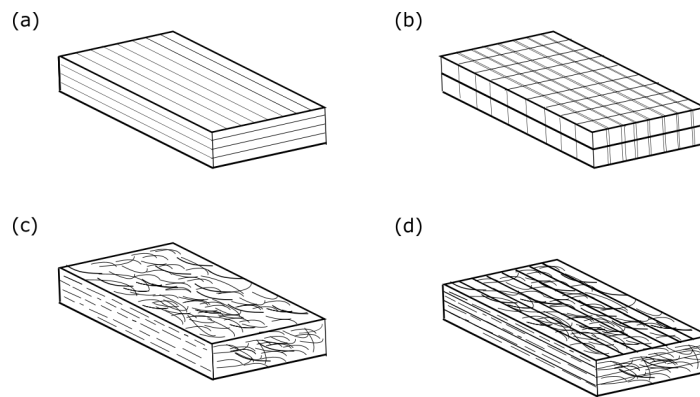


Fig. 2.1 Types of fibre reinforced composites (a) continuous fibre composite, (b) woven fibre composite, (c) chopped fibre composite, (d) hybrid composite

Even if fibrous materials demonstrate better mechanical properties, they have disadvantages in terms of efficient usage. Fibres need to be clustered with the help of matrix or binder material as a support of transverse reinforcement, because fibers alone can only endure longitudinal loads. While the fibres carry the load, the matrix helps to retain them in required position as a load transfer member and to protect them from environmental effects such as moisture and temperature. Laminates are the commonly used form of fibre reinforced composites as it can be seen from Figure 2.1. Thin layers of fibres and matrix have been stacked to create a part with desired thickness. Mechanical and physical properties of laminates can be adjusted by controlling the fibre orientation and the array of the layers [1]. Matrix materials are explained in detail in the next section.

2.1.2 Matrices

Matrix is the load carrying member of a composite material, which supports the fibres in the preferred orientation. Even though the fibres determine the mechanical properties of the final parts, matrix material also characterizes the shear and compressive strength by influencing the interlaminar bonding. Delamination of the layers can occur during the static or cyclic loading due to the weak toughness and resistance [1]. Therefore, it is important to choose the right characteristics of the matrix to achieve the desired final properties specific to the application [21]. For example, composite materials can be supported with a tough matrix where cracks are likely to propagate, whereas a brittle and stronger matrix can be preferred where the load transfer and stiffness of the material are prominent [22].

Composites are categorised by their matrix types in three major groups [23];

- Metal matrix composites
- Ceramic matrix composites
- Polymer matrix composites

Figure 2.2 shows the creation of composites by indicating the relationships between the categories of materials.

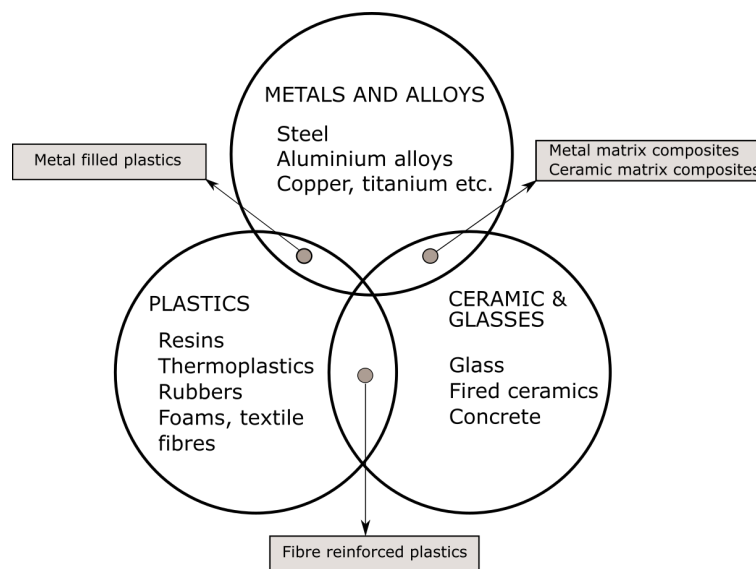


Fig. 2.2 The relationships between groups of engineering materials [24]

2.1.3 Metal Matrix Composites

Metal matrix composites (MMC) are manufactured by inserting a reinforcement material in metal matrix. Typical MMCs are Al, Mg and Cu based. In aircraft and automotive sectors, aluminium and its alloys are used due to their higher strength, stiffness and corrosion resistance. The fibre material can be selected depending on the requirements of the application. For example, aluminium fibres are suitable for lightweight applications. Different common processes are available to manufacture aluminium based composites. Aluminium matrix composites are appealing materials due to their high mechanical properties. They are easily processable in conventional techniques. However, the reinforcements should not be affected by the required service temperature. Problems in controlling the chemical reactions between the fibres and the molten metal decreases the mechanical properties of the composite due to fragile interphase. The cost of the fibre increases when surface treatments are applied to reduce the risk of this problem occurring, which limits their use [2].

One of the advantages of MMCs are greater electrical and thermal conductivity. A variety of new fibres are continuously introduced or improved but acceptance of new fibre products for structural applications is slow. A large number of characterization tests are required to assure safe and effective application under a variety of conditions. While great strength and stiffness to weight ratios are advantageous for aircraft applications, other characteristics of the composites that can be produced with these fibres are likely to be the limiting factors in their application [10].

2.1.4 Ceramic Matrix Composites

Ceramic matrix composites (CMC) are made of high-performance ceramics like silicon nitride and carbide used in different applications from engines to implants. The most important advantage of CMC is that they are durable to high temperature. However, the ceramic matrix is not strong to failure when it is compared with metal or polymer matrix. A pre-existing crack in the matrix could result in catastrophic failure down the line. CMCs have low toughness and fragile structure which limits their applications. Although they have unique characteristics like high resistance to heat, abrasive and chemicals, they are not easy to fabricate in an effective way due to their brittleness [1, 3].

2.1.5 Polymer Matrix Composites

Polymer matrix composites (PMC) are used as a principal material in aerospace, automotive industries, high-speed trains and ships where the weight and the strength of the components are significantly important. The reason for using them instead of many conventional metallic materials is their mechanical properties such as low density, large strength and stiffness to weight ratios and stability under force [1, 4, 5].

Polymers can be processed at lower temperatures compared to metals and ceramics for an extended period, which makes them flexible to use in different manufacturing techniques. Figure 2.3 gives the comparison of service temperature limits of polymers, metals and ceramics [3].

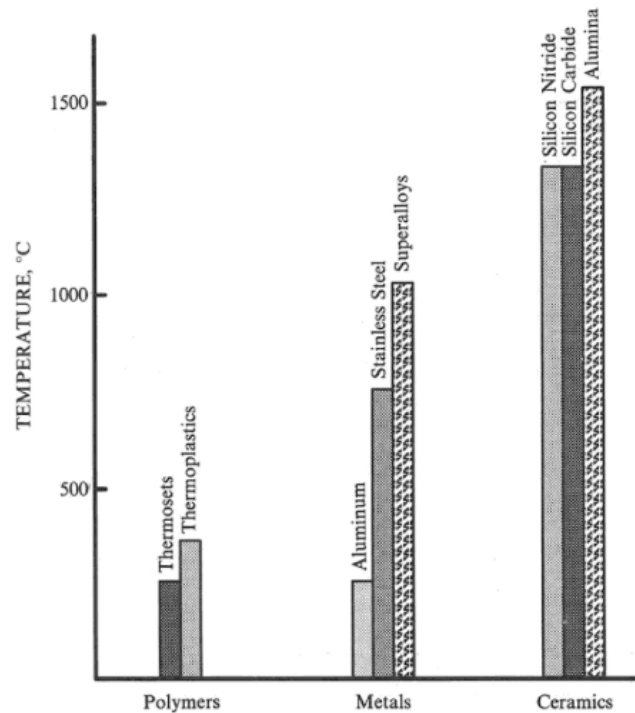


Fig. 2.3 The maximum service temperatures of polymers, metals and ceramics [3]

While MMCs suffer from high cost, complex fabrication methods and limited service experience, PMCs are more advanced in the manufacturing technology and are cheaper in terms of raw material cost. Lower density of PMCs is another important advantage compared to MMCs and CMCs.

Polymer matrix can be either thermosetting or thermoplastic polymers, which are explained in the following sections.

Thermosetting polymers

Thermosetting polymers provide relatively higher strength, stiffness and stronger interfacial fibre-matrix bond for composite matrices compared to thermoplastic polymers. Aerospace, automotive and marine industries commonly use thermosets in the production of lightweight and high performance structures. Thermosets initially have oligomers or polyfunctional monomers which are cured to form three dimensional network of covalently bonded chains, which is an advantage for creating a strong bond for the reinforcement surface [2]. In the pre-curing period (A-stage), good impregnation of the thermoset resins into the fibres can be achieved. The curing process starts once the resin has fully penetrated into the fibre during processes such as the resin transfer moulding (RTM) and injection moulding. Pre-impregnated forms of composites, called prepreg sheets, can be also produced by partial curing (B-stage). In this stage, the majority of chains are not cross linked, which allows an easy handling of the material to form a desired shape by using lay-up process. Lastly, an autoclave or hot press machine can be used to fully cure and consolidate the prepreg layers (C-Stage).

Thermosets are brittle due to the rigidness of the polymer chains, which results in poor fracture toughness [25]. They do not have formability or melting processability like thermoplastics do.

Thermoplastic polymers

Thermoplastic polymer chains do not form cross-links like the thermosetting polymers do, therefore they can be re-melted by adjusting the temperature according to their melting point, and can be reshaped under pressure. The polymer crystallization occurs when they are cooled to room temperature in two steps; crystal nucleation and growth. Crystal nucleation can happen either in homogenous or heterogeneous way in fibre reinforced semi crystalline composites. While spherulitic structures are formed inside the polymer in homogeneous nucleation, columnar structures are observed in the heterogeneous nucleation due to the growth of nuclei on the surface of fibre. The whole crystallization process readjusts the molecular chains, releasing exothermic heat and producing shrinkage [26].

Figure 2.4 shows the difference between molecular structures of thermoplastic and thermosetting materials. As a result of not forming cross-links, thermoplastic materials have high melt processability. It is easier to adopt thermoplastics to new manufacturing techniques whereas thermosetting polymers like epoxy resins are not very flexible to work with. Using

thermoplastics such as polyketone and nylon instead of an epoxy matrix provides high performance parts in a cost-effective way [27]. However, they are not preferred when there is a need for dimensional stability. Despite all these, they can provide high impact and fracture resistance as well as high strain-to-failure ratio [28, 29].

Thermosetting polymer matrices have been widely used for long and continuous fibre over the past 40 years in the aerospace industry. For this reason, in chopped fibre reinforced composites, thermoplastics are more common compared to long and continuous fibre reinforced composites. Even if thermosetting polymers provide more dimensional stability, disadvantages such as the storage conditions, longer curing time with complex parameters, and some irreversible defects due to problems with handling of fibre fabric make them hard to use. Therefore, thermoplastic polymers can be used as a good replacement for thermosetting resins, providing better chemical endurance. They can withstand intense forces and they are flexible to use in wide range of temperatures. [30, 31].

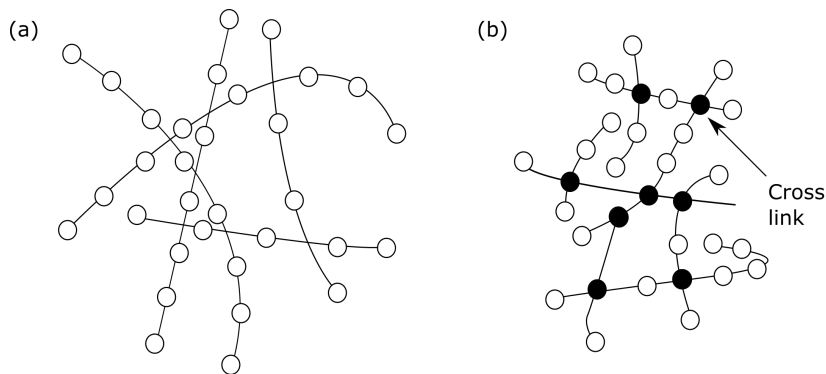


Fig. 2.4 Chain formation of (a) thermoplastics and (b) thermosettings

Thermoplastics can be categorized into two; amorphous and semi-crystalline. While amorphous materials have a temperature range where they get semi-molten, semi-crystallines remain solid until their melting point. Both types of thermoplastic material can be reshaped while cooling. The difference is that amorphous thermoplastics forms random structures whereas the semi-crystalline materials have organized molecular formation, called crystal lattices [32].

In the case of thermal analysis of thermoplastic materials, three transition temperatures are important to understand how their particles rearranges; glass transition temperature (T_g), melting temperature (T_m) and crystallization temperature (T_c). Glass transition temperature is the only important factor for amorphous polymers since it is the beginning of the temperature interval where their structure starts gradual melting and flowing. As the

temperature rises, more amorphous bonds break and the viscosity of the material decreases. Melting and crystallization temperatures are important for semi-crystallines. Crystalline structures break only when the melting temperature is achieved, and they rearrange when the temperature decreases to the crystallization point. Figure 2.5 shows the typical thermal analysis output, which is acquired from differential scanning calorimetry, for both amorphous and semi-crystalline materials [33].

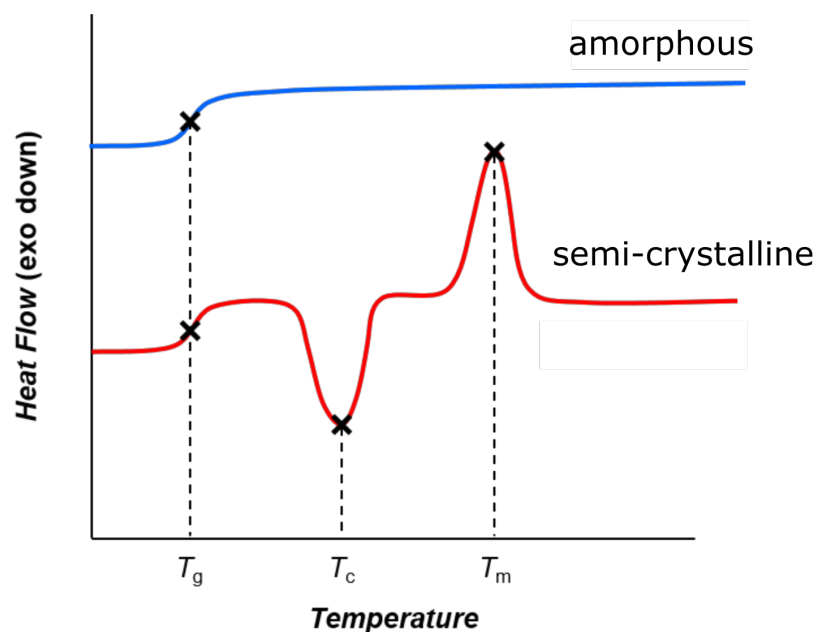


Fig. 2.5 Thermal analysis of thermoplastics

2.1.6 Carbon Fibre Reinforced Polymer (CFRP) Composites

Carbon fibre is the most commonly preferred reinforcement material. At a microstructural level, carbon atoms of fibres are joined parallel to the fibre axis and carbon fibres have extremely small thickness in between 5-10 microns in diameter, which makes the composites light and strong. Therefore, CFRP composites, containing carbon fibre reinforcements and polymer matrix, offer lightweight solutions. They have been demonstrated to have wear and corrosion resistance. Their high thermal conductivity provides also improved fatigue properties against thermal stresses. Even if they are expensive, the superior properties of CFRPs make them one of the most important materials for structural applications, especially in aerospace industries [34, 27]. Still, many types of failure may be observed in fibre rein-

forced polymers. Typical failure modes of fibre reinforced polymers include fracture, poor adhesion and interlaminar delamination between fibre and matrix. Many factors can affect the failure behavior, such as the loading nature, fibre orientation and the fabric form, but most importantly the manufacturing techniques [35].

In the following sections, conventional and additive manufacturing techniques for composite materials, focusing mainly on CFRP composites and their final properties are presented.

2.2 Conventional Manufacturing Techniques of Fibre Reinforced Composites

The manufacturing of composites presents many challenges. To be able to reach the maximum performance of the final products, a manufacturer must be aware of the processing requirements of the fibre and matrix materials. Unlike metals that are homogeneous and have predictable properties, it is hard to have consistent final part properties in the production of composites [31]. The anisotropy given by the fibre orientation adds complexity to the process. Both the raw material and final components are generally made together in a single manufacturing operation. This operation should also include the requirements to produce the desired final shape. Furthermore, the chosen manufacturing technique affects the surface quality [1].

Most composite parts are created layer by layer followed by a consolidation since the feedstock material is supplied as dry or prepregged plies. Composite laminates can be produced by manual lay-up process, followed by curing. The laminates then can be cut according to the final desired shape. Autoclave and hot press processes are often used to provide heat and pressure to form a compact composite laminate. Uniform distribution of heat and pressure must be provided to avoid any void formation and achieve a low porosity part with high performance. Vacuum bagging in clean room conditions is used to provide inert gas like nitrogen to the laminate in an autoclave machine. The bagging materials are usually expensive. During the curing cycle under pressure, the resin viscosity is reduced and trapped air is removed. As the compaction pressure is increased, the higher performance of the final part can be achieved [21]. Compression moulding is used to create more complex geometries. The type of mould and compression varies with the part geometry. Thermosets reinforced with random discontinuous fibre are often produced by this technique. An hydraulic hot press is used to provide the necessary compaction pressure. Injection moulding is another

mature technique to produce fibre reinforced polymer composites. Molten state material is injected with pressure by a screw plunger into a mold cavity to form a final part. This process is suitable for mass production since multiple numbers of products can be formed with one injection simultaneously. Epoxies and polyimides often combined with glass fibre reinforcements are economically available for injection moulding. The drawbacks of this technique are the fibre degradation and limitation in part design as well as the long set-up times and expensive tools [36].

In recent years, advanced manufacturing techniques for carbon fibre reinforced composite materials have been investigated. Manual lay-up and moulding are labour intense and costly. There are limitations for complex shaped parts and it is hard to control material properties for every cycle of production, which results in lower efficiency and lack of reliability [7, 37]. Automated conventional manufacturing techniques which are filament winding, automated tape lay-up and automated fibre placement are developed to overcome these disadvantages [4]. However, they still require additional compaction to obtain high quality parts [38]. In the next sections, automated techniques are reviewed.

2.2.1 Filament Winding

Filament winding is one of the oldest process. Mainly cylinder-shaped parts such as pressure vessels or pipes are produced with this process [39]. It is an automatic method of creating composite parts with either wet or dry winding prepreg sheets. The first step of the wet winding process is gathering and bundling the fibres, followed by a pass through a resin bath which includes liquid resin and catalyst. Then the amount of the resin on fibre can be controlled by squeeze rollers and the excess resin can be wiped off. After the roving are impregnated, they can be straightened up to form a flat band and positioned on the mandrel. The helical winding pattern is formed by the movement of flat band back and forth. To obtain the desired winding form such as hoop and helical for the part, the speed of the carriage and the mandrel can be altered. The material is cured on the mandrel after the chosen thickness for the product is acquired. The mandrel is removed after curing [1, 4]. Figure 2.6 shows the representation of the filament winding process. Production of cylindrical composite parts by filament winding includes three stages. First stage is the design during which the material selection, shape and fibre orientations has been done. Fibre placement is the second stage, which involves arranging the fibre positions. The last stage is the selection of the process parameters that should be under control during the manufacturing process [40].

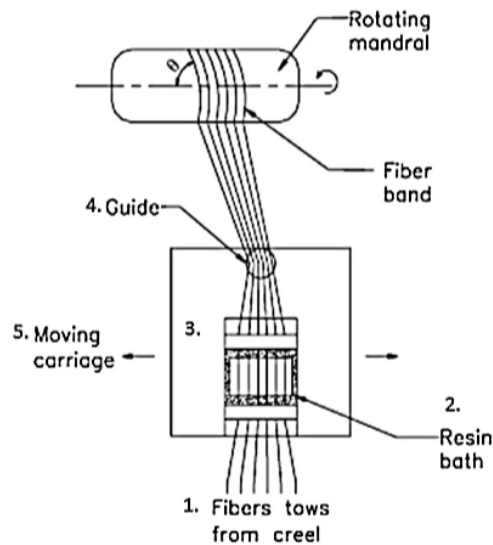


Fig. 2.6 Filament winding diagram. (Figure reproduced with permission from [40])

The main disadvantage of this process is voids which arise from inconsistent wetting of the fibres. Bubbles in the resin bath or excess resin create voids. Delamination and fibre wrinkles are also common defects on filament winding parts. While unsuitable adhesion due to joining of dry layers to formerly wound layers can cause the delamination, fibre wrinkles are the result of poor winding tension and misalignment of rovings [41, 42].

2.2.2 Automated Tape Lay-up

Automated tape lay-up (ATL) is a process which has been available since 1980 for both thermoset and thermoplastic materials. While hand lay-up technique has been used to manufacture earlier composite structures, the aim of inventing ATL was to increase product quality and the productivity since the former is labour intensive and time consuming [43]. In ATL process, continuous fibre sheets are laid by ATL machine onto a smooth floor in several orientations. By the help of a roller, prepreg tape is deposited onto the mold as a first stage of composite fabrication. Then the machine continues the deposition of the tape depending on the desired part shape. When lay-up process is complete, a secondary rotation process cuts the tape automatically. As the complexity of part geometry increases, the speed of the machine might decrease accordingly. Figure 2.7 shows automated tape lay-up system.

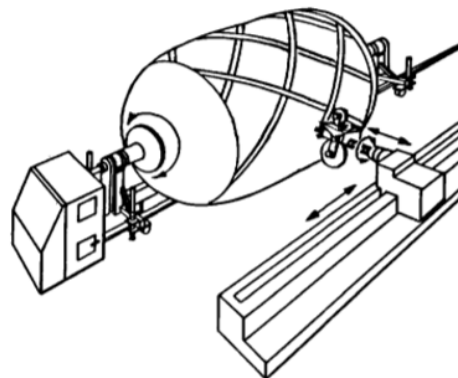


Fig. 2.7 Automated Tape Lay-up system using filament winding machine (Figure reproduced with permission from [44])

ATL is used as an efficient way to manufacture large flat structures or parts with single curvature. To manufacture more complex structures, ATL laminate sheet is shaped second time. However, the disadvantage of this process is warping and buckling of the laminate, if the machine has to draw a large curve [4]. For such complex parts, prepreg tapes need to be routed to reach the preferred fibre orientation [43]. This makes the process not adequate for creating complex parts.

2.2.3 Automated Fibre Placement

Automated Fibre Placement (AFP) is one of the automated production technologies that is capable to lay strands on complex curvatures with the chosen fibre orientations in series production. It combines the advantages of ATL, and filament winding processes and has much in common with ATL. ATL is mainly suitable for flat surfaces. However, it is possible to use AFP for more complex shapes, since narrow tows can be laid which can be routed over surfaces with large curvatures. On the other hand, wider tapes can be placed only by buckling some of the fibres; process which makes the laminates weak. In AFP, the machine is fed prepreg tows, places them onto a surface to shape a continuous prepreg strand. An AFP head can be attached on a multi- axis conveying arm that travels around the tool. As an alternative way, a software program can control the rotation of the tool under a static head [45]. Figure 2.8 shows an automated fibre placement robot.

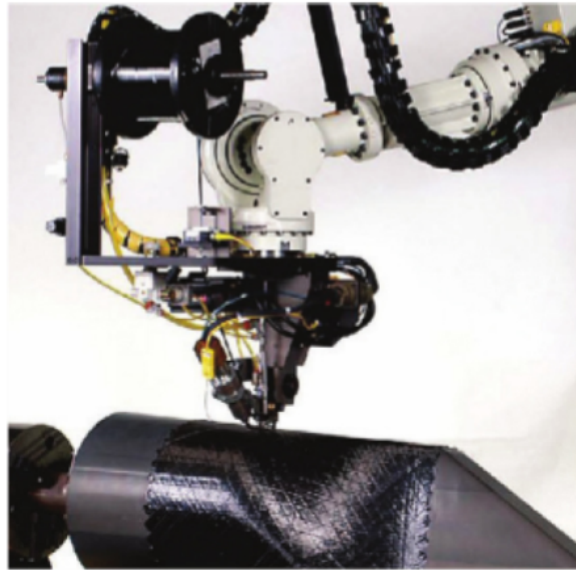


Fig. 2.8 Automated Fibre Placement robot (Figure reproduced with permission from [45])

There are limitations in automated manufacturing processes. The fibres tend to wrinkle out-of-plane as it is illustrated in Figure 2.9, which is the reason for decreasing of load carrying abilities of the cured laminate. These defects are called “ply waviness” which have many effects on stiffness and static strength [43].

In addition, the main limitation of possible AFP is the shortest cut length. Machine can place only limited tow. The cost of obtaining the desired equipment is also a major issue. The use of robotic arm style AFP machines has become a potential way to decrease the cost in manufacturing industries [4].

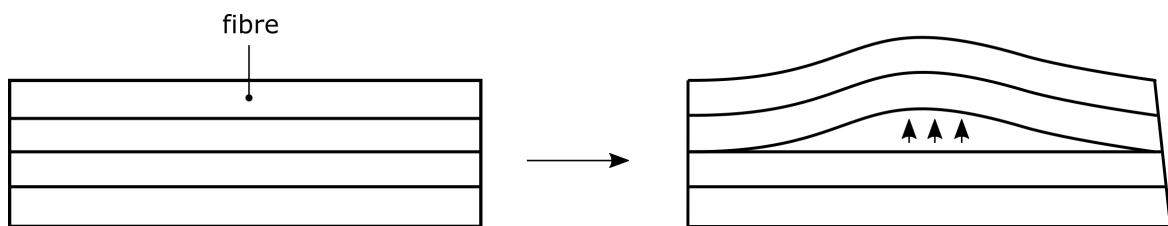


Fig. 2.9 Local buckling of steered fibres

2.3 Additive Manufacturing Techniques of Fibre Reinforced Composites

Additive manufacturing (AM) is a manufacturing process where materials are bonded layer-by-layer to create parts from a 3D Computer-Aided Design (CAD) model. The standard process of AM can be listed in 6 steps;

- A CAD model of the designated part is created.
- The CAD file is transformed into a STL (stereolithography) file and then sliced into thin layers.
- After the transfer of the STL file to the 3D printer, with the help of a 3D printing software, the last alterations are done such as scale, position and the thickness of layers.
- Manufacturing process can be started after the process parameters are adjusted.
- Part is removed from the 3D printer.
- If it is needed, post processing techniques are applied and the part would be ready to use [46, 47].

Adopting AM techniques in aerospace, automotive, healthcare, and other fields has become common due to the properties and benefits that AM can bring to these industries [5]. The design flexibility is the defining advantage of AM. Producing complex parts in a material effective way has made producing low volume products economically viable. However, the quality and performance of the AM parts are still not standardised compared to the traditional techniques.

Although most commercial AM systems can only produce single-material parts, recent research has questioned, and demonstrated the capability of producing multi-material parts as well [46, 48]. Being able to use multi material layer-by-layer can be a great benefit to the tailoring of mechanical properties and performance of a part, as well as solving the quality problem that single-material AM systems suffer from [49]. Fabrication of composite materials, involving multi material, can be interpreted as an oldest form of additive manufacturing. Automated tape lay-up, and fibre placement technologies use the layer by layer approach when the prepreg materials stacks together to form a laminate. Therefore, the composites can be adopted to advanced additive manufacturing.

AM of composites is a major area of interest in academia and industry, it presents an opportunity to combine the benefits of high strength to weight ratio of composites with design freedom in AM to create functional, lightweight, complex geometries efficiently and cost-effectively [50]. Even though AM composites are behind the traditionally made composites in terms of mechanical performance for critical applications such as aerospace and automotive industries, design flexibility is the main attraction point. AM is preferred as a cost-effective alternative in the applications where the end-use products have complex geometry and low volume. The development of composite tools such as brackets and fasteners that are used in the assembly of an aircraft can be efficiently manufactured with the AM processes. Composite bike frames and drone frames are among the most popular end-use products. Recently, medical applications also become common for composites AM. 3D printed carbon fibre reinforced composite implants and foot prosthetics provide more dynamic responses and load resistance than any other materials. Prosthetics with customizable designs can be manufactured in hours with AM [51].

Discontinuous or short fibres (a few millimeters in length) are currently more widely utilised in AM compared to continuous fibres due to the ability to enhance the mechanical properties of the materials without a significant modification to the manufacturing process. Short fibres are more easily integrated into standard feedstocks used in AM, providing an advantage over continuous carbon fibre manufacture which is more challenging to manufacture using current AM techniques [52–54]. The addition of short fibre to polymer-based AM not only improves the strength and stiffness but also enables a flexible selection of matrix materials, which makes them more processable using AM methods. Thermosets are the conventionally preferred epoxy matrices used in the aerospace industry as they provide strong adhesion, however, thermoplastics usage is becoming more common due to their advantages in additive manufacturing, such as melt processability and chemical resistance. The characteristics of thermoplastics decrease the complexity of curing cycles and make them available for rapid manufacturing. Therefore, they can be more easily used for processing using AM techniques [6].

AM of fibre reinforced polymer composites can be classified into powder bed fusion, stereolithography, material extrusion and sheet lamination according to ASTM International Technical Committee F42 [55]. Each group of composite AM will be elaborated in the next sections.

2.3.1 Powder Bed Fusion AM Processes

In powder-based additive manufacturing technologies, powder is used to join the layers of a part together. After deposition of powder for the first layer of the part, the second layer is engraved selectively. This process is repeated until the last layer of the part is finished. Then, the removal and cleaning of the part can be done since it is only enclosed by powder. Selective Laser Sintering (SLS) and Selective Laser Melting (SLM) are the most well-known processes of this technology [56]. Figure 2.10 shows the schematic of the process. Just as in the other AM techniques, the most important advantage of the process is that there is no need for mold and subtractive machining techniques to create complex geometries, which makes the process material effective [57]. The materials which are used in this process are generally wax, metals, polymers and ceramics.

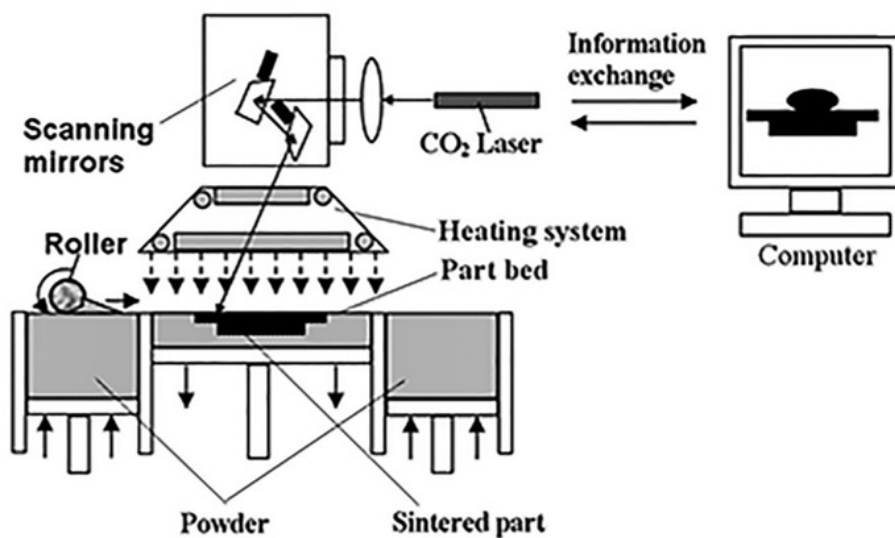


Fig. 2.10 Schematic of SLS process (Figure reproduced with permission from [58])

In SLS/SLM, three methods are mainly used to manufacture composites; combining multiple types of powder, using in-situ reactions to form a compound and application of post processing such as furnace treatment to create chemical reaction or infiltration [59]. The first one is the most common technique to explore SLS composites. In this technique, either ceramic or polymer powder can be selected, and laser sintered to produce composite materials with or without fibres. It is preferred to use the reinforcement powder to avoid formation that disrupts the smoothness of powder feedstock. Secondly, in-situ particles can be created by chemical reactions during laser sintering. This is a way of producing composite materials such as formation of TiC-Al₂O₃ composite using TiO₂, Al and C [60]. This technique is not

desirable since the products have porous structures and they have low strength and stiffness. Using furnace treatment is the third method to manufacture composites by SLS/SLM. It again includes chemical transformation on the laser sintered parts with the help of post processing techniques. There are so many chemical conditions which can influence the mechanical properties [59].

Fibre reinforced polymer composites can be manufactured using the first method by combining the matrix powder with reinforcement. Mechanical properties of the final parts can be potentially enhanced with the addition of short fibre to the powder feedstock in SLS processes. One of the SLS process, called High Speed Sintering (HSS), produces nylon parts with a maximum of 38 MPa ultimate tensile strength and minimum of 4.71% porosity using PA2200 polymer powder (EOS GmbH) [61]. Salazar et al. added short fibre glass (25%wt) to the PA12 powder and produced composite parts that have 43.7 MPa tensile strength [62]. Jing et al. achieved 80 MPa tensile strength not only by combining CF with PA12, but also applying a surface modification with nitric acid and heat treatment to the carbon fibres [63]. The porosity of the CF/PA12 parts were decreased from 38.12% to 4.68% thanks to the post-processing. However, the resultant parts still had a high amount of porosity compared to the conventional CFRP parts.

As it is highlighted in the literature, the main disadvantages of this process for composites are the poor dispersion level of the fibre in the powder feedstock as well as the internal porosity of the final parts. It is also not possible to include continuous or long carbon fibre in this technique [64]. Although SLS is one of the fast growing AM technique, there has been limited research on composites due to the limited improvements on the mechanical properties and negative effect on the quality of the final parts [6].

2.3.2 Stereolithography

Stereolithography (SLA) is a distinguished methodology which is based on photopolymerization. Liquid resin is transferred into a solidified polymer when is exposed to ultra-violet laser radiation. The layers of resin are cured in a bath to fabricate the parts until the parts are completely shaped [65]. A diagram of the process is presented in Figure 2.11.

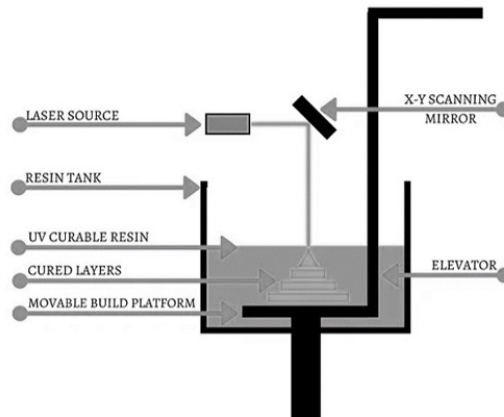


Fig. 2.11 Schematic of SL process

3D parts which are fabricated with SL have low mechanical properties. For this reason, their applications in load carrying components can be limited. Photopolymer-fibre mixture can increase the strength and stiffness of SL-produced parts. Therefore Stereolithography is another AM technique that adopted nonwoven mats of carbon fibre, e-glass and para aramid fibres to produce composite parts with epoxy based resins. The highest tensile strength and stiffness reported are 55.2 MPa and 2.85 GPa respectively for the e-glass fibre reinforced acrylic based resin (17 grams per square fibre mat) [66, 37]. Similar to SLS processes, limited research has been carried out on SLA of composites due to the challenges in dispersing the fibre on the surface of the resin. Fibre addition causes an increase in the viscosity of the photopolymer. This makes the layer coating process more complicated. Non-uniform distribution of the fibres on the surface of resin, poor bonding and high volume fraction of voids between the layers due to the partial curing are the drawbacks of adopting fibres in the SLA technique [67, 65]. Heat treatment was observed as a post processing method that improved the mechanical properties [55, 23].

2.3.3 Fused Deposition Modelling

Fused deposition modelling (FDM) is the most popular technique among AM processes for thermoplastic materials like acrylonitrile butadiene styrene (ABS), polylactic acid (PLA) and nylon. In this process the material in filament shape is heated and extruded with the help of spools through the nozzle. Semi molten filament is printed as a first layer of the part with specific thickness. The same process is repeated layer by layer and layers are joined and solidified together, while the printed head moves according to the defined path. A 3D part

with desired geometry is created with the completion of final layer [68]. A schematic of the FDM process can be seen in Figure 2.12.

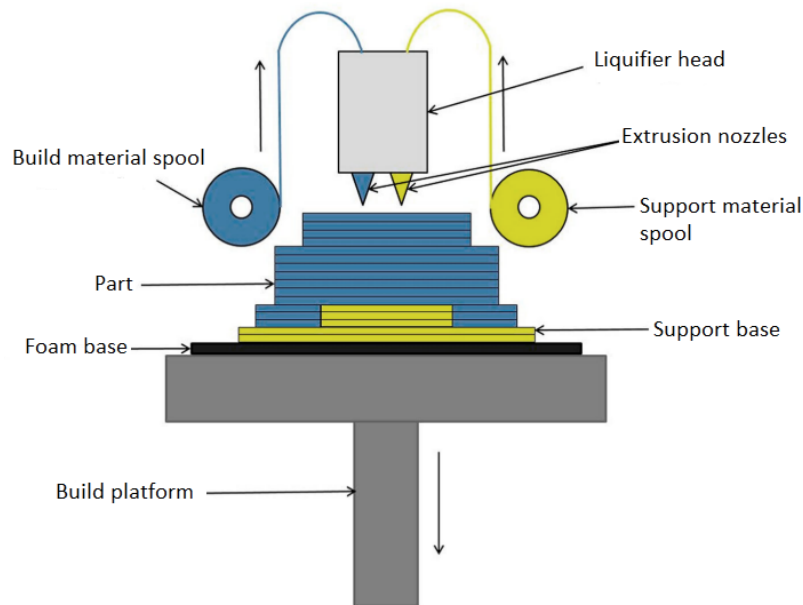


Fig. 2.12 Schematic of FDM process (Figure reproduced with permission from [69])

Material extrusion-based techniques such as fused deposition modelling are the most common methods used for the production of fibre reinforced thermoplastic components. Continuous fibres have been introduced to AM with FDM. Printing of short fibres requires almost no alteration in FDM printers, whereas continuous fibres need some modification. Therefore, short fibre filaments are accessible and printable with desktop 3D printers. There are three different FDM methods to manufacture composite parts which can be seen in Figure 2.13.

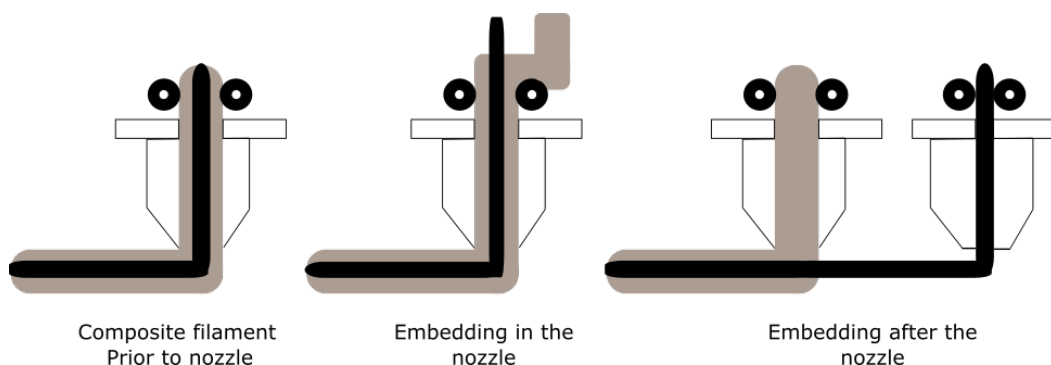


Fig. 2.13 Fibre implementation methods for Fused Deposition Modelling

First of all, the composite filament can be produced before the printing process which is the most straight-forward method as there is no need to make considerable changes in the system. The main advantage of this approach is the homogeneity of the composite filament in terms of fibre and matrix as the continuous supply of those is provided.

Embedding in the print head is the second approach where reinforcing fibre is extruded as a dry roving while the matrix is added independently. Therefore, fibre volume ratio can be adjusted by machine control during the printing. However, there could be disadvantages in terms of air inclusions [70]. In both methods of fibre operation 'before the nozzle' and 'inside the nozzle', the part becomes ready after printing since the printing process is made by fibre reinforced polymer [71].

The third method that is embedding on the component after the nozzle, is very similar to traditional fibre placement processes. Deposition of fibre and matrix can be also made through separate nozzles which increases the complexity of the machine. Proper adhesion should be provided during the process as the risk of occurrence defects is increased [70].

The US company Markforged developed Mark One 3D printer as a desktop 3D printer which enables the manufacturing of carbon, Kevlar and glass fibre composite parts. Currently, Markforged is the most popular desktop printer for AM of composites, since it is based on Fused Deposition Modelling (FDM). Continuous fibre filaments have been introduced to AM with the technique that Markforged developed. The working principle is same with FDM and the filament is extruded layer by layer. The difference is the second nozzle which prints fibre filament feeding the material, which is called Continuous Filament Fabrication (CFF). Figure 2.14 shows Mark One Composite 3D Printer and the schematic of the process.

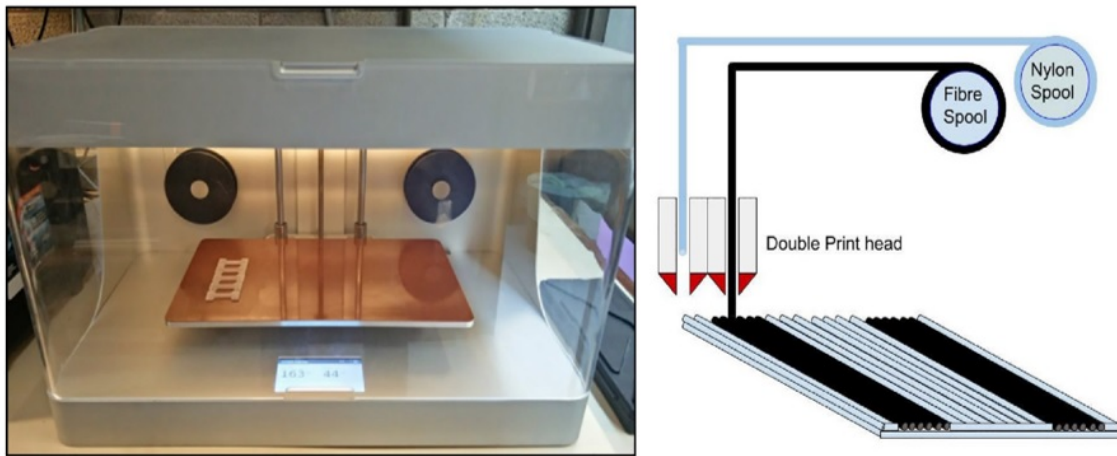


Fig. 2.14 Mark One Composite 3D Printer and the schematic of the process (Figure reproduced with permission from [72])

The Mark Two machine is 320 mm x 132 mm x 154 mm in size and working with composite filament fabrication approach. Parts made with CFF comprise of strand of fibres embedded in a thermoplastic matrix that hardens during printing [73]. There have been many studies on the performance of the parts made by Mark One system in the literature. Van Der Klift et. al. examined the manufacturing capabilities of Mark One by 3D printing carbon fibre reinforced thermoplastic polymer (CFRTP) specimens, in which carbon fibre and nylon were supplied by the Markforged Company. Mechanical properties of those specimens were assessed by tensile testing. Continuous carbon fibre reinforced nylon parts with 6 CFRTP layers produced by MarkOne achieved average of 464.5 MPa tensile strength and 35.7 GPa stiffness, which is the highest for composites AM without applying any post treatment. However it is still lower than traditional composites (tensile strength 1500 MPa and stiffness 135 GPa) [74]. Discontinuity of fibres due to printing pattern caused an early tensile failure in some samples. These discontinuous areas were cut and post processed, which also affected the strength of the samples. Dickson et. al. [45] investigated mechanical properties of Kevlar, glass fibre and carbon fibre composites with nylon matrix to make comparisons between Markforged filaments. In their study, different parameters such as volume fraction and fibre orientation on the mechanical properties were analysed. Table 2.2 shows the results of tensile test for different types of specimens. It can be seen that carbon fibre composites have higher tensile strength than the other types.

Table 2.2 Tensile test results of materials printed by Markforged MarkOne [72]

Specimen	Tensile Strength (MPa)	Elongation at break	Elastic Modulus (GPa)
Nylon	61	439	0.53
Carbon Fibre	216	4.22	7.73
Kevlar	150	4.23	3.61
Glass Fibre	194	8.97	3.12

In the field of composites AM, studies have been focused mainly on FDM. There have been many studies performed to improve the final performance of continuous and discontinuous fibre reinforced polymer composites made by FDM. It was pointed out that there is a trade-off in performance and processability in terms of selection of continuous or discontinuous fibres. In the case of discontinuous fibre composites, the strength and stiffness of the parts are relatively lower. As the performance of the parts increases with the length of the fibres, the processability of the material is reduced [54]. Therefore, continuous fibre reinforcement were mainly possible to process via FDM among AM processes.

Another important observation is that a high void content is common in FDM continuous fibre composites due to the occurrence of triangular gaps between the printed tracks [75]. Justo et al. [76] stated that the lack of compaction in the FDM process caused a high percentage of porosity between layers. 12% of porosity was observed in continuous carbon fibre reinforced PA (Nylon) composite manufactured by additive layer manufacturing using the MarkOne 3D printer. Tekinalp et al. [77] observed that the percentage of void volume in FDM printed carbon fibre reinforced ABS parts were between 16% and 27% regardless of fibre content. As the fibre content increased, tensile strength of the parts increased from 35 MPa to 65 MPa. High fibre reinforcement loading resulted with nozzle clogging. Zhang et al., [78] printed short carbon fibre reinforced ABS composites that have tensile strength and stiffness of 13.74-39.05 MPa and 2.19-5.89 GPa respectively for different raster orientations. The parts had 4.18 - 8.54% porosity level. Blok et al. achieved 1.1% porosity for the short fibre reinforced nylon composites ($V_f = 6\%$), while 9% porosity was found in the parts printed by continuous CFRP filaments ($V_f = 27\%$).

Few research reported an improvement in the final part performance with the use of heat and pressure as a post-process application in FDM composites. Ueda et al. used hot compaction during 3D printing of continuous CFRP, which reduced the void content and improved the

tensile and flexural properties of final parts. The void fraction has been reduced from 10% to 3%, while the tensile strength improved 24% with the use of hot compaction [79]. Mei et al. were able to increase the tensile strength of the FDM composite parts by 24% by applying hot press, causing the void content to reduce [80]. An impregnation and a powder compression post-curing methods were used in [81] and significant increase was obtained in tensile properties of 3D printed continuous fibre reinforced thermosetting epoxy resin parts due to the high fibre fraction of 48%. Compression post-curing reduced the void fraction from 10% to 2.5%.

There are other FDM technologies involving robotic arms developed to print composites. Arevo Labs, a specialist in additive manufacturing of composite materials, has developed a robot-based additive manufacturing (RAM) platform to manufacture composite parts. There is an additive end-effector hardware which includes a head with a nozzle with advanced thermal management technology. Continuous carbon fibre reinforced filaments with a thermoplastic resin that are PAEK or PEEK can be processed. The robotic head has six degrees of freedom which makes the printer head different from the other heads. This enable the construction of parts with 3D surfaces in variable orientations for the first time [6]. The company claims that the resulting parts have strength and great finishing surface when it is compared with the other parts produced with Cartesian-based additive manufacturing software. The delamination problem can be minimized with this technology. Furthermore, the part build envelope can be scalable from 1000 mm³ to 8 m³ depending on the size of the robot [82]

Stratasy also released a Robotic 3D Composite Demonstrator which has a robotic arm that can move in 8-axis (6-axes robot with 2-axis work table) [83]. There is a potential that the 3-axis fibre alignment can be achieved, which would result in composites with higher performance than conventional ones. However there has been no research reports investigating the properties of composites produced by these techniques.

The summary of the FDM composites review is presented as discontinuous and continuous in Table 2.4 and 2.3 respectively.

Table 2.3 Summary of literature review for FDM of continuous fibre composites

Reference	Material	FDM Equipment	Tensile Strength (MPa)	Elastic Modulus (GPa)
Melenka et al. [84]	Continuous Kevlar/Polymer	Markforged MarkOne	82.9	9
Matsuzaki et al. [85]	Continuous carbon fibre/PLA	Blade 1 Printer	185.2	19.5
Dickson et al. [72]	Continuous carbon fibre/Nylon	Markforged MarkOne	216	7.73
Dou et al. [86]	Continuous carbon fibre/PLA	RepRap Kossel 3D Printer	243.5	25.77
Van Der Klift et al. [74]	Continuous carbon fibre/Nylon	Markforged MarkOne	464.4	35.7
Blok et al. [54]	Continuous carbon fibre/Nylon	Markforged MarkOne	968	62.5
Ming et al. [81]	Continuous carbon fibre/thermosetting epoxy resin	Impregnating/ Printing/ Post-curing	1476	100

Table 2.4 Summary of literature review for FDM of discontinuous fibre composites

Reference	Material	FDM Equipment	Tensile Strength (MPa)	Elastic Modulus (GPa)
Shofner et al. [87]	Nanofibre/ABS	Stratasys FDM 1600 Modeler	26.9	0.49
Blok et al. [54]	Chopped carbon fibre/Nylon	Lulzbot TAZ 6 printer	33.5	1.85
Ning et al. [88]	Carbon fibre powder/ABS	EB-1, ExtrusionBot Co. (USA)	35	2.27
Zhang et al. [89]	Chopped carbon fibre/ABS	QIDI Tech dual-nozzle 3D printer (China)	39.05	5.89
Liao et al. [90]	Chopped carbon fibre/PA12	Hueway 3D-304 (China)	47	0.96
Ferreria et al. [91]	Chopped carbon fibre/PLA	BQ Prusa i3 Hephestos	53.4	7.54
Mahajan and Cormier [92]	Chopped carbon fibre/UV cured resin	nScript 3Dn-Tabletop micro-extrusion system	65	4
Tekinalp et al. [77]	Chopped carbon fibre/ABS	Solidoodle 3	67	13.7
Jiang and Smith [93]	Chopped carbon fibre/PLA	Makerbot Replicator 2	68.4	9.28
Love et al. [94]	Chopped carbon fibre/ABS	Solidoodle 3	70.69	8.91

2.3.4 Sheet Lamination

During the sheet lamination production method, parts are manufactured by bonding the sheets of material as shown in Figure 2.15. A Laminated Object Manufacturing (LOM) technique, which is another term for sheet lamination, to produce fibre reinforced polymer composites called Selective Lamination Composite Object Manufacturing (SLCOM) has been developed by Envision Tec company. Selective Lamination Composite Object Manufacturing (SLCOM) uses both additive and subtractive manufacturing techniques. Fibre reinforced sheets are cut by using ultrasonic blade cutters. Then these sheets are stacked together to form a 3D object by applying heat and pressure [95]. The advantage of this technique is its flexibility to adopt a wide range of reinforcement (carbon fibre, glass fibre, aramid fibre) and thermoplastic materials such as PEEK (polyetherketoneketone), PE (polyethylene) and PA (polyamides: Nylon 6, Nylon 12).

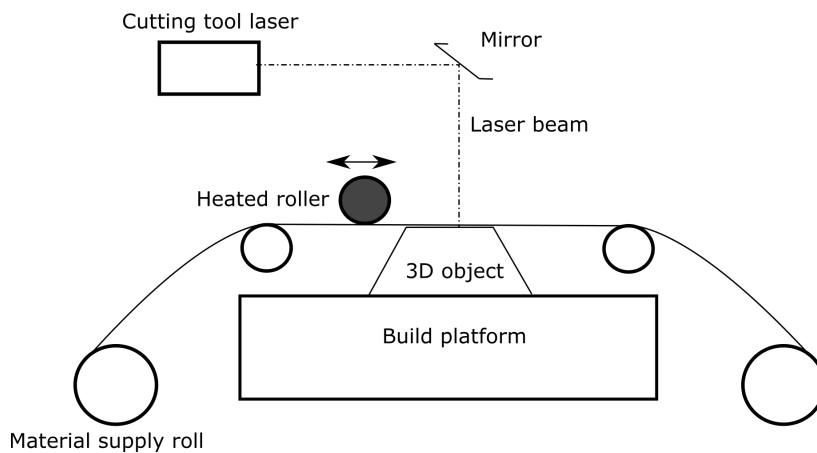


Fig. 2.15 Schematic of Laminated Object Manufacturing (LOM)

Impossible Objects developed a commercial composite AM technique known as Composite Based Additive Manufacturing (CBAM) based on sheet lamination that does not require cutting. CBAM falls under this category even though it is slightly different than the traditional LOM method. Inkjet printing is used to print a liquid binder on a carbon fibre substrate layer. Then, a thermoplastic powder is deposited on the substrate. Excess dry powder is removed, leaving an adhered powder behind in the shape of printed geometry. After a sufficient number of layers have been produced, a hot press is used to compress printed sheets together and melt the polymer layers together. Lastly, the excess region of substrate layers is removed using a sandblaster [96, 97]. Figure 2.16 shows selectively deposited polymer powder onto a discontinuous carbon fibre reinforced substrate [98].



Fig. 2.16 Deposition of polymer powder in CBAM process [99]

CBAM system requires a facility for manufacturing and it is not a desktop-based like Markforged. However, the problems encountered by desktop carbon fibre printers can be overcome by integrating fibre reinforcement with numerous matrix materials. It could be theoretically faster. The company claims that the parts with CBAM can be up to 10 times stronger when they are compared with the other parts made by FDM or other 3D printing processes. Figure 2.17 shows some example parts made with CBAM process. Additionally, as matrix materials are not extruded in CBAM, wide range of thermoplastics are available for 3D printing, such as PEEK. The goal of the company is constructing a CBAM machine capable of 3D printing at rates of 100 meters per minute. The machine has a maximum scale of 12 in x 16 in (305 mm x 406 mm) and the cost of the technology, the first CBAM machine, is \$ 250,000 USD in 2022. The cost of heated press and bead blast cabinet, which are necessary to have a full solution capable of producing parts, is excluded. Currently, the carbon fibre parts made by CBAM do not have better mechanical properties than that of parts made by conventional techniques. However, they can compete with other AM technologies [96].



Fig. 2.17 Parts produced by CBAM [96]

Sheet lamination processes can potentially enhance the strength and stiffness of the discontinuous fibre reinforced polymer parts by applying heat and pressure to consolidate the layers. They provide strong inter-laminar bonding, resulting in smaller air gaps. To date no independent academic study has been performed using this approach to produce components or study effects of processing conditions on resultant part properties.

The next section describes inkjet printing which is the first manufacturing step in CBAM process.

2.4 Inkjet Printing

Inkjet printing (IJP) is an additive manufacturing technology, which produces constant size droplets of liquid phase materials in order to form a desired shape. The volume of the droplets are varied from picolitres (pL) to microlitres (mL) and they can be positioned on a substrate selectively. Desired patterns without any complexity limitations can be designed and printed onto various substrates. Multiple inkjet heads can be used to deposit multiple materials, which reduces printing time and set-up cost. 2D structures can be printed, and the technology can be extended to allow the stacking of droplets, layer by layer, to form a 3D object [100]. This deposition technique that was created initially in graphics industry, is being developed

to be used in manufacturing due to the progress in the composition of functional inks [101]. Many fields such as fabrication of electronics [102–104] and tissue engineering [105–107] employed inkjet printing to print sensors, resistors and cells.

Inkjet technology has been used to improve the mechanical properties of CFRP materials. Thermoplastic microphases are printed between the carbon fibre laminate plies, which increases mode I interlaminar fracture toughness [108]. Furthermore, the effect of printing parameters on the formation of microphase structure were investigated [78]. In another research, IJP is also used to print self healing polymer formulation to improve interlaminar properties of composites [109]. Alongside providing toughening mechanism for composites by printing polymer solutions, inkjet printing became an important step of sheet lamination processes to produce carbon fibre reinforced thermoplastics which is the main focus of this thesis.

Inkjet printing can be categorized in two groups which are Continuous Inkjet (CIJ) and Drop on Demand (DOD). While CIJ discharges droplets continuously, DOD generates droplets only when needed. In CIJ, a continuous stream of droplets is ejected from a nozzle by the direction of an electric field towards to the substrate as shown in Figure 2.18(a). Droplets that are not printed are collected with a gutter to be recycled for future printing [110]. In Drop on Demand, a droplet can be formed by creating a pressure pulse. Droplets are printed only where they are needed in the designed pattern, otherwise the generation of droplets pauses. Therefore, the waste of material is reduced significantly. Risk of contamination is also low since there is no need for recycling gutter. The working mechanism of DOD printer is shown in Figure 2.18(b).

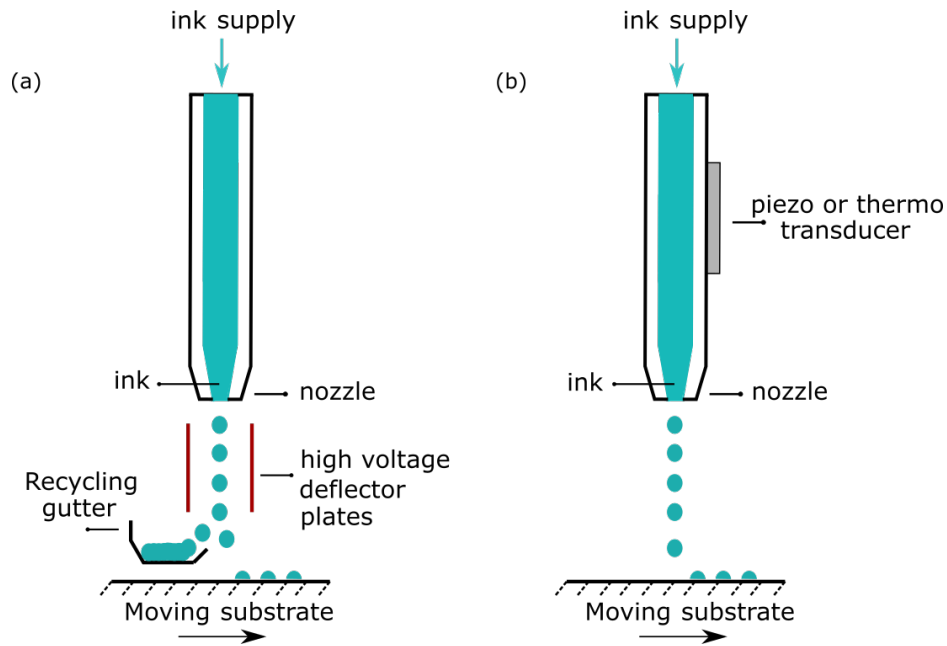


Fig. 2.18 (a) Continuous inkjet printing (CIJ), (b) Drop on Demand (DOD) inkjet printing

The pressure pulse in DOD can be produced commonly in two ways; thermal and piezoelectric [111]. The difference between the working mechanisms is illustrated in Figure 2.19. Thermal inkjet technology is mostly used in desktop printers. In this technique, heat is used for drop formation. Ink is contained by a resistive element in a small chamber which is heated up to 400 °C. Vaporization of the ink by this high temperature causes a bubble formation, which creates a pressure pulse. Therefore drops can be ejected through the nozzle. Piezoelectric inkjet is more common in industrial applications. In this technology, deformation of a piezoelectric actuator is used to generate a pressure pulse, which ejects an ink drop [112, 113]. Thermal inkjet can use limited number of the inks since it should withstand high heat. The rapid changes in temperature also affects the life time of the print-head negatively. On the other hand, a wide range of fluids are available for piezoelectric inkjet, however it is expensive compared to thermal inkjet technology [113]. Electrostatic DOD is another way of generating droplets by using electrostatic forces [114]. In this technique, an electric field is created by the hardware and short response time is very advantageous [115]. However the implementation is expensive. Table 2.5 summarizes the advantages and disadvantages of inkjet printing mechanisms.

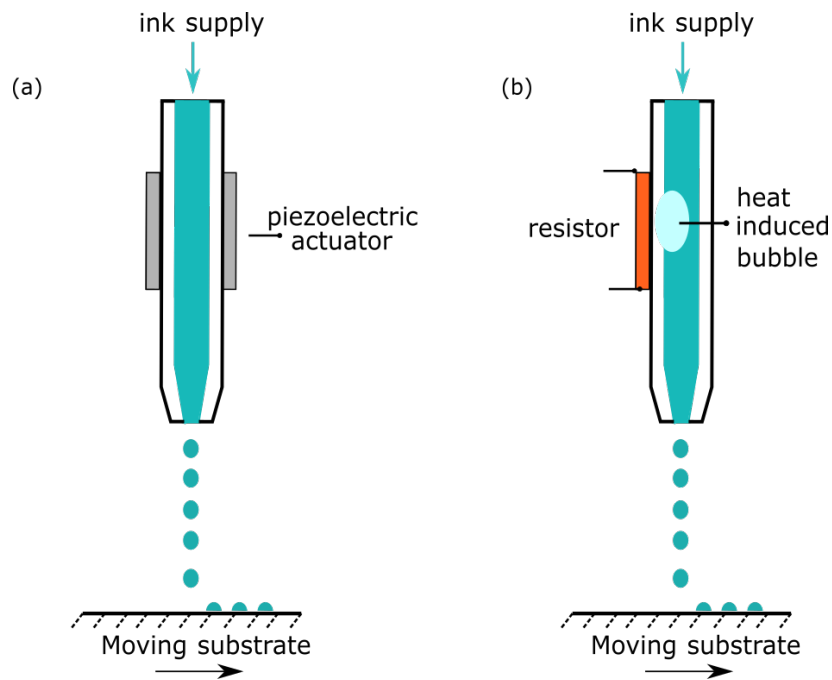


Fig. 2.19 (a) Piezoelectric DOD, (b) Thermal DOD

Table 2.5 Comparison of inkjet printing mechanisms

	Advantages	Disadvantages
CIJ	high drop frequency high drop velocity ink based on volatile solvents	low print resolution high maintenance environmentally friendly
Thermal DOD	micro scalable droplets high nozzle density lower cost	limitations of the fluids short printhead life
Piezoelectric DOD	long printhead life flexibility of ink production	higher cost of printheads
Electrostatic DOD	more concentrated fluid higher resolution micro scalable droplets	only conductive fluids higher cost of application

Drop formation process in a glass capillary tube of a piezoelectric printhead is illustrated in Figure 2.20. An electric field is applied to deform the piezo-ceramic plate which creates a pressure wave into the ink, causing droplet generation. A typical trapezoidal pulse provided to the piezoelectric DOD actuator is also presented step by step during the drop formation process. Figure 2.20 (a) shows the expansion of the piezoelectric transducer by the application of a voltage. The dwell period in Figure 2.20 (b) represents the pressure wave splitting up and traveling in negative (reservoir) and positive (nozzle) directions inside the tube. Since the nozzle is seen as a close end, the wave is conserved and the meniscus is retracted by the pressure wave reflecting at the nozzle. When the pressure waves meet back in the middle of the tube, the contraction of the piezoelectric actuator happens as shown in Figure 2.20 (c). The wave travelling to reservoir direction is cancelled with the compressive pulse, whereas the wave travelling to nozzle direction is amplified, which results in a formation of a droplet [116] (Figure 2.20(d)). This duration is called as fall time, following by echo time where the negative voltage is applied. Finally, the printhead can go back to the initial rise state to form another droplet (Figure 2.20 (e)). The factors such as voltage, pulse duration and the diameter of the nozzle affect the size of the ink droplets significantly [117, 118]. Prior the printing process, the waveform must be optimized to obtain a single droplet without any satellite droplet or a tail. The optimized droplet size can be measured to calculate the volume of ink that is printed onto substrate.

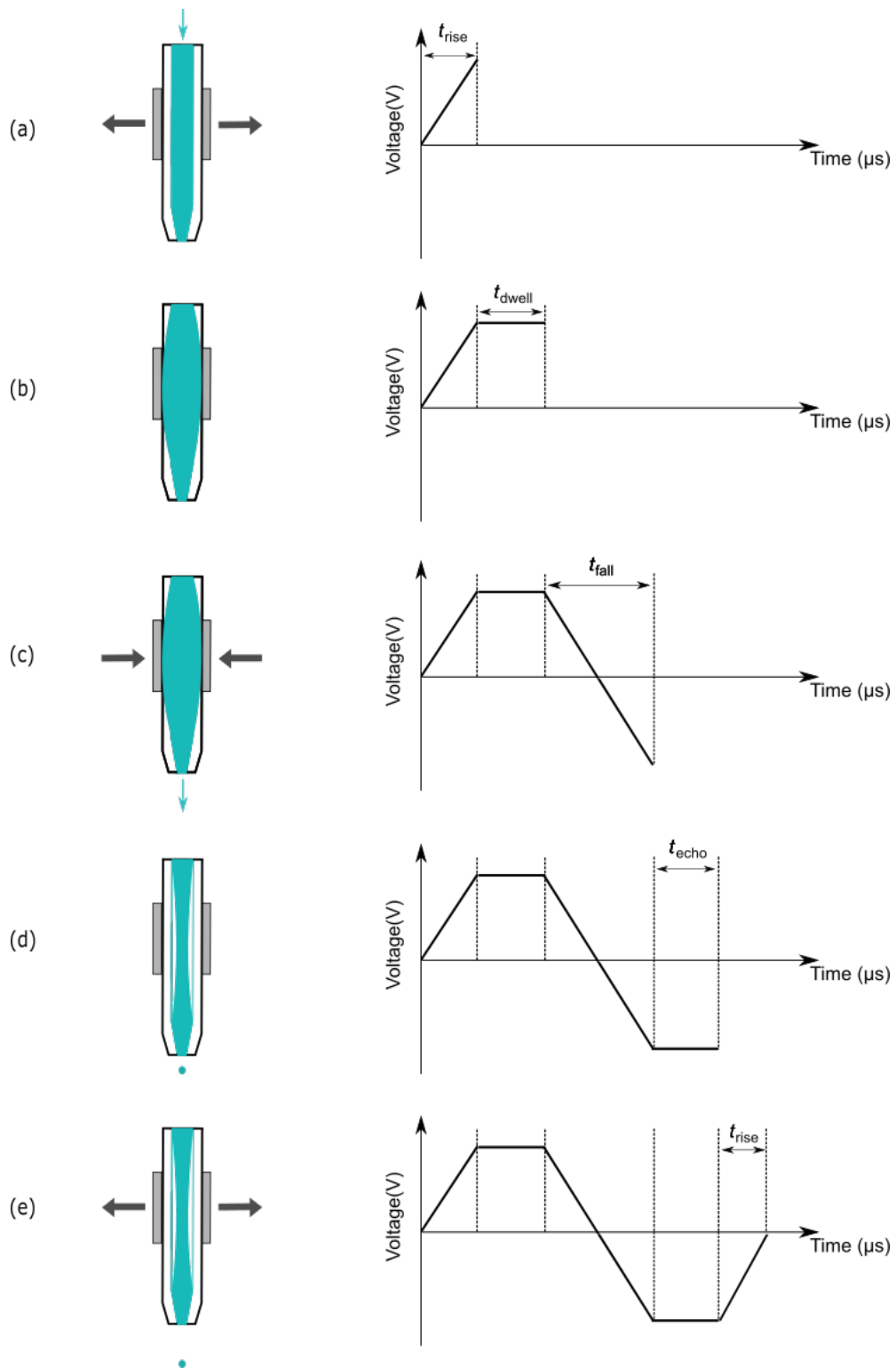


Fig. 2.20 Droplet formation process in piezoelectric DOD printhead with the step by step pressure waveform generation

2.5 Literature Review Conclusions

AM of composites has many challenges, including the limited availability of materials and a high percentage of porosity in the final parts. AM composite parts currently possess lower strength and higher void content than parts manufactured with conventional methods due to lack of layer-to-layer compaction.

Traditional composite manufacturing techniques use autoclave machines or heated rollers to improve the consolidation of the layers which in turn improves mechanical performance of components [119]. The effect of applied pressure on mechanical and microstructural properties of traditionally made composites have been widely investigated in the literature. It has been identified that there is a correlation between the amount of pressure applied and the void content. An increase in the amount of pressure is expected to result in a lower porosity level, which improve the strength and stiffness of the parts [120–123].

There is currently no useful pressure applied in AM of composite structures (e.g FDM and powder bed fusion processes [54]). Research shows that post-processing of FDM printed composites using a hot press can significantly improve the tensile and flexural properties of FDM composite parts by decreasing the void content [124]. However, the application of high heat and pressure is not practical to preserve FDM component geometry [125].

The sheet lamination processes can potentially enhance the strength and stiffness of the discontinuous fibre reinforced polymer parts by applying heat and pressure to consolidate the layers. This provides strong inter-laminar bonding, resulting in smaller air gaps. To date no independent academic study has been performed using this approach to produce components or study effects of processing conditions on resultant part properties.

In this study, discontinuous CFRP composite parts are manufactured using a custom built system at the University of Sheffield, described as Composite Fibre Additive Manufacturing (CFAM), and this approach is based upon a sheet lamination technique similar to CBAM.

Chapter 3

Experimental Methodology

Summary

This chapter describes the methodology used throughout this study. First of all, the reinforcement, matrix and ink materials are presented.

Then, the development of custom built manufacturing process is explained step by step. Inkjet printing mechanism, which is the first step of the manufacturing process, is described. Optimization of drop formation process based on the prior information given in Chapter 2 is performed. Surface treatment of fabric sheets and contact angle measurements are given. Verification of hot press process is explained in detail.

Finally, this chapter covers the characterization techniques to analyse the mechanical and microstructural properties of final composite parts.

Part of this chapter is published: : Karaş, B., Beedasy, V., Leong, Z., Morley, N.A., Muntaz, K., Smith, P.J. Integrated Fabrication of Novel Inkjet-Printed Silver Nanoparticle Sensors on Carbon Fiber Reinforced Nylon Composites. Micromachines 2021, 12, 1185. <https://doi.org/10.3390/mi12101185>

3.1 Materials

A carbon fibre surfacing veil, supplied by ACP Composites, incorporating carbon fibres approximately 25 mm in length is bonded into a polyester matrix. A 0.12 mm thick surfacing veil with 16.95 gsm (gram per square) has been selected since this fabric is suitable for use in a wet layup and hot press applications. The high air permeability allows the fibre move between the layers during compression, which creates homogeneous distribution of fibre inside the part. As a matrix material, virgin PA 2200 (polyamide-12) supplied by EOS GmbH (Krailling, Germany) was used [126]. This polymer powder has a melting point of 185 °C and average grain size of 56 µm. It is commonly used in AM powder bed fusion processes. HP Instant Ink 67/305 (Hewlett-Packard, Inc., Palo Alto, CA) was used to print on the carbon fibre sheets before applying the polymer powder [127].



Weight	16.95 gsm
Thickness	0.127 mm
Fiber	PAN Carbon Fibre
Binder	Polyester
Average tensile	1.22 MPa
Air permeability	0.39 m^3/s

Fig. 3.1 16.95 gsm carbon fibre veil supplied by ACP Composites and properties

3.2 Development of the Composite Fibre Additive Manufacturing (CFAM) Process

A sheet lamination technique, CFAM, was developed in The University of Sheffield to produce discontinuous carbon fibre reinforced thermoplastic composite parts. Figure 3.2 shows all the steps involved during the manufacture of components within this study. In this process, the carbon fibre sheets are cut according to the size of final geometry, after which they undergo a surface treatment to improve the accommodation of ink. These sheets are then inserted into one of two printing system; thermal and piezoelectric inkjet printing. These systems are a HP Deskjet Plus 4130 inkjet printer (Hewlett-Packard, Palo Alto, CA,

USA) and a drop on demand inkjet printer JetLab IV (MicroFab Technologies Inc., Plano, TX, USA) respectively (represented as inkjet head in Figure 3.2 Step 1). The CAD file is converted to STL file which is uploaded to the open source slicer software Slic3r Manual. This software helps to produce Scalable Vector Graphics (SVG) output for other type of 3D printers in which an image representing a layer is required. Each output stands for a 2D slice of the final object. The slices are uploaded to the printer as a separate bitmap/SVG file to be able to print layer by layer. After the first 2D slice of the part is printed onto the fibre sheet, PA2200 nylon powder is spread out onto the printed area (see Figure 3.2 Step 2), resulting in a coating/sticking of nylon over the printed area with the dry excess powder being easily removed with some mild suction over the surface of the fibre sheet (see Figure 3.2 Step 3). This process is repeated until the last layer of carbon fibre is stacked.

The layers of carbon fibre sheets coated with the polymer powder are aligned and stacked on top of each other. Figure 3.2 Step 4 shows the hydraulic hot press machine used to form a compact part bonded with melted nylon powder. Three different pressure levels (0.3, 0.6 and 0.9 MPa) have been selected for comparison of processing parameters. The hot press chamber is heated to 210 °C (30 degrees above the melting point) to allow the nylon powder to melt completely. After 20 minutes of ramping up time, the sample is left under pressure with three different dwell times (0.5 hour, 1 hour and 2 hours), following by cooling time at ambient conditions. All the samples are cooled down using a cooling rate of 1 °C per minute to stabilise the crystallisation conditions. The compressed part was removed from the hot press when it reaches a temperature of 40 °C.

Finally, a sandblasting process with the blast media of brown alumina with low metallic iron content called Guyson Saftigrit Brown (Guyson International Ltd., Skipton, UK) was used to remove the excess carbon fibre layer which were not printed/coated with nylon powder (see Figure 3.2 Step 5). Step 6 shows the final CFRP part obtained with the desired geometry.

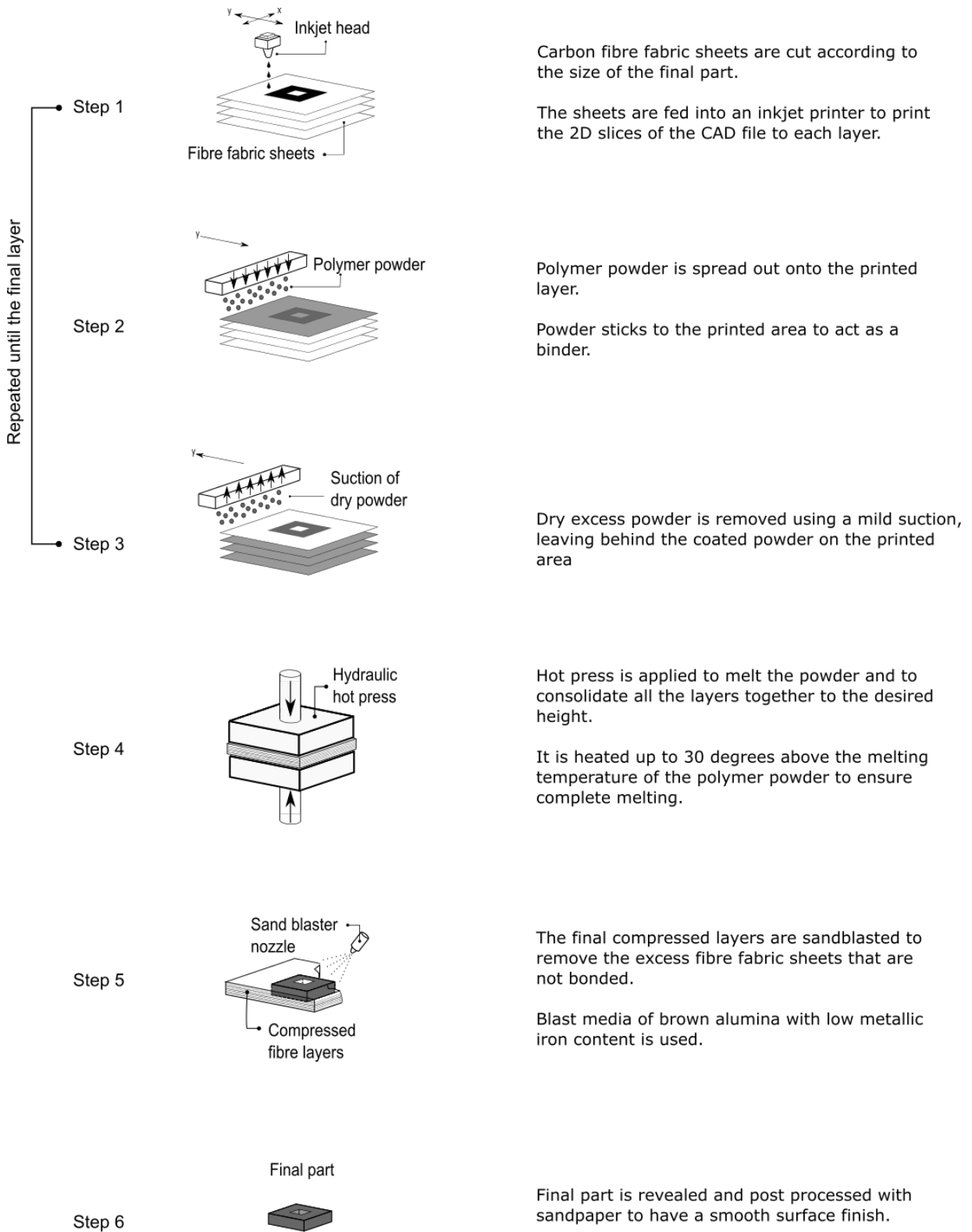


Fig. 3.2 Steps of Composite Fibre Additive Manufacturing process

Figure 3.3 shows an example of a complex shape that the CFAM process developed at The University of Sheffield was able to produce as a proof of concept. The 3D object was designed in Fusion360 Autodesk Inventor. The bitmap file was created from a 2D slice of the part as shown in Figure 3.3(a). While the Figure 3.3(b) shows one of the printed layers, the final part can be seen in Figure 3.3(c).

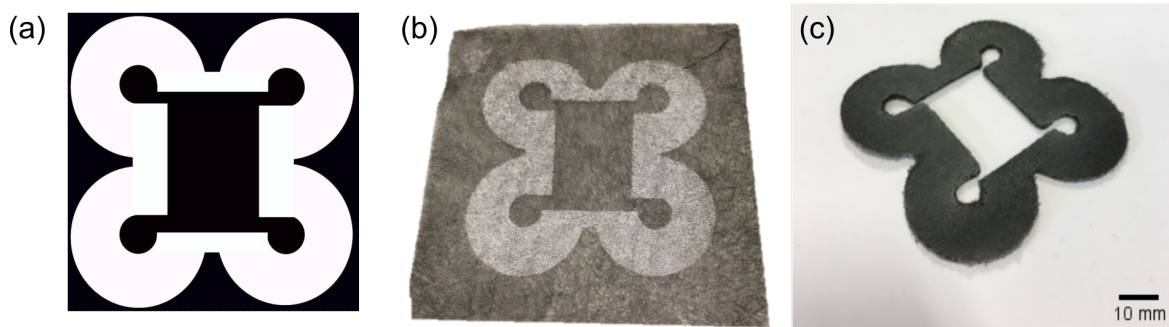


Fig. 3.3 Example of composite component made using CFAM approach; (a) bitmap file for a 2D slice, (b) printed layer before compression, (c) final part with 24 layers (60x60 mm)

3.2.1 Printing Process

Microfab JetLab IV Inkjet Printer

Jetlab IV DOD printer manufactured by Microfab Inc. (Plano, Texas, USA) is used to print on carbon fibre substrates. Figure 3.4 shows the printer. The workbench area of the Jetlab 4 system is approximately 130 x 250 mm. The printing stage is protected with an enclosed cabinet to provide a stable environment for the process. Therefore, fluctuations in temperature and humidity due to the external laboratory environment were negligible during the printing process. There is also an outdoor humidifier inside the cabinet which can be used to control the humidity level required by the process. A humidity indicator is attached to read the percentage of humidity. The workbench is controlled by stepper motors driving screws in the x and y directions. The platform can move only the x and y directions, while the position is maintained in z axis to increase the printing accuracy. Ink is supplied from a reservoir into the nozzle by a pneumatics controller. Negative pressure is also applied to hold the ink back to pause the printing by preventing ejection due to the force of gravity.

An MJ-AT-01 piezoelectric printhead with a nozzle diameter of 60 μm has been supplied from Microfab Inc as shown in Figure 3.4. It is actuated piezoelectrically. An annular piezoelectric (PZT) element, poled radially, is bonded to a glass tube with an integrated nozzle and orifice. A protective housing bonded with a fitting is used to hold the glass capillary inside [128].

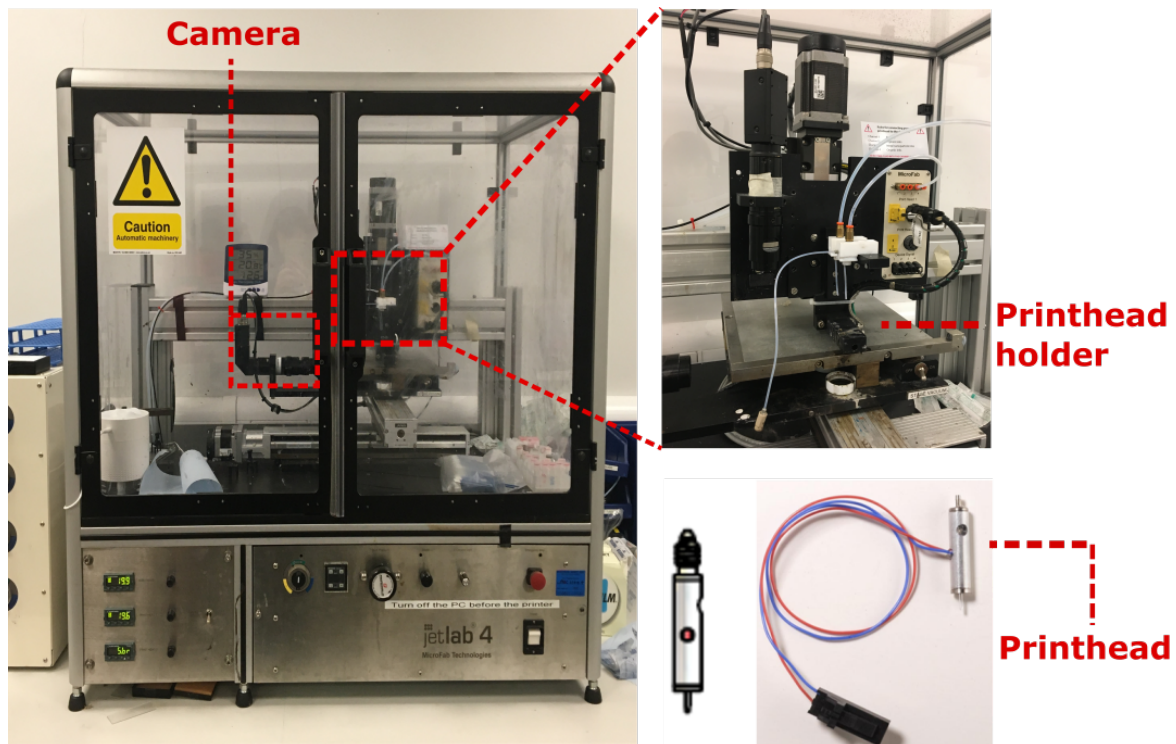


Fig. 3.4 JetLab IV piezoelectric DOD inkjet printer by Microfab Inc. and Microfab MJ-A style drop-on-demand single jet dispensing device

Jetting parameters for piezoelectric printheads can be set up using a graphical user interface designed to drive the Microfab JetLab IV printer. As mentioned previously in section 2.4, jetting parameters must be optimized to obtain a high resolution printing. A single droplet without any noise or satellite droplets gives a high quality finish. Once the drop generation process is completed, the optimized parameters can be saved as a file to use it in the future printings. However, these jetting parameters would often require minor alterations since the drop formation can be affected easily by the outside conditions, even though the cabinet is closed. Optimization of drop generation process for HP Instant Ink 67/305 is shown in Figure 3.5. The photos of droplet generation were taken at the real time when the pressure waveform at the right hand side were applied. While there is a satellite droplet formation in the images (a) to (d), an optimum droplet has been formed in (e) with the optimized voltage level and the durations of rise, dwell and fall. The volume of optimized droplet has been measured as 14 pL on average. The optimized parameters have been saved and used throughout the experimental process to stabilise the volume of ink.

It was observed that during printing process the humidity level needs to be kept above 50% to avoid evaporation of the printed ink. Due to the use of single piezoelectric printhead,

the printing process of one tensile coupon takes approximately 10 minutes with 140 pL ink per mm. Figure 3.6 shows the partially powder coating on top of the printed substrates. The evaporation starts from the areas that are first printed onto. As the humidity level increases gradually, the evaporation of the printed ink decreases, causing more powder to attach.

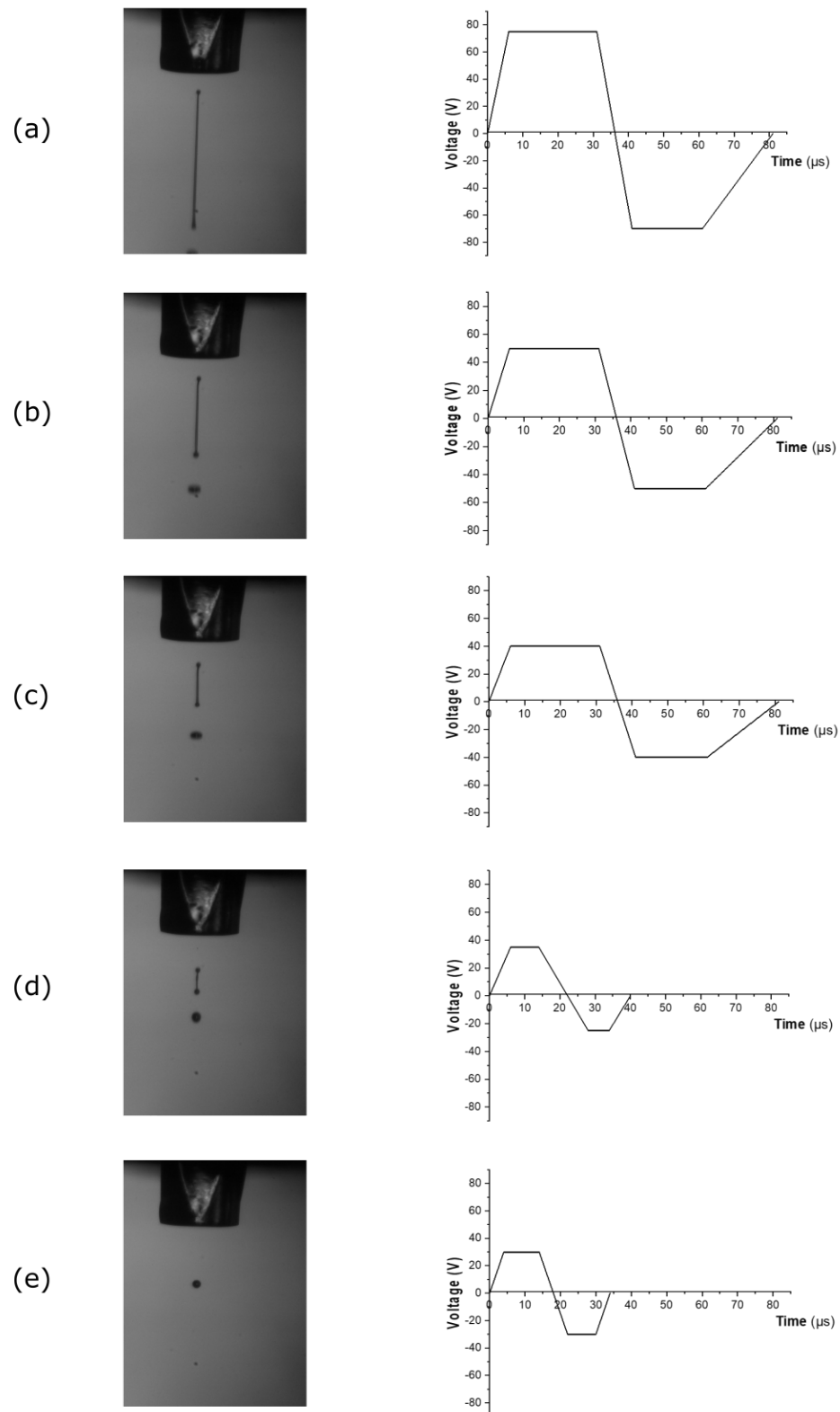


Fig. 3.5 Waveform optimization process for HP Instant Ink 67/305 in JetLab IV inkjet printer

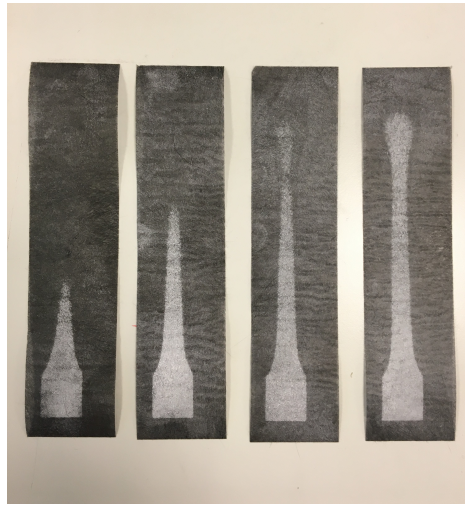


Fig. 3.6 Affect of humidity level for evaporation of ink in JetLab IV inkjet printer cabinet, humidity increases from left to right

HP Deskjet Plus 4130 All-in-One Printer

HP Deskjet printers are commonly used for research purposes especially in tissue engineering [105, 129] and sensor fabrication [130, 117]. It is easy to modify the hardware and the printheads specific to the applications. In this study, a HP Deskjet Plus 4130 drop-on-demand thermal inkjet printer has been utilised to be able to print in higher dots per inch (DPI) settings in a shorter time compared to the piezoelectric printhead. There was no modification needed in the system. The volume of droplet ejected from the printhead was 17.9 pL.



Fig. 3.7 HP Deskjet Plus 4130 drop-on-demand thermal inkjet printer

Surface treatment and contact angle measurements

Discontinuous carbon fibre fabric sheets used in this study have a high surface wettability and can absorb the printed ink which is undesirable in the CFAM technique. The ink is expected to hold a sufficient amount of powder on the surface, so the melted powder can bind the sheets. To decrease the wettability of the surface, an all purpose fabric protector spray was used effectively. Scotchgard™ Fabric Water Shield [131] supplied by 3M (Berkshire, United Kingdom) sprayed onto the substrates prior to the printing process in a fume cupboard, followed by a drying period up to 12 hours at room temperature. Unfortunately, there is no way to measure the amount of spray that has been applied on the fabric sheets since it is evaporated and does not make any difference in the weight of the sheet. However, the contact angle measurement, which is a way of analysing the interaction between the ink and the surface, can be used to understand if there is any considerable difference between the sheets that undergo surface treatment. JetLab jetting station was used to measure the contact angle of the HP ink on the carbon fibre substrates as shown in Figure 3.8.

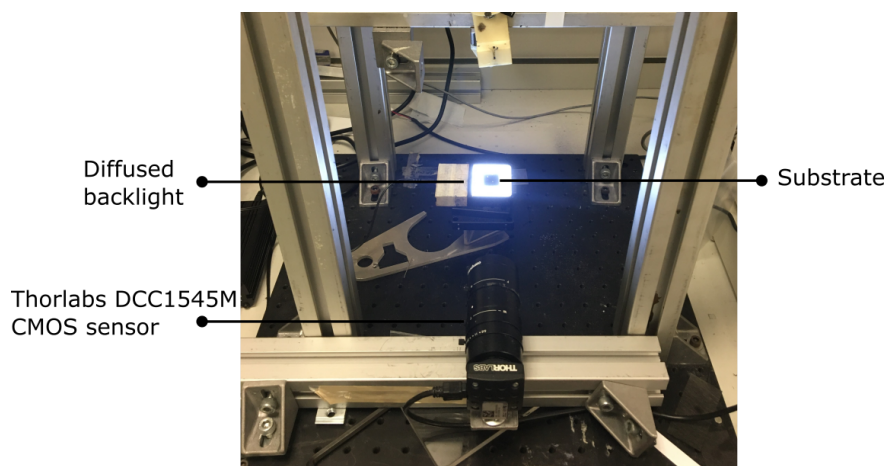


Fig. 3.8 Jetting station with the sensor used for contact angle measurements

The ink was dispensed using a micro-syringe, with a controlled back pressure supplied by a built-in vacuum pump. The droplet formed on the substrate was visualised with a Thorlabs DCC1545M CMOS sensor fitted with a zoom lens. Images were taken using The Thorcam software. ImageJ software pack FijiJ distribution was used to measure the contact angle by ellipse best-fit feature. Figure 3.9 shows the difference between the 2 hours and 12 hours drying periods after the surface treatment. The contact angle of the droplets were found as 6° and 112° for the un-sprayed and sprayed sheets respectively. While the carbon fibre sheet without any surface treatment has a small contact angle with the printed droplet, the sheet got exposed to the treatment has hydrophobic surface, which creates high contact angle.

Therefore, the powder can be deposited on the droplets with high resolution.

The ink behaviour on five different carbon fibre sheets that have been dried for 12 hours after the surface treatment have been also compared to understand the control over the volume of applied water shield spray. The difference between the contact angles was negligible, therefore it can be said that the surface treatment conditions are stable for the all carbon fibre sheets.

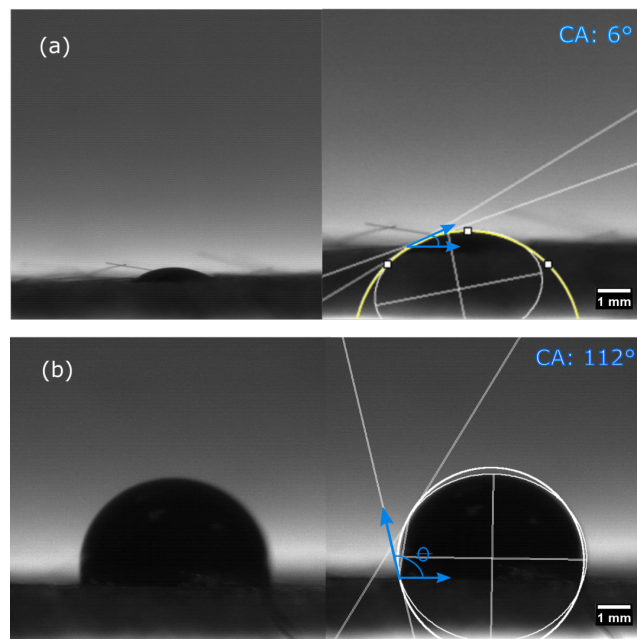


Fig. 3.9 Contact angle measurements (a) Surface treated substrate with 2 hours drying period, (b) Surface treated sample with 12 hours drying period

3.2.2 Deposition of Powder

After printing, the second operation is selective deposition of thermoplastic material in powder form. In this study, a Nylon-12 powder PA2200 with a melting point of 185 °C and an average grain size of 56 μm supplied by EOS GmbH was used. It was coated on the carbon fibre sheets with a stainless steel sieve in a fume cupboard. The excess dry powder was removed with a mild suction leaving behind the attached powder to the printed area. Powder must be deposited on the printed area before the ink gets dry or evaporated in order for it to adhere to the carbon fibre and result in a high resolution geometry. The fabric sheets printed with the same amount of ink were weighted to investigate if there is consistency

between the amount of powder that is accommodated on the surface. Three different dots per inch printing setting have been compared by weighing the samples printed with the same geometry. As the volume of ink increases, the volume of powder adhered to the printed area increases logarithmically as shown in Figure 3.10. Three different volumes of ink have been experimented as 140, 423 and 845 pL per mm defined by the droplet volume and DPI setting of the printheads as it will be explained in detail in Chapter 4. While a tensile dog bone printing (24 cm^2) with 140 pL per mm ink can accommodate 0.1 g ($\pm 0.003 \text{ g}$) polymer powder, the same specimen with 423 and 845 pL per mm ink hold 0.5 g ($\pm 0.012 \text{ g}$) and 0.7 g ($\pm 0.018 \text{ g}$) respectively. It has been concluded that the volume of ink determines the volume of polymer powder that can adhere to the surface of the fabric sheet. Small standard deviations show that the difference between the amount of powder that belongs to the same printing setting is negligible. Therefore the same volume of powder between the layers is ensured. However, the error level increases as the volume of ink rises. There is likely to be a more variation in powder volume on each layer with the higher DPI printing setting.

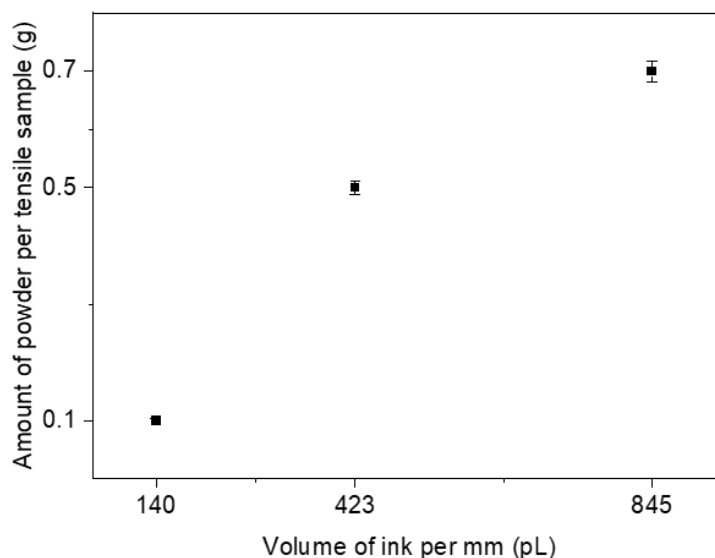


Fig. 3.10 The amount of powder that is adhered to the printed surface for each printing setting

3.2.3 Hot Press Process

A hydraulic hot press machine, which is shown in Figure 3.11, has been used to melt the nylon powder and compress the stacked layers together. A temperature of 210 °C, which is 30 °C above the melting temperature of polymer powder, was used to ensure the complete

melting. The size of the specimens need to be limited by the area of hot press, which is 190 x 170 mm. Teflon sheets are used between the substrate surface and the hot plates to prevent any adherence.



Fig. 3.11 Hydraulic hot press machine

The polyester binder in the fabric starts shrinking with the high heat, and melts. The microstructural investigation proved that the melted polyester is mixed with the semi-molten nylon polymer under pressure, which might contribute the internal porosity at a finished part, however the effect of this material on porosity and mechanical properties has been neglected in this study, since the material could not be detected in the microscopy and DSC investigations.

The hot press process is a critical step which has a significant effect on final part properties. Adding heat and pressure element to additively manufactured parts is possible with this operation, which makes the manufacturing process different than other AM techniques. Therefore, it is essential to make sure that there is a uniform temperature distribution and the controller is able to monitor the real time data.

A picolog has been used to measure the temperature in between the hotpress plates at specific locations as shown in Figure 3.12. To cover the whole surface area, 8 measurements along the X axis, repeating 8 times along the Y axis for 30 secs were taken. Four different target temperatures as 120, 140, 170 and 190 °C were defined since the polymer powder

melting and crystallization points are expected to be in this temperature region. Figure 3.13 shows the measurements taken from the 8 thermocouples. Each of the steps represent the each X axis line. It can be observed that the target temperature is likely to be reached in the centre of the hot press, whereas the error increases from the central thermocouple to the thermocouples at the edges.

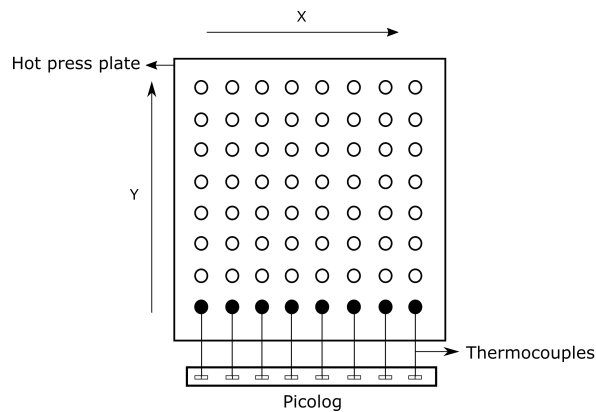


Fig. 3.12 Hydraulic hot press machine temperature verification with thermocouples

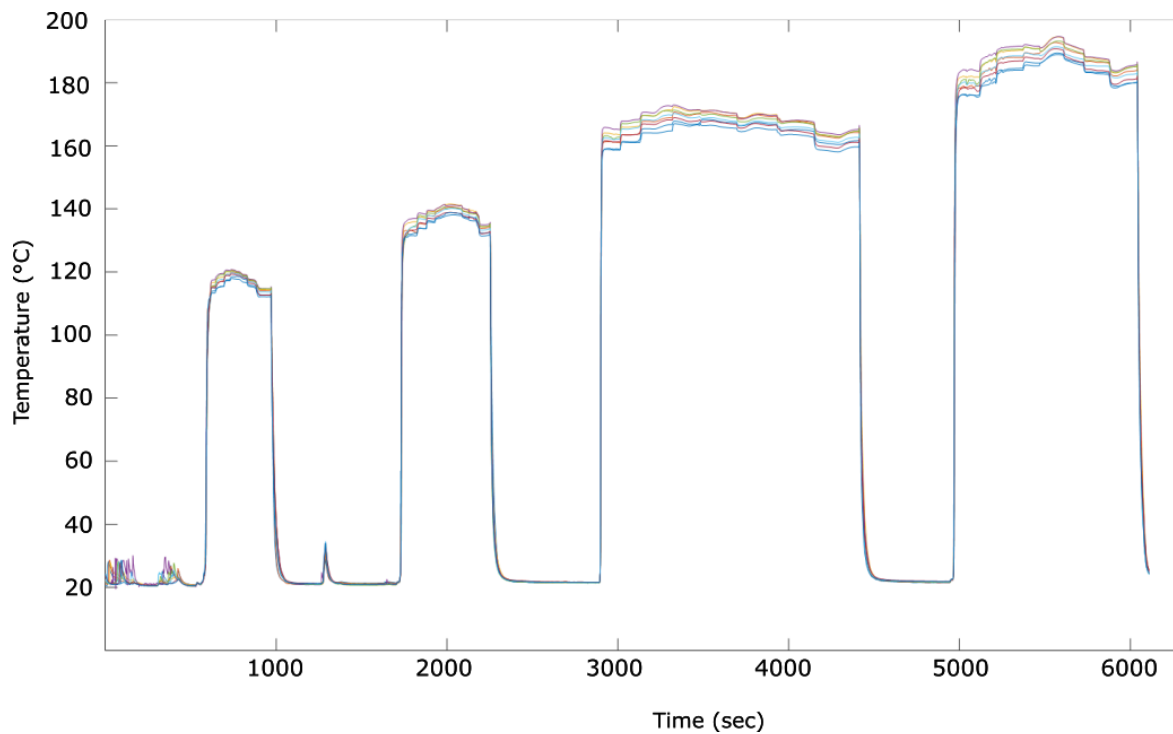


Fig. 3.13 Hydraulic hot press machine temperature verification with thermocouples

Data was processed using MatLab to investigate the average temperature and the deviation respect to the target. Figure 3.14 shows the temperature distribution along the surface of

hot press plate. It appears that the error slightly increases as the temperature rises. An approximately circular region in the centre of the plates reaches the target temperature and has a relatively uniform temperature distribution. 1-2% of error has been found in the centre, whereas at the edges the deviation was measured up to 6%. It can be concluded that the control temperature needs to be above the target temperature to ensure the complete and uniform melting. It is also recommended to use the central region of the hot press.

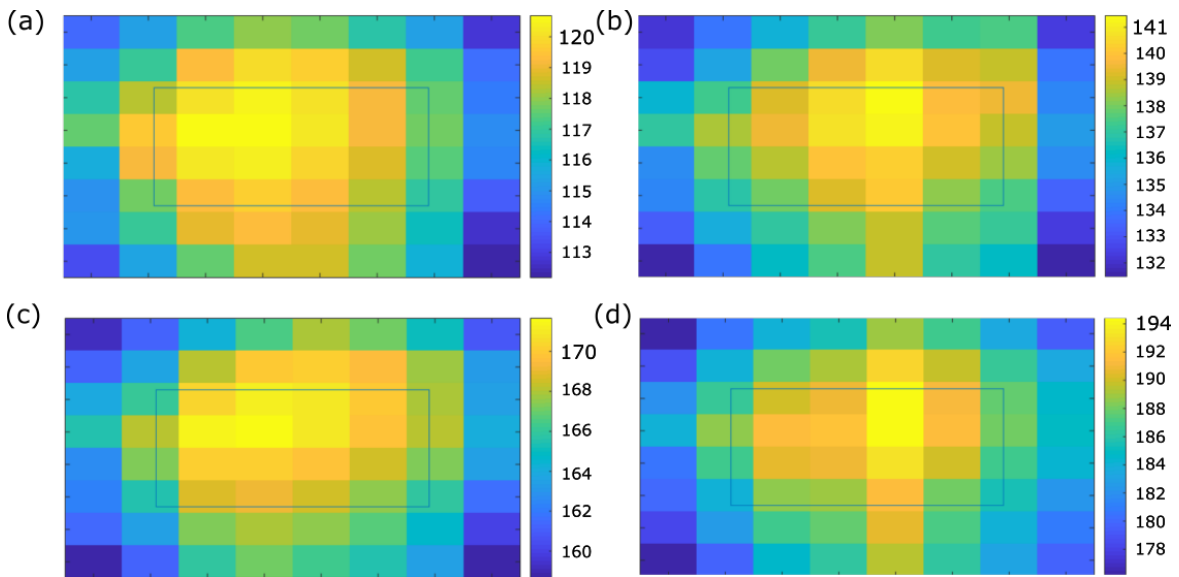


Fig. 3.14 Heatmap of a hydraulic hot press machine (a) 120°C, (b) 140°C, (c) 170°C, (d) 190°C

3.2.4 Sand Blasting Process

Abrasive blasting, commonly known as sand blasting or bead blasting, is a process where a stream of abrasive media used with a high pressure to clean or smooth a rough surface of a material. It is commonly used for postprocessing of additively manufactured parts made by FDM or powder bed processes [132, 133]. Polymer parts produced with SLS have small polymeric materials that remain on their surface, which can be removed by using glass beads. In this study, same approach was followed initially and a Guyson Euroblast 4 sandblaster with a media recovery unit has been utilised. Guyson 16 grade glass bead was used to remove the excess carbon fibre fabric. However, the glass bead media was not successful in removing the excess fibre if the thickness of the compressed laminate was higher than 2 mm. There was need for a stronger media that can remove the fabric sheets easily. Therefore, a blast media of brown alumina with low metallic iron content called Guyson Saftigrit Brown (Guyson International Ltd., Skipton, UK) was used. This type of media was able to remove

the unprinted fabric sheets in a very short time. 10x10 mm area can be removed in a second, without any damage on the surface of the part. Figure 3.15 shows the sand blasting machine used in this study.



Fig. 3.15 Guyson Euroblast 4 sand blasting machine

3.3 Characterisation

3.3.1 Differential Scanning Calorimetry (DSC)

The differential scanning calorimeter, Perkin Elmer DSC6, has been used to understand the thermal behaviour of nylon-12. First of all the samples with 6 mm diameter were punctured out of the laminates and weighted using a Mettler Toledo balance. Then they were placed in a sealed DSC pan (02190041, Perkin Elmer). The sealing is important for the polymer materials due to the expansion of material. An empty pan was used to create a baseline thermal curve before the analysis of the actual specimens. During the scanning, the temperature was raised from 30 °C to 210 °C with a rate of 10 °C per minute, followed by 5 minutes hold at the maximum temperature. The sample was then cooled back to room temperature at a cooling rate of 1 °C per minute, which mimics the melting and cooling rate of the hot press. The ramps were performed under a nitrogen purge of 50 mL/min. Pyris software was used to acquire the enthalpy of fusion by obtaining the integral of the area under the curve where the temperature is maximum (melting temperature). This data is used to calculate the degree of crystallinity as it will be demonstrated in Chapter 5.

3.3.2 X-Ray Computed Tomography (CT)

The specimens for the tomography were manufactured in a cylindrical shape of 5 mm in diameter with an average thickness of 1 mm. They were scanned using the Zeiss Xradia 620-Versa system. The scanning voltage was 70kV with an X-ray source power of 8.5 W, and the current was 108 μ A. Exposure time was 2.0 s per projection to obtain a pixel size of 1.5 μ m. The porosity and fibre volume fraction has been calculated using the Dragonfly and FEI Avizo 9 software with segmentation by the Otsu method [134]. After applying thresholding operations to extract the region of interest and contour meshes, the unrepresentative image slices and small defects (noise) can be removed. Parameters can be automatically calculated in the software. Dynamic colouring helps to visualise and the data such as volume, porosity, particle and void is given by statistics table. Figure 3.16 shows the stacked samples mounted on a pillar in the X-ray CT system.

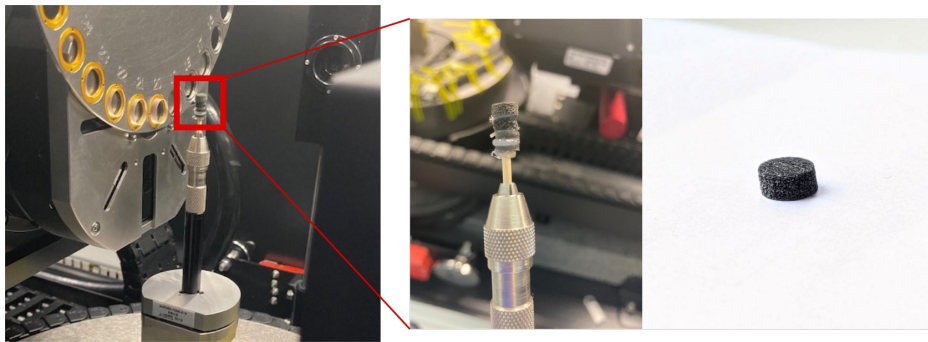


Fig. 3.16 Mounted samples to be scanned in X-ray CT system

3.3.3 Sample Preparation for Optical Microscopy

Samples were wet cut using a diamond saw machine. Cold mounting method was applied prior to grinding and polishing with a Buehler Automet Grinder-Polisher. P320, P600, P1200 and P2500 grit papers were used respectively for grinding process. 10 N force were applied for 40 seconds with a plate speed of 200 rpm and head speed of 60 rpm in complimentary head rotation direction. Then the samples were polished for 4 minutes using MEtaDi lubricant with the same parameters mentioned in grinding in contradirectional way. Lastly, the samples were cleaned by using MasterPrep polishing cloth with water for 2.5 minutes. Samples were used for optical microscopy that will be explained in the next section.

3.3.4 Optical Microscopy

To cross-check the porosity and fibre volume fraction calculations obtained from X-ray CT, optical microscopy was used. This technique is commonly used for microstructural analysis along with the Archimedes method. Previous studies show that the Archimedes method may not give accurate results [135]. Unconsolidated powder trapped inside pores may cause misleading of porosity calculations [136]. Therefore, optical microscopy was preferred for this study to be able to gain more information about the pore morphology.

A Nikon Eclipse ME600 Metallurgical Microscope was utilised for imaging. Cross section of the samples were investigated by using ImageJ software pack FijiJ distribution. Images were stitched to take advantage of the whole surface area. Stitched images were overlapped and cropped to the same size to make a consistent comparison. Same thresholding level was applied to all samples for examination of the fibre volume and porosity factions.

3.3.5 Scanning Electron Microscopy

Scanning electron microscopy (SEM) was used to analyse the void formation and shear failure modes in the samples. Tescan Vega3 LMU scanning electron microscope in the facilities of BioMedical Sciences at University of Sheffield has been utilised. Beam intensity was adjusted to 5 kV to obtain high resolution images at a distance of 12 mm under three different magnification (x100,x200 and x500).

3.3.6 Tensile Testing

Tensile specimens have been manufactured in dog-bone shapes according to the BS EN ISO 527-4:1997 Standards Type 1B specimen [137] The dimensions are presented in Figure 3.17. Tensile tests have been performed utilising a Zwick tensometer 2020 Proline with a video extensometer (see Figure 3.18) and Tinius Olsen H5K5. Specimens were tested at a crosshead speed of 2 mm/minute.

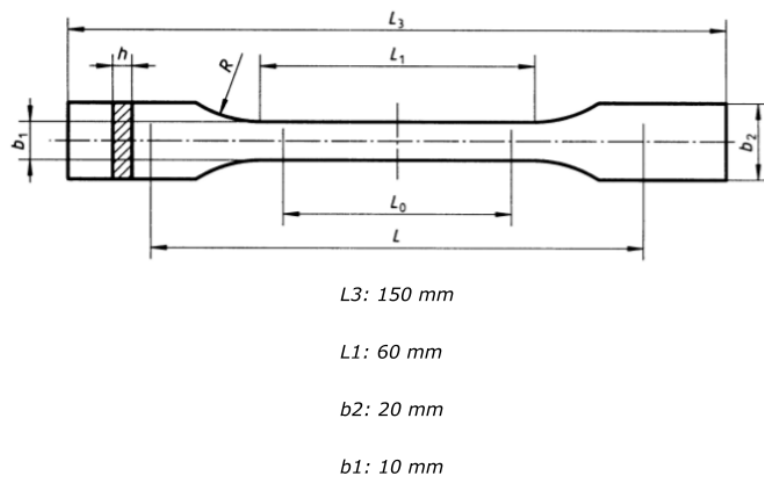


Fig. 3.17 BS EN ISO 527-4 standards-Type 1B specimen

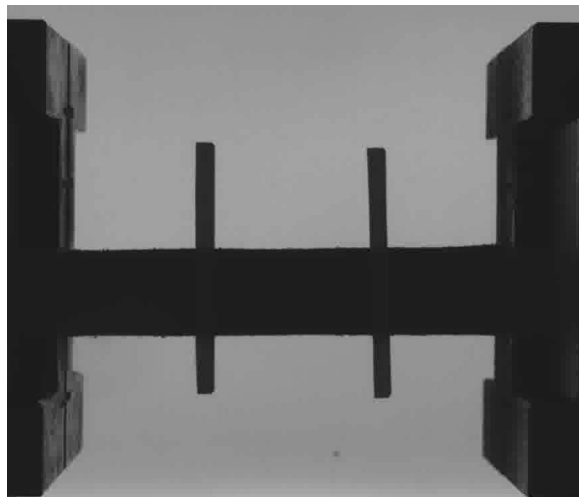


Fig. 3.18 Zwick Tensometer 2020 Proline with a video extensometer

3.3.7 Flexural Testing

The flexural specimens have been manufactured according to ASTM D7264 standard for three point bending test as 168 x 13 x 4 mm rectangles [138]. The thickness of the samples was varied depending on the process parameters, however, the 32:1 support span- to-thickness ratio kept constant. Flexural tests have been performed using a Zwick tensometer 2020 Proline with a crosshead speed of 1 mm/minute and Tinius Olsen H5K5. Figure 3.19 shows the dimensions of flexural specimens that were produced with CFAM process alongside a photo of the tensometer during testing.

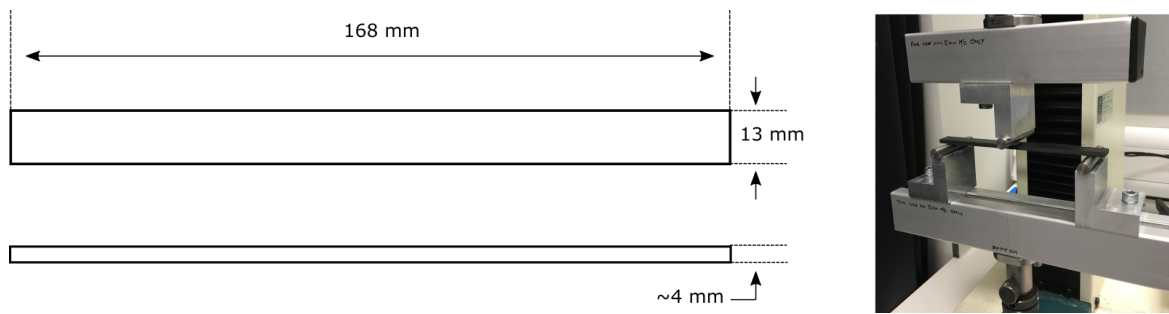


Fig. 3.19 Standard flexural test specimen and flexural test setup

3.3.8 Short Beam Shear Test

Short beam shear (SBS) tests have been performed according to the BS EN ISO 14130:1998 standard [139] to calculate the apparent interlaminar shear strength (ILSS) of carbon fibre reinforced polymer parts made by CFAM process. Test samples were cut in different directions from a laminate using a ProtoMAX abrasive waterjet system (Washington, USA), followed by polishing with 600 grade SiC sand paper to remove the free edge effects. The samples have been then dried for 12 hours. The dimensions of SBS test specimens and the test setup using H5K5 Tinius Olsen are shown in Figure 3.20. The speed of cross head of SBS tests was set as 1 mm/min similar to flexural testing. The distance between two supporters was 10 mm, the span/thickness ratio was 5 which is recommended by the SBS test standard to encourage the shear failure.

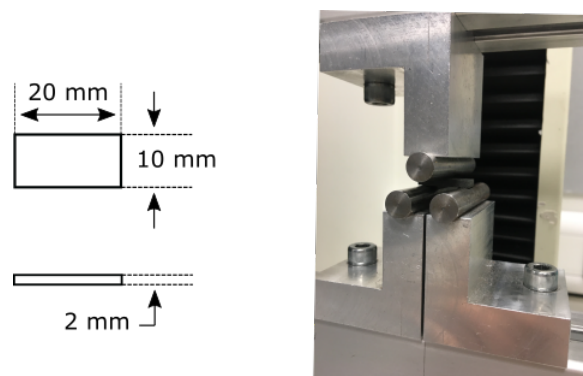


Fig. 3.20 Standard flexural test specimen and flexural test setup

Chapter 4

Optimization of CFAM Process Parameters

Summary

This chapter presents the optimization process for CFAM process parameters. First of all, the importance of manufacturing process optimization is discussed. Design of experiments (DOE) techniques such as full factorial design, Taguchi analysis, and ANOVA are presented and evaluated. Studies that used these DOE techniques to optimize the AM processes are reviewed.

Secondly, the critical process factors and their parameters for the CFAM process are established, which are pressure level, compaction time, and the volume of printed ink per mm. Taguchi orthogonal design is presented to create a combination of different experimental conditions. The effect of process parameters on the final part properties is investigated.

Finally, the results of Taguchi analysis and ANOVA are presented and the relation between the process parameters and output is discussed. The chapter is concluded with the comparison of mechanical and microstructural properties of CFAM and those of current composite AM processes producing CFRP composites.

This chapter is published: B. Karaş, P. J. Smith, J. P. A. Fairclough, and K. Mumtaz, "Additive manufacturing of high density carbon fibre reinforced polymer composites," Additive Manufacturing, vol. 58, p. 103044, 2022, doi: <https://doi.org/10.1016/j.addma.2022.103044>.

4.1 Introduction

Manufacturing processes have their own unique process parameters that affect the final part quality in terms of mechanical and microstructural properties. It is essential to understand the relation between these factors and the outputs especially in a newly established process in order to obtain maximum efficiency. There are many combinations of factors and their levels, therefore it is difficult to determine the most impactful parameters without a systematic approach [140]. When the cost of fabrication and part characterization techniques is also considered, statistical tools and design of experiments (DOE) techniques are important to reduce the waste that results from an optimization process [141].

Taguchi analysis is one of the DOE methods that allows the researcher to find the influential factors for a process with reduced number of experiments. While a full factorial design would have to test all possible combinations, using Taguchi one can reach the conclusion by saving time and resources [142, 69]. Taguchi analysis has 3 main objectives which are; determination of the “main effects” of each factor to find out their influence, investigation of factor levels that give the best result, and finally evaluation of contributions made by each factor to the output. The last objective is performed with Analysis of Variance (ANOVA), which is a statistical tool to inspect the significance of the factors [143, 144].

Additive manufacturing processes include innovative and advanced methods, hence achieving a quality standard with reliability in the final possess a challenge [145]. To improve the built part properties, optimization of process parameters is typically performed for many AM processes. Recent research demonstrated the benefit of using Taguchi analysis together with ANOVA. FDM printing parameters such as layer thickness, orientation angle and filling pattern were investigated by using Taguchi analysis and ANOVA with the aim of improving the dimensional accuracy [146]. Five different factors and their parameters were successfully optimized by analysing only 27 experiments with Taguchi analysis, and the best trade-off among the factors was established. Wankhede et al. used this statistical analysis method to investigate the effect of FDM process parameters on the surface roughness and build time of the final parts. Only 8 experimental combination was sufficient to obtain the best parameter levels [147]. Zhu et al. improved the surface characteristics and reduced the porosity of High Speed Sintering (HSS) parts by optimizing the HSS process parameters using Taguchi analysis. Orthogonal design of L9 was efficiently used to analyse the relationship between the outputs and a variety of process factors [61].

Sheet lamination process parameters have not been investigated previously due to the novelty of this manufacturing technique. Thus, the traditional composite manufacturing was taken as a reference to determine the critical process parameters. Hot press process is the primary element of this manufacturing technique, bringing the heat and pressure application to AM with the aim of reducing porosity and improving the mechanical properties. Aligned with this idea, investigation of the effects of autoclave process factors such as pressure and curing time on microstructural and mechanical properties of CFRP composites is widely carried out in the literature. It has been observed that the optimum amount of pressure and vacuum application time improved the mechanical properties significantly [148, 120, 122]. Kiran et al. used the Taguchi technique to investigate the hot press forming process parameters on tensile, flexural, and impact properties of green composites. Heating time, temperature, and pressure were among the chosen factors. The effect of pressure and heating time were found to be significant on tensile and flexural properties, while the cooling time had a significant effect on impact properties. Kumar et al. also found that processing temperature, compaction time and mould pressure influenced the flexural properties of composites significantly [149]. Another research showed similar findings for tensile properties of SiC whisker Al composites [150]. Results from both studies showed that the mechanical properties of composites improve as the pressure level increases up until a threshold point where the high pressure starts to damage the fibres. Processing temperature has not been considered in this study as a parameter since the melting and crystallization temperature of the polymer powder are constant even though the heat goes higher. Therefore, the polymer morphology would not be affected.

Inkjet printing is another essential step that has influence on matrix properties. The ink volume determines the volume of powder that can be coated on a printed layer. The resolution of a desired geometry and adhesion of the layers can be affected by printing parameters. Rahul et al. investigated the inkjet printing parameters to fabricate ceramic coatings with optimized layer thickness. The parameters involved ink content, substrate temperature and nozzle open time [151]. Similarly, the thickness of printed films was used as output in an experimental design where the factors were chosen as drop spacing and ink concentration. The authors found that the thickness of the film can be predicted successfully by the model considering the ink concentration, contact angle and droplet spacing [152]. In the CFAM process, the thickness of the printed ink does not need to be very precise since it is supposed to act only as a binder. Therefore, the volume of the ink is regarded to be a sufficient criterion to benchmark the process.

CFAM process factors that are potentially influential on the mechanical properties are explained in detail in the next section.

4.2 Design of Experiments

4.2.1 Process parameters

Based on the literature review and observations made during the development of CFAM process, three factors have been chosen: pressure level, compaction time, and ink areal density.

Ink areal density: The amount of ink per m^2 that is printed onto the carbon fibre sheet. This parameter value can be determined using the volume of the ink droplet ejected from the printhead and dots per inch (DPI) setting of the printer. To calculate the total volume of ink printed per m^2 , one can multiply the volume of ink per droplet and the DPI setting of the printer as shown in Equation 4.1 and Equation 4.2. Thus the printed ink volume can be varied by changing the DPI setting of the printer. The droplet ejected from the printhead has a volume of 17.9 pL for HP Deskjet 4100 as reported by the company, while it is 14 pL for the JetLab IV system, which was measured in ImageJ by capturing an image of the droplet with the camera. The lowest volume of ink has been possible to print by using JetLab IV since the system gives more flexibility. The parameter levels are determined as 24, 223 and 892 g/m^2 due to the printer settings of 254, 600 and 1200 DPI respectively.

$$\text{Volume of ink per mm (pL)} = \frac{\text{Droplet volume (pL)} \times \text{DPI}}{25.4 \text{ mm}} \quad (4.1)$$

$$\text{Ink areal density} = \text{Volume of ink per mm (pL)}^2 \times \text{Ink density} \quad (4.2)$$

Pressure level: The pressure applied on the stacked carbon fibre layers to form a compact part bonded with melted nylon powder. Due to the limitation of sensitive control over the hot press and the size of the test specimens, factor levels have been chosen as 0.3, 0.6 and 0.9 MPa in this study. Autoclave pressures between 0.3-0.6 MPa have been reported in [120, 153] as well. It has been found that the final part width expands if a higher pressure than 0.9 MPa is applied due to squeezing the melted powder out of the printed region. Therefore, 0.9 MPa

was the highest pressure level that can be applied. Section 4.4.1 gives more information about the results of applying higher pressure than 0.9 MPa.

Compaction time: The amount of time the part is kept under pressure during the dwell period. Factor levels have been chosen as 0.5, 1 and 2 hours.

Table 4.1 shows three process parameters with three levels as low, medium, and high levels.

Table 4.1 Process parameters with three levels

Input parameter	Level-1	Level-2	Level-3
A=Pressure (MPa)	0.3	0.6	0.9
B=Compaction time (h)	0.5	1	2
C=Ink areal density (g/m^2)	24	223	892

4.2.2 Taguchi analysis

L9 orthogonal array is used as there are three factors with three different levels; low, medium and high. Table 4.2 shows the experiment sets with the chosen parameter levels.

4.3 Results

4.3.1 DSC analysis

The DSC curve related to Nylon 12 (EOS GmbH) is shown in Figure 4.1. This experiment focused on the melting and crystallisation temperature of polymer powder to understand when the removal of the specimen from the hot press equipment is safe. If the sample is removed earlier than the crystallisation time, carbon fibre layers will delaminate since the polymer molecular chains cannot be aligned and work as a binder. In this case, the crystallisation temperature range of Nylon 12 has been found to be 160-165 °C as it can be seen from the exothermic peak at the cooling DSC graph. Therefore, samples placed in the hot press, have been heated up to 210 °C (30 °C more than the melting temperature found from the endothermic peak at the melting DSC graph) to make sure the powder was melted

Table 4.2 Taguchi L9 orthogonal array for the design of experiments

Experiment Set	Pressure (MPa)	Compaction Time (h)	Ink areal density (g/m^2)
1	0.3	0.5	892
2	0.3	1	223
3	0.3	2	24
4	0.6	0.5	223
5	0.6	1	24
6	0.6	2	892
7	0.9	0.5	24
8	0.9	1	892
9	0.9	2	223

entirely, and they were removed from the hot press when they were cooled down to 40 °C for health and safety reasons.

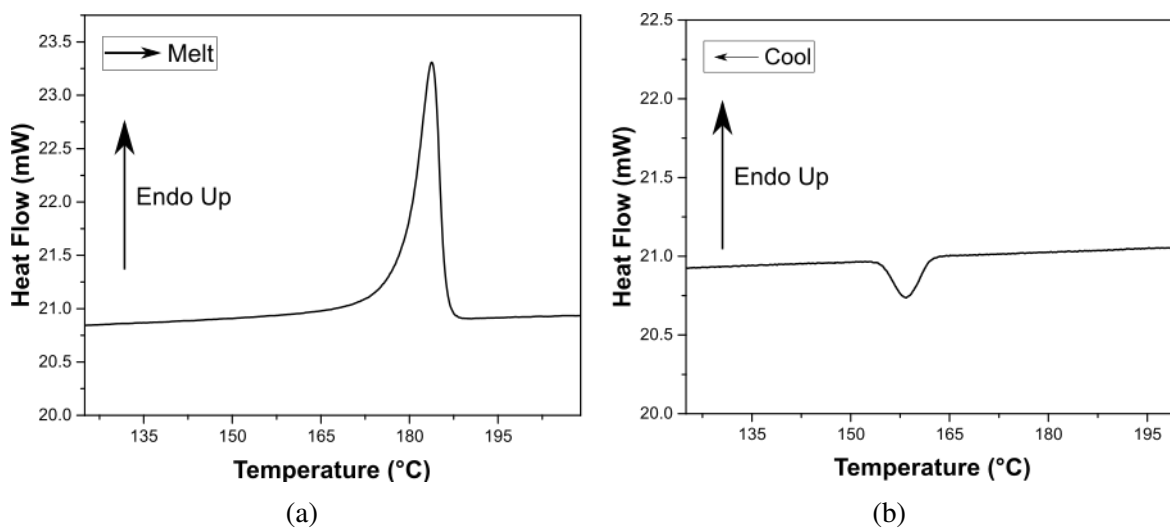


Fig. 4.1 DSC Analysis of raw CF/Nylon 12 (1.2 mg) specimen

4.3.2 X-ray CT and optical microscopy

High-resolution X-ray tomography is a non-destructive characterisation technique to understand the volumetric content of the parts. Many researchers used this technique to successfully determine the porosity and fibre content in composites [154–157]. In alignment with the literature, percentages of porosity and carbon fibre volume fraction (FVF) calculated by the segmentation method for each sample are shown in Table 4.3. Each sample has been fabricated with the same number of layers. Higher process pressure resulted in the end part being thinner and formed with better consolidation.

X-ray CT images from low, medium and high pressure levels are shown in Figure 4.2. Images on the left side present the top view of the cylinder part, while the images on the right show the cross-sectional view. The layer by layer structure cannot be observed due to consolidation and random alignment of the fibres. It can be seen that large voids occurred when low pressure of 0.3 MPa has been applied to the component. Increasing the pressure has been correlated with a decrease in void size.

Table 4.3 Porosity and fibre volume fraction of the samples for each experiment set

Set Number	Pressure (MPa)	Compaction Time (h)	Ink areal density	Porosity (%)	FVF (%)
1	0.3	0.5	892	15.01	8.15
2	0.3	1	223	12.09	11.04
3	0.3	2	24	9.39	10.77
4	0.6	0.5	223	4.19	12.8
5	0.6	1	24	4.65	13.75
6	0.6	2	892	5.16	11.12
7	0.9	0.5	24	2.72	16.1
8	0.9	1	892	7.12	14.34
9	0.9	2	223	1.52	15.16

Figure 4.3 shows the 3D pore distribution for the Sets 1, 4, 6 and 9 respectively. The thickness of the specimens decreases as the pressure level increases from a to d. There are pores up to 0.08 mm^3 for the Set 1 specimen that is produced with a 0.3 MPa pressure level. The maximum pore size is reduced to 0.03 mm^3 with the increase in pressure level to 0.6 MPa in Figure 4.3(b) and 4.3(c) representing Set 4 and 6 respectively. The big pores are more frequent in Set 6, compared to Set 4, even though they have been manufactured with the

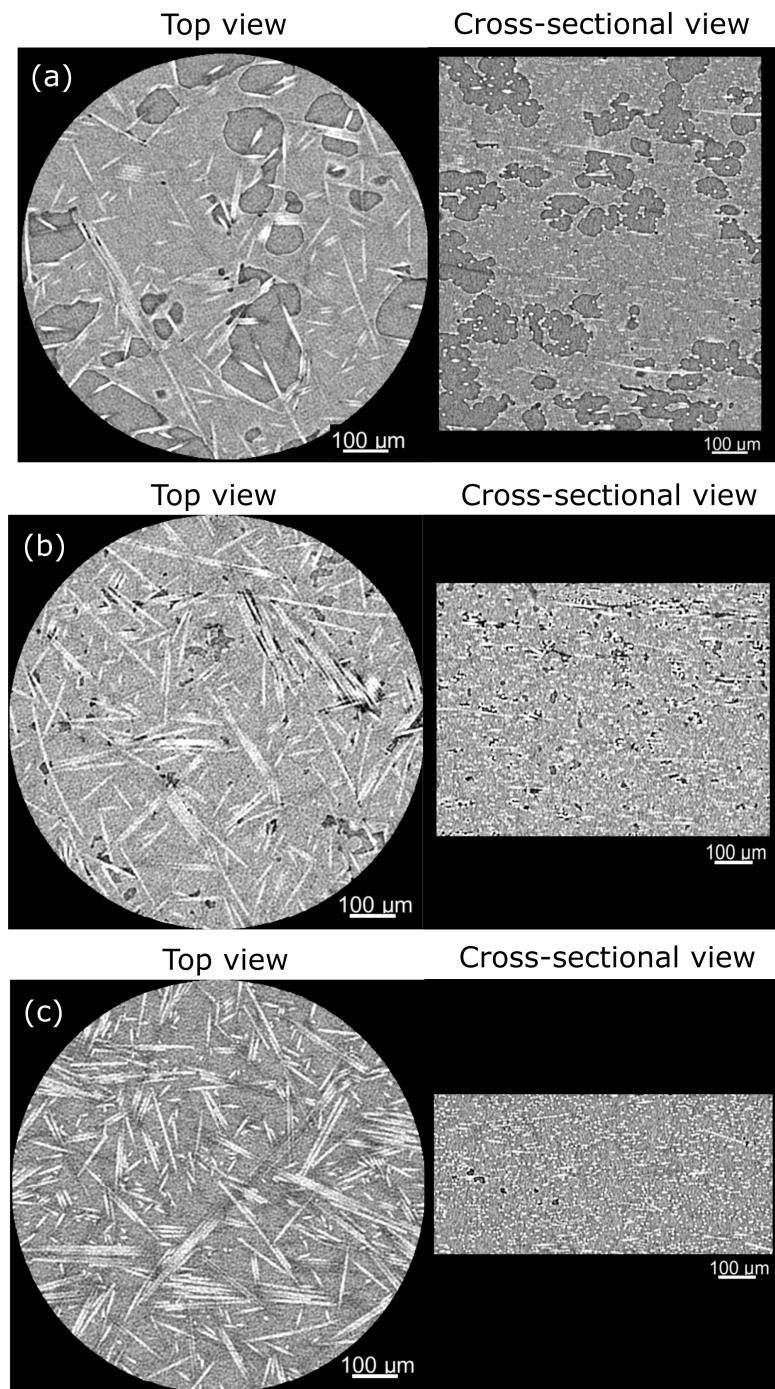


Fig. 4.2 X-ray CT images of different pressure settings; (a) Void content at low pressure level (0.3 MPa) (Set2) – Porosity: 12.09%, (b) Void content at medium pressure level (0.6 MPa) (Set4) – Porosity: 4.19%, (c) Void content at high pressure level (0.9 MPa) (Set9) – Porosity: 1.52% Tensile properties of each experimental set

same pressure level. The difference in pore density might be originated from the different compaction times or volume of ink. The combination of both can be also the reason. Set 6 has a higher amount of ink, hence more polymer powder in between the sheets, yet it has a high number of big pores. Set 4 was produced with a shorter compaction time. The origin of the difference in microstructure can be understood from the Taguchi analysis, revealing the significance of the factors. Set 9 presented in Figure 4.3(d) has little number of small pores due to the pressure level of 0.9 MPa.

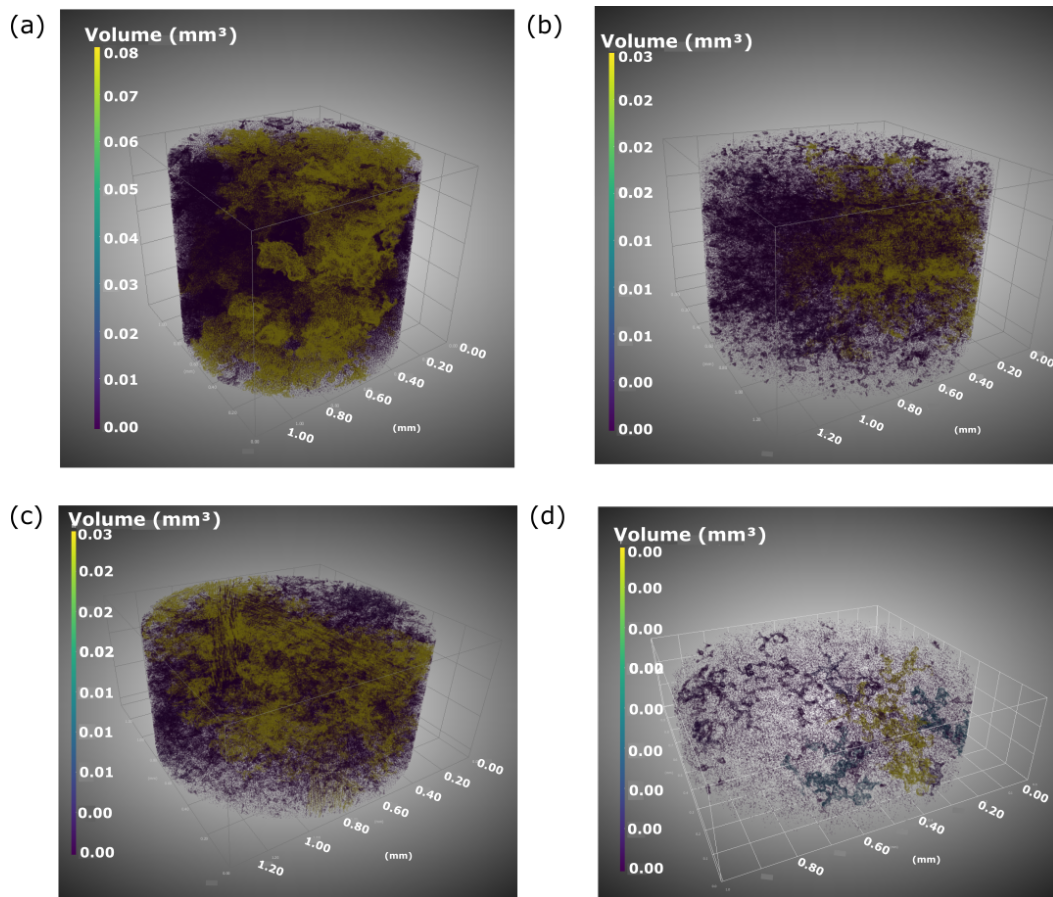


Fig. 4.3 3D porosity distribution in X-ray CT with the pore segmentation; (a) Set 1, (b) Set 4, (c) Set 6, (d) Set 9

The porosity and fibre volume fraction calculations have been cross-checked with optical microscopy measurements. 4 samples have been manufactured using the parameters of Sets 2, 4, 6 and 9 from Table 4.3. These sets have been selected in order to analyse the difference between the pressure levels. Sets 4 and 6 are also compared to confirm the difference occurred in X-ray CT results. The results are consistent with the X-ray CT results. 1.59% porosity was found in the sample manufactured with Set 9 parameters, which is aligned with the

1.52% obtained from X-ray CT for the same experimental conditions. Fibre volume fraction has been measured as 15.89% for the same sample, which is also aligned with the value determined from the X-ray CT scan of 15.6%. Figure 4.4 shows the optical microscopy images. The white coloured dots are fibres and they are surrounded by polymer matrix which is the grey area, while the dark regions are the pores. Thresholding can be seen from 4.4-a which was applied to the stitched image presented in 4.4-b. Figure 4.4(c) is one of the stitched images with a high magnification for the sample that has the lowest porosity (Set 9). Figure 4.4(d) and (e) show the samples from 0.6 MPa and 0.3 MPa respectively. The amount of porosity was measured as 6.3% (Set 4) and 14.5% (Set2) using the stitched images, while the X-ray CT samples produced with the same experimental conditions has a porosity level of 5.16% and 12% respectively. The difference between the X-ray CT and optical microscopy might be because of X-ray CT missing some of the features due to the pixel size.

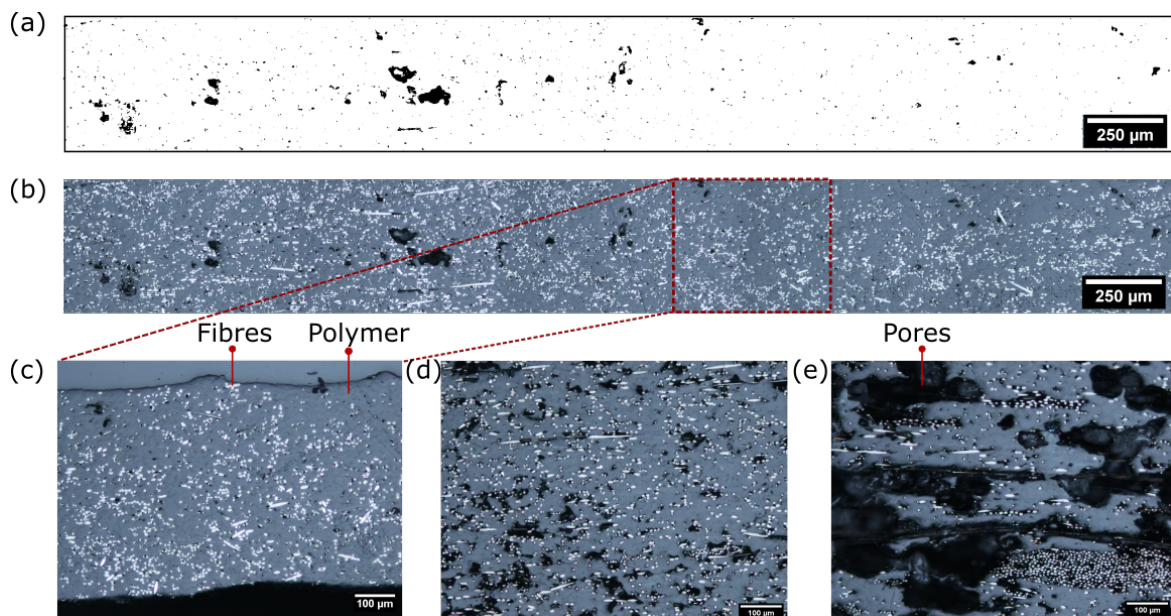


Fig. 4.4 Optical microscopy images; (a) Thresholded stitched images of Set 9 sample (0.9 MPa), (b) Actual stitched images of Set 9 sample (0.9 MPa), (c) Set 9 sample, (d) Set 6 sample, (e) Set 2 sample

Moreover, the difference between the porosity content of Set 4 and Set 6 samples was investigated with optical microscopy. It has been confirmed that Set 6 has more porosity level (10%) than Set 4 (6.3%), in agreement with the results obtained in X-ray CT analysis. The difference between the pores was investigated and it has been observed that the pores are more uniformly scattered in Set 6, while Set 4 shows localized pore formation. This supports the argument that ink volume, consequently the volume of polymer matrix between the sheets, has an effect on pore formation.

Finally, Figure 4.5 shows the images taken using SEM to visualize the pores. While the fibers of the Set 9 sample produced under high pressure are supported with the matrix material without any void, the melted polymer is not united in the Set 1 sample. The molten polymer cannot be conveyed to all regions on the surface of the fibre sheet due to the lack of sufficient pressure.

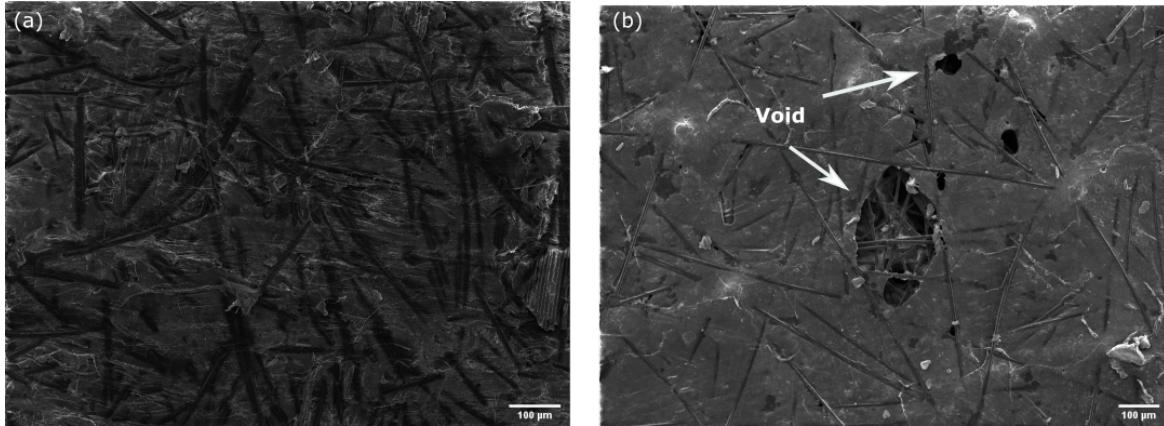


Fig. 4.5 SEM images to investigate the voids (a) Set 9 sample top view (b) Set 1 sample top view

4.3.3 Mechanical testing

As it is mentioned in Chapter 3, mechanical testing, including tensile and flexural tests, have been performed to investigate the strength and stiffness of the final parts according to the BS EN ISO 527-4:1997 and ASTM D7264 standards respectively. The reason for following the British Standards for tensile test experiment is its suitability to the chopped carbon fibre reinforced polymer parts. Since there is no unidirectional fibre in the parts, end tabs are not need to be used for tensile testing grips. Figure 4.6-a shows the 2D slice of printed geometry on one carbon fibre substrate. To achieve the average thickness of 2 mm, 40 layers of carbon fibre fabric have been printed and stacked layer by layer. Figure 4.6-b shows the compressed part after the hot press process, while Figure 4.6-c shows the part during sandblasting process. Finally, Figure 4.6-d shows the final cleaned parts. The manufacturing steps of flexural test samples are also given in Figure 4.7. Figure 4.7-a also shows the rig that was used for alignment. 2 points have been sufficient to align the flexural samples since the geometrical tolerance is not crucial for the purpose of this test.

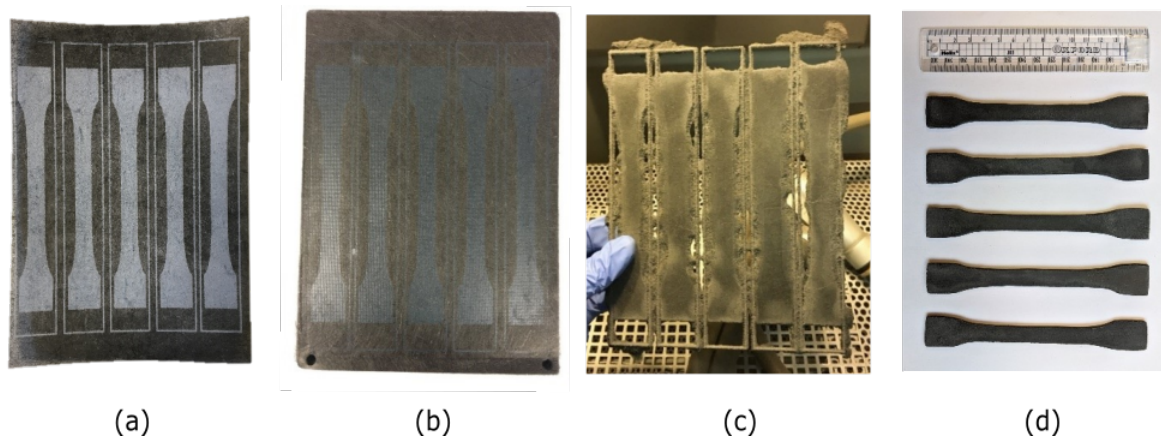


Fig. 4.6 Stages of manufacturing process (a) carbon fibre sheet after printing and deposition of powder; (b) stacked carbon fibre layers after hot press process; (c) sandblasting process halfway through; (d) final dog bone samples

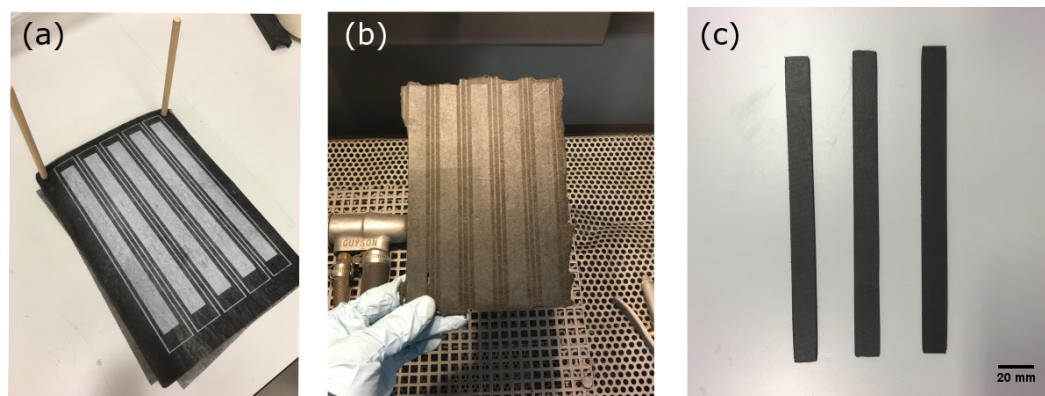


Fig. 4.7 Stages of manufacturing of flexural testing samples (a) stacked and aligned carbon fibre sheets after printing and deposition of powder; (b) sandblasting process halfway through; (c) final flexural test samples

Figure 4.8 shows the stress strain graphs for both tensile and flexural testing for different pressure levels since it is dominantly significant factor for both properties. A considerable improvement can be observed as the pressure level increases from 0.3 MPa to 0.9 MPa. Set 2,4 and 9 have been chosen for comparison since they have the same parameter levels of compaction time and volume of ink. High pressure samples shows a brittle behaviour, whereas the low pressure samples have better ductility. The samples produced with low pressure level can be plastically deformed without fracture for a longer period of time, which shows that the fibres are not consolidated enough to reinforce the polymer and add brittleness to the material, whereas the high pressure samples show brittle behavior without significant plastic deformation.

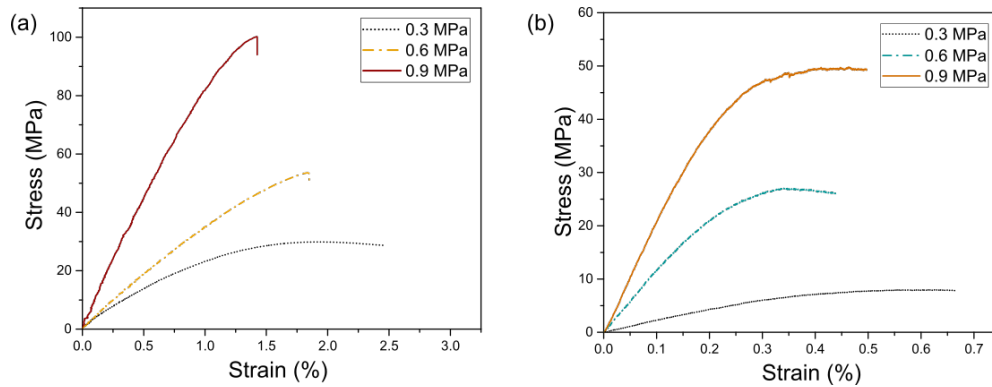


Fig. 4.8 (a) Tensile and (b) flexural test results for low, medium and high pressure levels (Set 2, 4 and 9, respectively)

The results of the tensile tests of all samples are shown in Figure 4.9. The error bars demonstrate the standard deviation of five composite samples from each experimental set. The maximum average tensile strength and stiffness have been determined to be 97 MPa ($\pm 1.79\%$) and 8.9 GPa ($\pm 1.49\%$), respectively, for a sample that has a 15% fibre volume fraction. The flexural properties of each experimental set are shown in Figure 4.10 with the error bars representing the standard deviation of five repeats. The maximum average flexural strength and stiffness were found to be 42.4 MPa ($\pm 5\%$) and 12.7 GPa ($\pm 2\%$), belonging to the same experimental condition (set 9) with the sample that has the maximum tensile properties. An improvement in both mechanical properties can be observed as the pressure increases from experimental set 1-2-3, to set 4-5-6 and lastly to set 7-8-9. The difference between the sets belonging to the same pressure level is not very significant. However, this fluctuation increases as the pressure is at the maximum level in sets 7, 8 and 9, suggesting that other process parameters have secondary effects on the mechanical strength of the parts. The tensile and flexural failure of the samples can be seen in Appendix A.

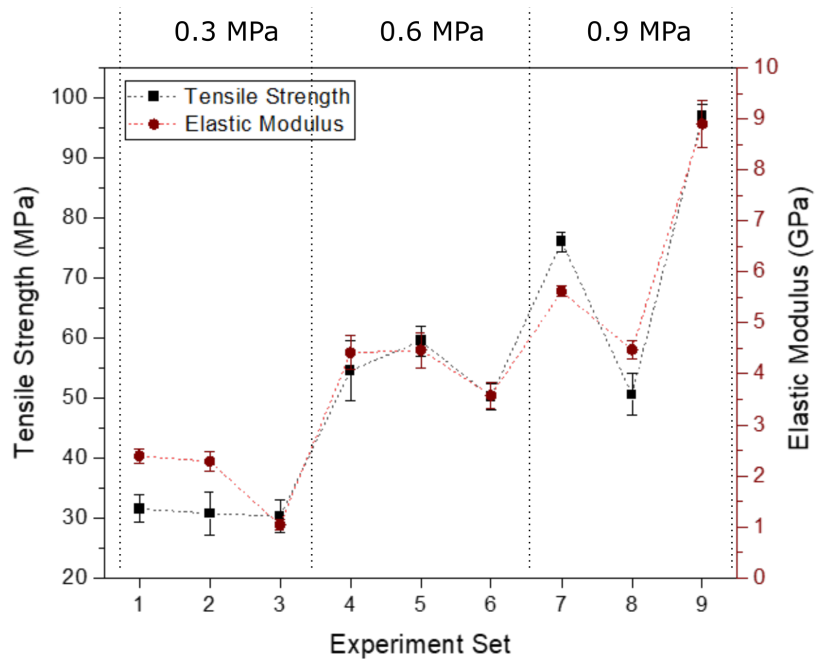


Fig. 4.9 Tensile properties of each experimental set

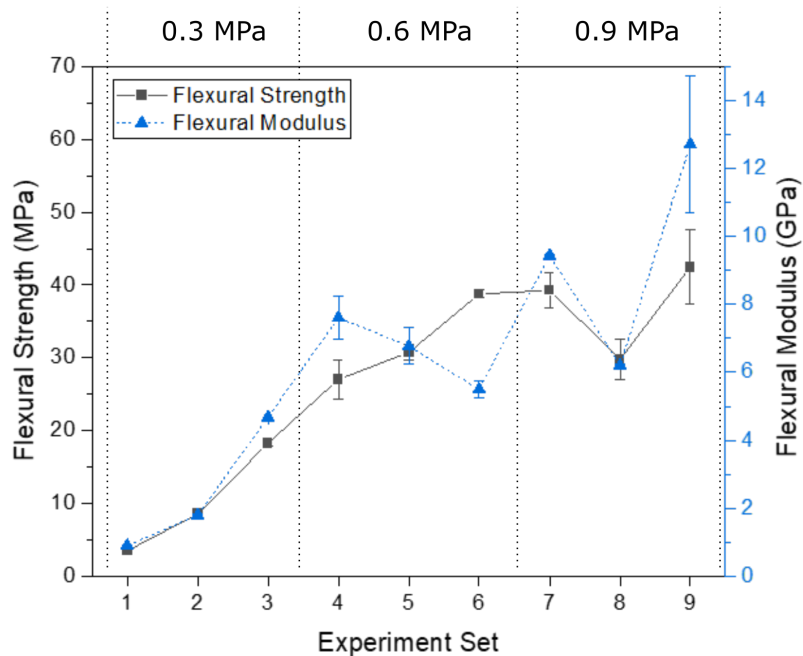


Fig. 4.10 Flexural properties of each experimental set

4.3.4 Taguchi analysis

The taguchi design has been analysed using Minitab 18 to determine the optimum parameter levels. Analysis of variance has been undertaken using R software. Table 4.4 shows the analysis of variance (ANOVA) table for the tensile strength outputs. All three factors have been found to be significantly influential since they are lower than 0.05 (95% confidence interval). The most significant factor that affects the tensile properties of the samples has been found to be the amount of pressure with the lowest p-value ($p=4.85E-15$) and the highest contribution (70%). Ink areal density has been determined to be the second significant factor with 10% contribution. Compaction time has been found to be the least significant factor for tensile strength in this experiment with 7% contribution.

Table 4.5 shows that pressure once again the most impactful factor with almost 80% contribution for improved flexural strength. Compaction time is the second most significant factor affecting the flexural strength with 13.4% contribution, unlike the effect of it on tensile strength. Volume of ink per mm was the least significant factor with 2.7% contribution.

Figure 4.11 shows the main effects plots for tensile properties. The highest level of pressure (0.9 MPa) gives the maximum tensile strength and elastic modulus. A logarithmic growth from 0.3 MPa to 0.9 MPa indicates that 0.9 MPa might be the parameter level that gives the maximum tensile strength, or the further increase is not going to make so much difference. 223 g/m^2 ink (medium level) has been found to be the optimum factor level generating the maximum tensile strength and stiffness, while the medium level of compaction time is worse than the other parameter levels. In the case of flexural strength output, the pressure level and compaction time parameter levels follow a similar trend as observed in main effect plot of tensile strength. However 24 g/m^2 ink gives the best flexural strength, while 223 g/m^2 gives the best flexural modulus. Since the contribution of this factor is very little compared to the other factors, the difference between the effects is accepted as negligible. The high amount of ink results in the lowest strength and stiffness for both tensile and flexural properties.

Table 4.4 ANOVA for tensile strength

	Degree of Freedom	Sum of Square	Mean Square	F-value	P-value	Contribution
A=Pressure	2	13780.7	6890.4	97.57	4.85E-15	69.7%
B=Compaction time	2	1398.9	699.4	9.90	0.00039	7%
C=Ink areal density	2	2099.1	1049.5	14.86	2.13E-05	10.6%
Residuals	35	2471.6	70.6			

Table 4.5 ANOVA for flexural strength

	Degree of Freedom	Sum of Square	Mean Square	F-value	P-value	Contribution
A=Pressure	2	6113.6	3056.80	329.755	<2.2e-16	79.5%
B=Compaction time	2	1029.6	514.79	55.53	9,958e-12	13.4%
C=Ink areal density	2	209.9	104.93	11.320	0.00015	2.73%
Residuals	36	333.7	9.27			

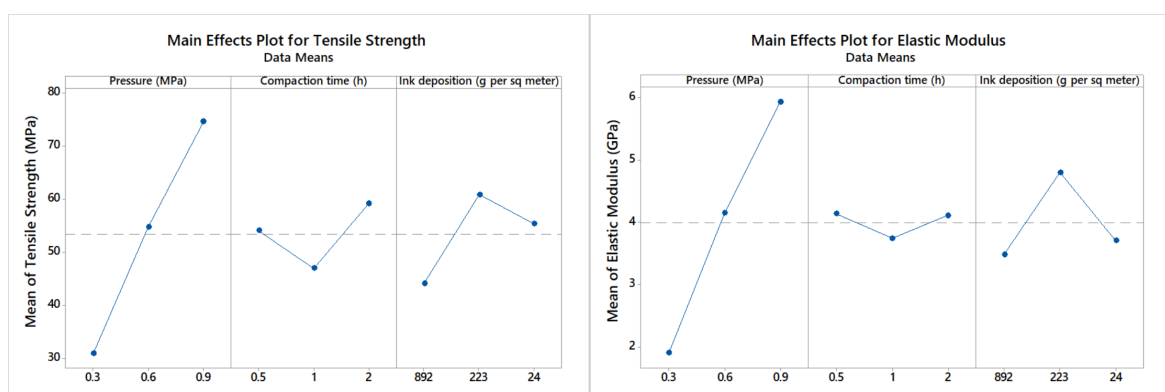


Fig. 4.11 Main effects plot for (a) tensile strength and (b) elastic modulus

4.4 Discussion

The results indicate that the amount of pressure, compaction time, and the ink printed on the substrate in the CFAM process have a significant effect on the porosity content and carbon fibre volume fraction of discontinuous CFRP composites. As the amount of pressure, the most significant factor for both tensile and flexural properties increases, the FVF of the samples also increases which can be explained through the reduced percentage of porosity. Therefore, the mechanical properties are improved. Flexural strength and stiffness of most of the samples were aligned with the tensile properties, however the compaction time has more impact than the volume of ink on the flexural properties due to the smaller p-value, whereas the volume of ink affects the tensile properties more than the compaction time. The effect of each parameter on the final properties and the manufacturing process are discussed in the proceeding subsections.

4.4.1 Effect of pressure on porosity and mechanical properties

Pressure is the most significant factor affecting the final part properties with the minimum p-value compared to other factors. The highest amount of pressure is preferred to improve both tensile and flexural properties. Since the layers are more compact, the thickness of the part is decreased, resulting in higher fibre volume fraction and lower porosity. Figure 4.12 shows the relation between porosity and tensile properties, as well as the fibre volume fraction relationship. Each point represents a data set from the experimental design. For fibre volume fraction, a sigmodial fit has been used, whereas in the porosity-tensile properties relationship, an exponential fit has been found to be more representative. As porosity increases, the tensile strength and elastic modulus of the parts decrease, presenting a strong correlation.

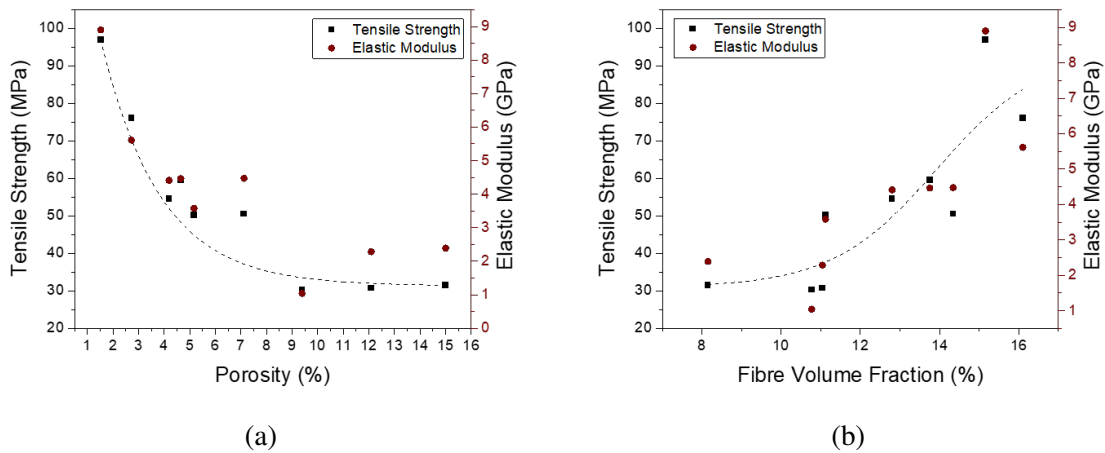


Fig. 4.12 Relationship between porosity and tensile properties (a), the relationship between fibre volume fraction and tensile properties (b)

Since the trend suggests that the mechanical properties keep improving with the higher amount of pressure, a follow-up experiment has been performed by applying 1.2 MPa of pressure during the process. Other parameters which are compaction time and volume of ink kept the same as the experimental set 9 to make a comparison. However, the experiments with 1.2 MPa pressure level resulted in 71.5 MPa ($\pm 2.7\%$) tensile strength and 3.52 GPa ($\pm 0.22\%$) elastic modulus for 10 repeats. Flexural strength and stiffness have also been determined to be only 53.7 MPa ($\pm 3.63\%$) and 8.1 GPa ($\pm 1.81\%$) respectively for 5 repeats. X-ray CT images of the sample produced applying 1.2 MPa is shown in Figure 4.13. Fibre volume fraction and percentage of porosity were calculated as 16.46% and 12.86% respectively.

It is interesting to find out that the porosity level is similar with the samples processed with 0.3 MPa, however the fibre volume fraction is higher than the one with 0.9 MPa. X-ray CT scan and the measurements of final dimensions of the part suggested that higher pressure level caused the void formation by squeezing the matrix material outside of the printed region, hence there is still high fibre volume fraction due to the compact final part. Higher pressure level might have also affected the fibre aspect ratio by damaging the fibres as it was mentioned in the studies investigating the effect of autoclave pressure on mechanical properties.

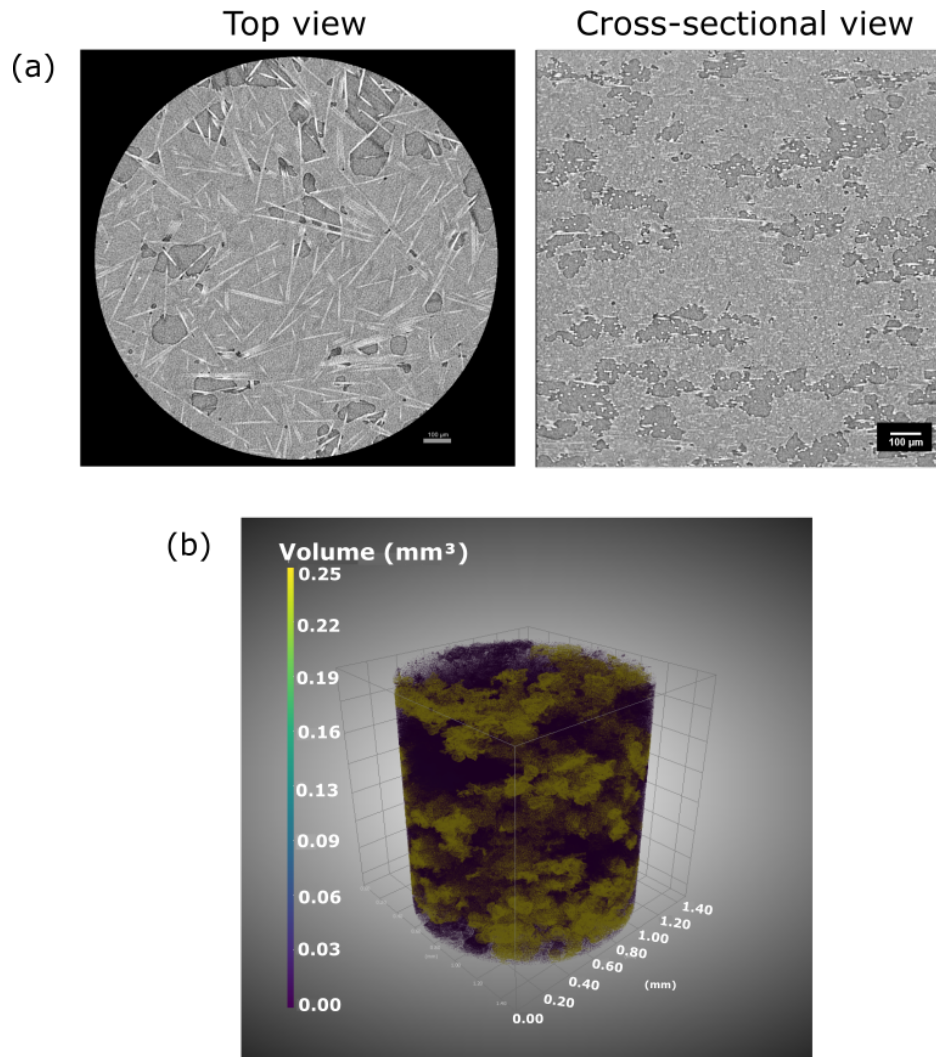


Fig. 4.13 X-ray CT images of the sample produced with 1.2 MPa pressure level (a) 2D view top and cross-sectional view, (b) 3D pore formation

The change in tensile properties with pressure level is shown in Figure 4.14. A pressure level between 0.9 MPa and 1.2 MPa could not be obtained due to the limitations of settings in hot press machine. Hydraulic pressure is difficult to control and adjust sensitively. The main effects shown in Figure 4.11 and ?? present a logarithmic increase in mechanical properties as the pressure parameter levels increased from low to high. It might be possible to reach a slightly higher strength and stiffness values with a pressure level between 0.9 MPa and 1.2 MPa than the properties 0.9 MPa can give. Some large voids created by trapped air might be removed, however, it is not expected to observe a significant jump since the porosity levels that are found in this study already very close to the traditional composites made by highly pressurised autoclave systems such as those reported in [153, 158].

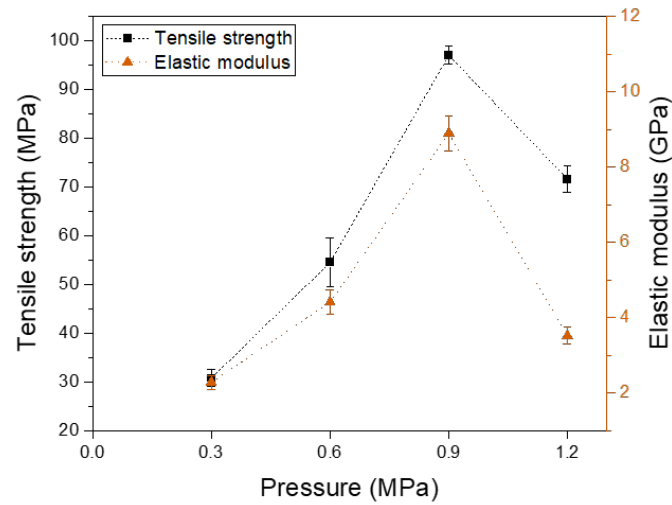


Fig. 4.14 Change in tensile strength and stiffness with the increasing pressure from 0.3 MPa to 1.2 MPa

One of the main disadvantages of additive manufacturing processes is the void formation between the layers of the parts [32]. It was expected to have a high amount of void formation in this process since it has many factors which could result in the trapping of air inside of thermoplastic powder and between layers. There has been limited research found on void formation in additively manufactured composite parts in the literature. Even if there is an analysis of the microstructure and the porosity, voids are not quantified [33]. However, it is possible to make a comparison with some of the studies that investigates additive manufacturing of composite parts. Tekinalp et al. observed that the percentage of void volume in FDM printed carbon fibre reinforced ABS parts was between 16% and 27% regardless of fibre content [77]. Justo et al. stated that the lack of compaction in the FDM process caused a high percentage of porosity between layers. 12% of porosity was observed in continuous carbon fibre reinforced PA (Nylon) composite manufactured by additive layer manufacturing using the MarkOne 3D printer [76]. Blok et al. achieved 1.1% porosity for the short fibre reinforced nylon composites ($V_f = 6\%$), while 9% porosity was found in the parts printed by continuous CFRP filaments ($V_f = 27\%$) [54]. This study achieved 1.52% porosity on average for the CFAM process ($V_f = 15\%$) with the optimum parameter levels; high pressure, medium amount of volume, and high compaction time.

4.4.2 Effect of ink areal density

It was observed that the ink areal density plays a vital role in the volume of powder that can be attached on the substrate, as a second significant factor after pressure. As the number of droplet increases, the amount of powder that can be used as a binding agent increases, resulting in a higher thickness of the final parts. This was verified by weighing the amount of powder for each parameter level. It has been found that the low, medium and high volume of ink can accommodate 41, 208 and 291 g of powder per m^2 respectively. However, increase in the amount of binder due to higher number of droplets can also decrease the fibre volume fraction since the volume of the final part increases, but the number of carbon fibre fabric used in the reinforcement stays the same. Therefore finding the optimal ink volume is essential to maximise the fibre volume fraction while providing a sufficient bonding between the carbon fibre fabric layers. Figure 4.15 represents the amount of ink deposited per unit area for each printing setting, which is calculated based on the droplet size, dot-spacing and the number of ink droplets printed per unit area. It can be seen that low and medium printing settings have discrete droplets, while the printing with highest amount of ink per unit area creates overlapped droplets, therefore a complete layer.

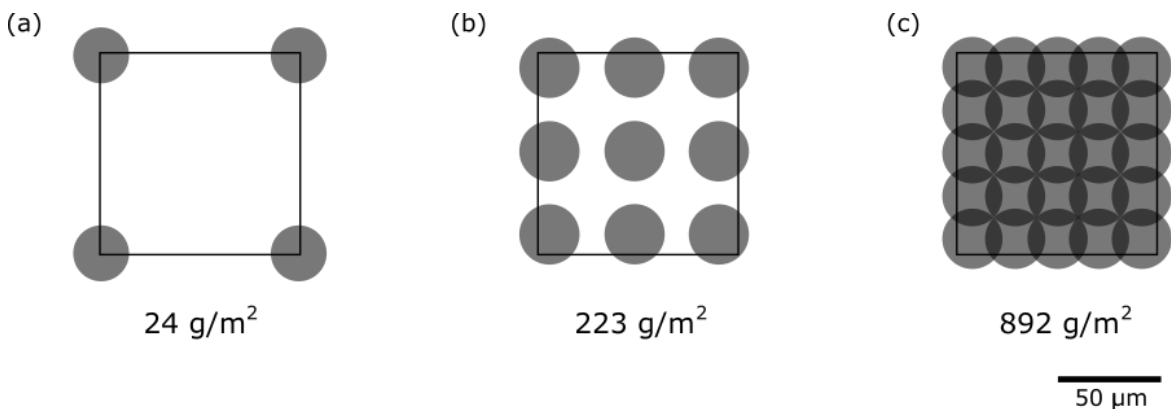


Fig. 4.15 Level of surface coverage for each printing setting (a) low - JetLab IV, (b) medium - HP Deskjet 600 DPI, (c) high - HP Deskjet 1200 DPI

The optimum parameter level for the maximum tensile strength and stiffness is 223 g/m^2 as this parameter level provides a strong fibre-matrix adhesion than the 24 g/m^2 of ink and a higher FVF than the 892 g/m^2 ink. Samples printed with a low amount of ink showed low strength and stiffness despite the high fibre volume fraction due to the delamination failure that occurred in the early stage of mechanical testing. Figure 4.16 shows the difference of failure modes between the samples printed with a low and medium amount of ink.

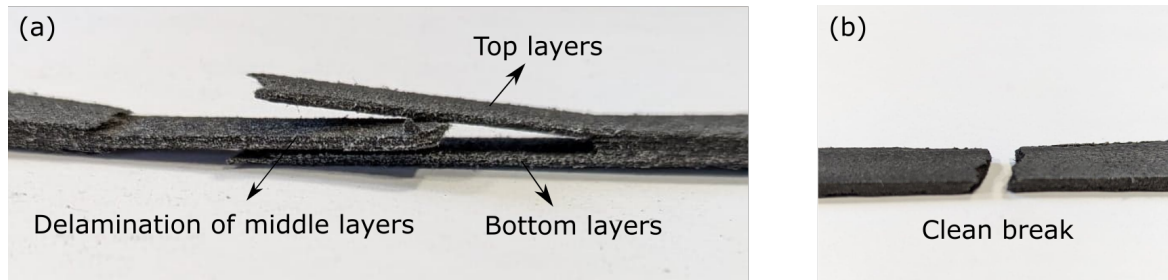


Fig. 4.16 Tensile failures of samples; (a) low, (b) medium (0.3 MPa pressure and 2 hours of compaction time kept constant)

On the other hand, the highest amount of ink exhibits the highest amount of evaporation, since around 82.5% of the ink is water. Non-uniform evaporation of the ink is likely to cause a high porosity level, as the amount of adhered powder is not distributed evenly. Since HP Deskjet printer has two automated high-resolution printing settings, it is not possible to adjust the dot-spacing in between the values shown in Figure 4.15b and c. JetLab IV printer can be used for this experiment, however, it is not practical to print larger geometries with a single nozzle, while the HP Deskjet printer has multiple nozzles that can print faster. Additionally, the optimal amount of ink found in this study shown in Figure 4.15b can cover the interfaces of different powder particles ($56 \mu\text{m}$), which is sufficient to coat the whole surface of carbon fibre sheet with uniformly distributed powder.

4.4.3 Effect of compaction time

In autoclave processes, it has been observed that the duration of pressure application affected the final part properties by influencing the thickness of the laminates [148]. In the CFAM process, pressure level has been found to be the most effective parameter on the final thicknesses of the parts. The compaction time has been found to be the least significant factor affecting the tensile properties with 7% contribution, whereas the flexural properties are affected more than the tensile properties by this factor. Since the thermal treatment has an impact on the thermoplastic matrix properties, an improvement in flexural strength and stiffness can be attributed to the compaction time.

Even though this factor is the least significant for tensile properties, as it was mentioned in DSC analysis, it is critical to keep the part under pressure during the cooling down period, since the polymer is at the molten state. Once the solidification is completed, the part can be removed from the pressure safely without any separation between layers. Crystallization must occur under pressure to ensure the strong adhesion.

4.4.4 Overall analysis of CFAM and comparison with state-of-the-art

Complex shaped discontinuous fibre reinforced polymer composites parts with high strength and stiffness can be manufactured in a fast and flexible way using CFAM. While thermal inkjet printing provides faster printing of 2D slices of geometry, the technique is flexible to acquire any long carbon fibre or glass fabrics and thermoplastic matrix materials such as a variety of nylon and PEEK powder. Therefore, there is no need for filament preparation like in FDM methods. Disadvantages such as nozzle clogging, discontinuities on printing patterns and inter-bead voids can be eliminated. However, many process elements need to be considered carefully to maximize the performance of the parts output from this manufacturing technique.

Inkjet printing is a useful technique to control the size of the droplets and the volume of ink, influencing the volume of powder that can be absorbed. JetLab IV system provides this flexibility in terms of adjusting the dots per inch setting by regulating the droplet spacing and the volume of droplets. In contrast, the HP Deskjet system only can print with constant droplet size and dots per inch settings. The uniformity of droplets is also critical to have a uniform distribution of powder on the substrate since this will affect the creation of voids during the melting process.

The hot press process is the most important stage of manufacturing. Uniformity of pressure and temperature is also critical to the final properties of the parts. It has to be ensured that the controller shows the real-time temperature for all surfaces of the hot press plates. Otherwise, there will likely be non-uniform crystallisation of the polymer powder. The fluctuation between the mechanical properties of samples might be originated from the differences between the thermal history due to the non-uniform distribution of temperature in hot press. For the parts with high thickness, a closed cabinet for the hot press operation can be considered to provide a uniform temperature distribution. Therefore, the simultaneous melting between all layers can be achieved.

The sandblasting process is the last step to subtract the complex geometry from the compressed laminate. Carbon fibre fabrics that are not bonded together can be easily removed with high pressure blasting. The laminate shown in Figure 4.6(b) was post-processed with this operation only in 15 minutes. It was observed that applying high pressure during the hot press process can increase the sandblasting time slightly since the un-bonded fabric layers can be more compacted. The top and bottom surfaces of the parts can be protected by using masking tape during the sandblasting. Following this process, the sides of the parts can also

be sanded by using 600 grit sandpaper to provide a better surface finish as it is commonly used in post-processing of FDM parts. Staircase effect (visible layer lines) can be removed from the final geometry in this way.

The performance of the additively manufactured composites is still low compared to traditional composite manufacturing [6, 54]. High quality composites using traditional methods typically have a porosity content lower than 1%, AM composite manufacturing techniques need to be improved in order to reach these densities. Reinforcing the polymers commonly used in AM techniques with fibres can improve the mechanical properties but can also increase overall porosity within the component [94, 90]. In the CFAM process, the addition of fibres to the same polymer (PA2200) that HSS uses increased the strength of the parts up to 97 MPa from 38 MPa. A lower porosity content of 1.52% compared to 4.71% in HSS is also achieved [61]. Compared with injection molding and LS of Nylon-12 parts with an average of 25 MPa and 40 MPa UTS respectively [159], the addition of fibres to the Nylon-12 in the CFAM process, increased the strength of the parts up to 97 MPa. This shows that fibres are effectively reinforcing the polymer matrix in CFAM process. Figure 4.17 shows the comparison of some of the reported mechanical properties for AM composites. It can be seen that CFAM parts produced parts with higher stiffness and tensile strength than discontinuous fibre FDM but lower than continuous fibre FDM (Markforged).

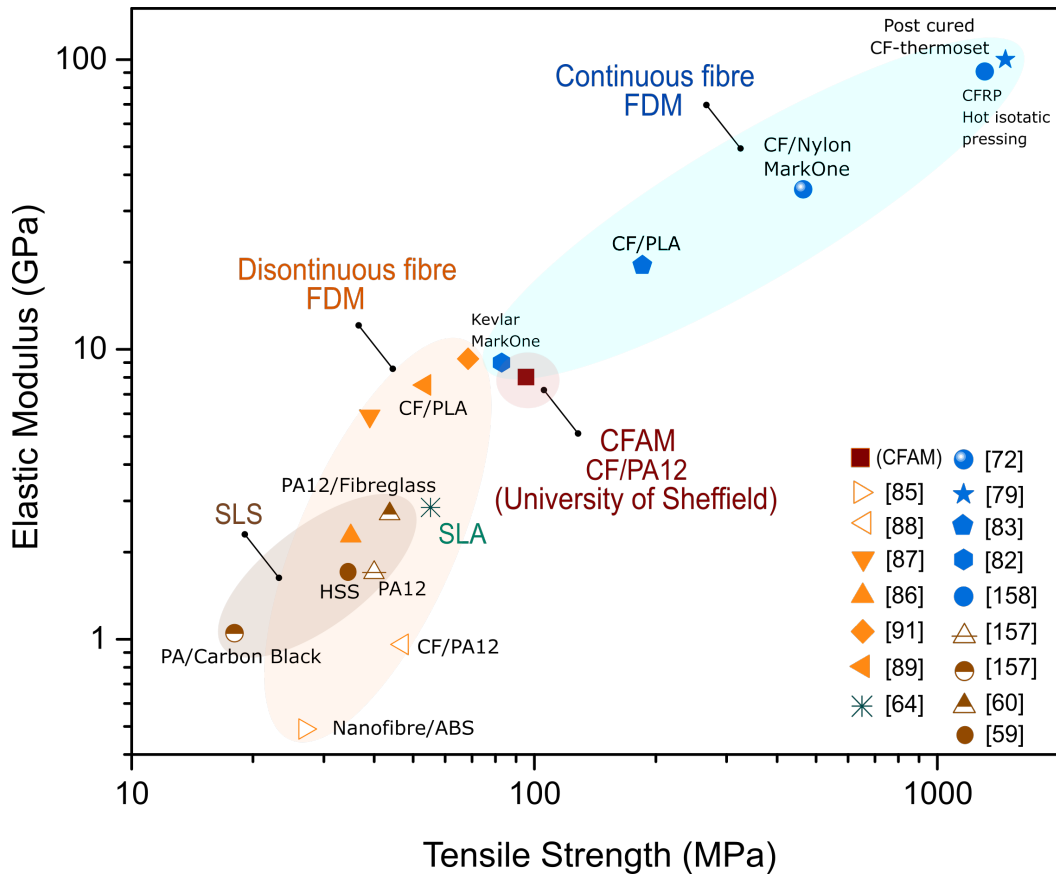


Fig. 4.17 Comparison between Composite Object Manufacturing and other AM parts with continuous and discontinuous fibre [62, 66, 74, 89, 90, 159, 88, 87, 93, 91, 81, 85, 84, 160]

4.5 Conclusion

In this chapter, a CFAM technique was developed based on Impossible Objects CBAM process using thermal inkjet printing technology to benchmark the performance of the process with mechanical testing and X-ray tomography. Discontinuous carbon fibre reinforced nylon composites were manufactured and tested. Critical process parameters such as the amount of pressure, compaction time and volume of ink were investigated by using Taguchi orthogonal array and ANOVA. Results showed that pressure is the most significant factor which is affecting the final part properties in terms of strength, stiffness and microstructural properties. A higher amount of pressure up to 0.9 MPa improves the consolidation, increasing the fibre volume fraction and decreasing the inner porosity, which further enhances the mechanical properties of CFRP composites. While compaction time has the lowest significance, the volume of ink plays an important role on absorption of the polymer powder on the substrate. It was observed that, low amount of ink increases the chances of delamination since there

is no sufficient binding between layers. However, as the volume of ink increases, the fibre volume fraction decreases due to higher volume of matrix material. Therefore, medium parameter level, 223 g/m^2 (600 DPI) can be used, which is also an advantage in terms of printing speed since the commercial desktop inkjet printers use this setting as standard.

With the optimized CFAM process, 1.52% internal porosity was obtained due to heat and pressure application during the manufacturing. Final parts that have low porosity achieved an average of 97 MPa and 8.9 GPa tensile strength and stiffness respectively, which is higher than the discontinuous fibre reinforced polymer composites produced with FDM, SLA and SLS techniques. CFAM parts still have inferior mechanical properties compared to conventionally produced short carbon fibre composites. However, this sheet lamination technique is promising to design complex shaped composites with the flexibility of fibre and matrix material selection.

Fibre length and fibre volume fraction determine the mechanical properties in composites. AM techniques need to be improved to process high volume of longer fibers, without losing the flexibility of creating complex geometries. Hybrid approach (continuous fibre mixed with discontinuous fibre) can be a way of reaching the properties of advanced composites, since the short fibre provides the formability while the continuous fibre increases the volume fraction and strength. CFAM technique can be developed to adopt the hybrid layers of carbon fibre fabric.

Chapter 5

Investigation of Polymer Morphology in CFAM Parts

Summary

This chapter introduces new knowledge relate to the dependency of matrix mechanical properties and polymer morphology. Previous research examining polymer crystallinity has been reviewed and is summarized in traditional polymer matrix composites and polymer AM parts.

The experimental section then explains the differential scanning calorimetry (DSC) analysis and the calculation method for the degree of crystallinity (DOC). The design of a compression rig that can be placed inside a furnace with the aim of adjusting the cooling rate, which is expected to impact the crystallinity, is then presented.

The fundamental differences between the single phase and double phase melting DSC curves are discussed alongside an evaluation of crystallinity. The relationship between the mechanical properties and melting behaviour is presented with a new approach. Finally, the interlaminar shear properties and failure modes of samples produced with different cooling rates are analysed.

5.1 Introduction

Fibre composites achieve high strength and stiffness due to the superior properties of the fibre. However, the matrix properties and fibre-matrix interface are as important as the fibre characteristics to obtain high-performance composites [161]. Polymer crystallinity is one of the thermoplastic material properties that is related to the fibre-thermoplastic matrix interface bonding [162, 163]. Mechanical properties, particularly matrix dominated characteristics such as compressive and shear strength are significantly affected by the changes in crystallinity since an interphase failure is a direct reflection of the interphase adhesion mechanism [32, 164]. For this reason, the characterization of polymer crystallinity is crucial in thermoplastic composites.

In traditional composites, the influence of crystallinity on interlaminar properties of final parts was widely investigated. The cooling rate in the hot compression moulding was observed to be strongly correlated with the crystallinity of polyphenylene sulphide [165]. Slow cooling improved the interfacial bond strength, which had a positive impact on compressive and interlaminar properties. Ye et al. reported that the interlaminar fracture toughness of glass fibre reinforced polypropylene decreased when the degree of crystallinity of the polymer increased [166]. Gao et al. examined a wide range of polymer crystallinity levels obtained with different process parameters. Tensile strength and stiffness of the samples decreased when the crystallinity was reduced, whereas the ductility found to increase. Interlaminar shear strength of the samples found to be not affected by the crystallinity significantly [164].

In additive manufacturing, one of the drawbacks of fibre reinforced composites is the weak fibre-matrix interaction. The nozzle system in FDM processes moves parallel to the interface surface, which weakens the strength of a part in the z-direction or stacking direction [167]. The extrusion of molten matrix material on top of a previously deposited layer at a lower temperature can cause the formation of residual stresses due to temperature gradient [168, 169]. Most studies so far investigated the relationship between the several types of composite AM process parameters and final mechanical performance by characterizing tensile properties. However, there is a lack of understanding of polymer morphology and how it affects the mechanical and fibre-matrix interfacial properties in additively manufactured parts. In polymer AM, few studies investigated the polymer morphology and the effect of crystallinity on mechanical properties. Majewski et al. investigated the effect of crystallinity on the tensile properties of Nylon-12 parts manufactured by Selective Laser Sintering [170]. DSC traces showed double phase melting which is a representative of melted and un-melted regions within the part. The proportion of these two regions is called Degree of Particle Melt (DPM)

whose effect on tensile properties has been found to be significant. Similarly, the effect of cooling rate on the crystallinity of SLS Nylon-12 parts was analysed by Zarringhalam [171]. The study revealed that there is no obvious trend in the crystallinity change as a function of cooling rate, except when comparing parts which went through significantly different cooling rates. For this reason, DPM is used to understand the relationship between polymer morphology and final properties. In composite AM, previous studies have explored the mechanical characterization of parts produced mainly by FDM as mentioned in Chapter 2. Limited research has focused on the polymer morphology of FDM parts. Heat treatment or annealing of the short carbon fibre reinforced polymer parts recreates the polymer crystallization with the aim of removing the residual stresses, which was used to improve the mechanical properties and layer-to-layer interaction [172, 173]. It was observed that change in annealing duration had an impact on the crystallinity, therefore the performance of final parts.

In this chapter, the crystallinity of the matrix polymer was examined under different experimental conditions by adjusting pressure level, compaction time and volume of ink. A compression mould that can be put in a furnace was designed to assess the effect of cooling rate on the interlaminar shear strength of CFAM parts. The aim is to understand the effect of process parameters on polymer morphology and interphase adhesion mechanism.

5.2 Methodology

5.2.1 Experiment I

Discontinuous carbon fibre reinforced nylon composite parts have been produced using the CFAM technique with the hot press process as mentioned in Chapter 3. Design of experiments according to Taguchi L9 orthogonal array that has been used in Chapter 4, is used in this chapter to understand the influence of process parameters on the crystallinity of matrix material. The significance of the factors is examined with Taguchi analysis and ANOVA. The relationship between resultant mechanical/microstructural properties and the degree of crystallinity is also investigated.

DSC analysis is conducted for the specimens produced under 9 different experimental conditions. Additionally, a sample produced with a pressure level of 1.2 MPa was also analyzed with DSC, which is named Set 10 in the experimental design. Three repeats from each experimental condition have been analysed and average crystallinity values have been

considered. The standard deviations of the crystallinity measurements for each sample were negligible. Figure 5.1 shows the region used in DSC curves to calculate the percentage of crystallinity. Phase 1 peak temperature is the representative of the un-melted regions in polymer powder, whereas the phase 2 shows the melted and crystallised areas [170]. The degree of crystallinity was calculated using the Equation 5.1, where ΔH_m is heat of melting and ΔH_f is the known heat of melting of 100% crystalline nylon samples. ΔH_f of a Nylon-12 is 209.3 J/g as it was determined by Gogolewski et al. [174].

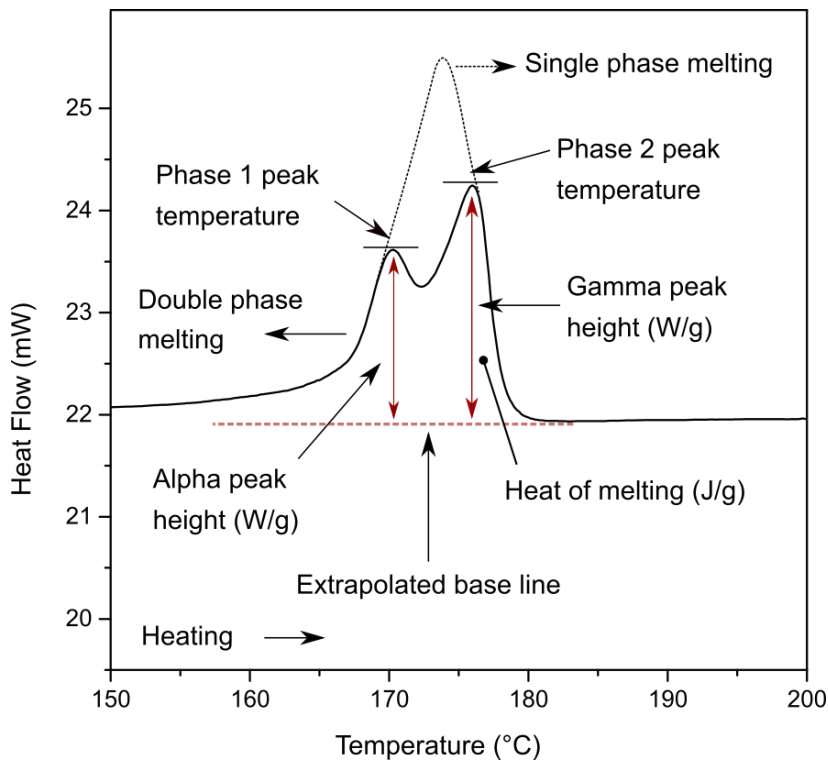


Fig. 5.1 DSC curves of samples from each experimental set (Endo up)

$$\%Crystallinity = \left(\frac{\Delta H_m}{\Delta H_f} \right) \times 100 \quad (5.1)$$

5.2.2 Experiment II

Cooling rate was proven to be influential factor in crystallinity, hence in the interfacial properties of the thermoplastic composites. The hydraulic hot press system presented in Section 3.2.3 does not have a controller to adjust the cooling time. Samples are left to cool under pressure and under the influence of ambient temperature. Therefore, a compression mould that can be located inside a furnace was designed and manufactured to allow the

control of the cooling time as shown in Figure 5.2. The amount of pressure is controlled by a Wera click-torque adjustable torque wrench and a pressure sensor to maintain consistency in pressure applied between parts produced in the hot press and those cooled in the oven.

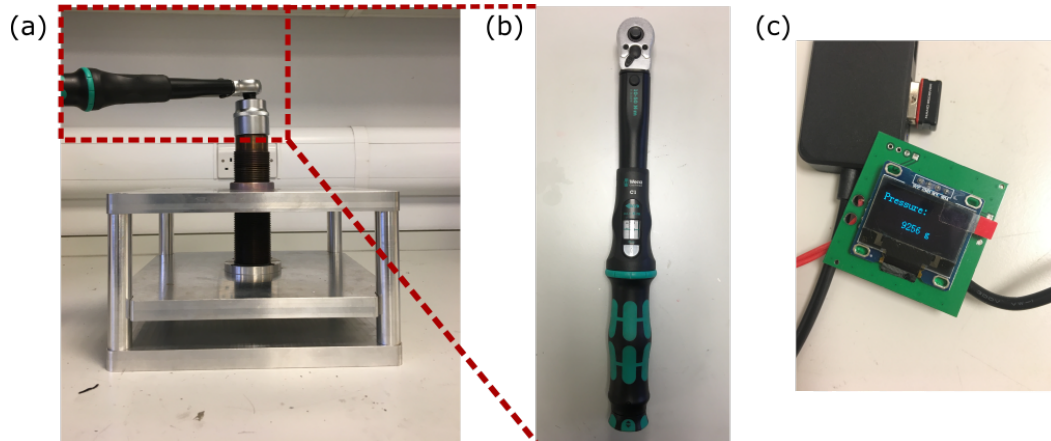


Fig. 5.2 (a) Compression rig, (b) Wera click-torque adjustable torque wrench, (c) pressure sensor

Interlaminar shear strength of the parts has then been determined using short beam shear testing according to the BSI EN ISO 14130:1998 standards. Short beam shear samples were printed using HP Deskjet 4130 (423 pL ink per mm) to be compressed by using compression mould and hot press system under the cooling rates of 5 °C and 1 °C per minute respectively. The reason for selection of 5 °C only is that the control over the cooling temperature in the oven was not successful at higher rates than 5 °C per minute. Thermocouples were used to understand the real temperature of the compression rig and it has been observed that the rig remained at high temperatures even though the furnace heat was reduced. For this reason, only the samples with 5 °C cooling rate were reliable for comparison. Five repeats were taken for each experiment. The short beam shear samples produced are shown in Figure 5.3. The pressure level and compaction time were kept constant at 0.9 MPa and 2 hours. The failure modes were examined using SEM and optical microscopy. DSC analysis was used to measure the crystallinity of the samples produced with the cooling times of 1 °C and 5 °C per minute.

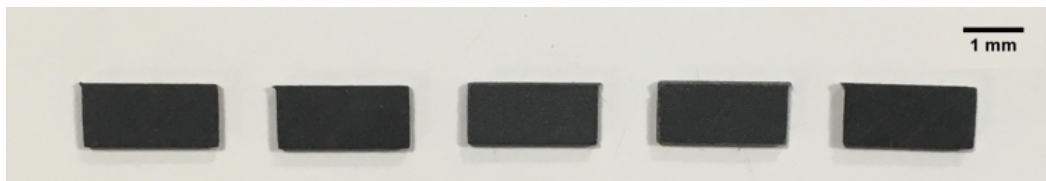


Fig. 5.3 Short beam shear test specimens

5.3 Results and Discussion

5.3.1 Effect of process parameters on polymer crystallinity

The DSC curves of the samples for each set of experiments are presented in Figure 5.4(a). They are lined up from top to the bottom according to their processing peak height. A double phase melting was observed in most of the curves. Only Set 5 and 9 demonstrated a single-phase melting. The three repeats were resulted in the same melting behaviour, which shows the consistency of the impact of processing conditions on crystallization process.

Double melting behaviour is the reflection of melted and un-melted regions of the polymer after the heat process. Three different types of melting behaviour can be observed in DSC analysis, which can be explained by different crystal formations, called γ , γ' and α -form [175]. The types of melting behaviour due to different crystal forms are shown in Figure 5.4 (b). The single endothermic peak represents the existence of γ -form or γ' -form, while the double peak shows α -form. Crystal in γ' -form as a variant of γ -form can be obtained commonly and the heat treatment under pressure can transform these crystals to α -form phase. In CFAM process, heat and pressure application might cause this transformation. The melting of α -form crystals in the core peak leads to the recrystallization of molecular chains into γ -form, which melts at the phase 2 peak temperature. Therefore it can be said that 7 out of 9 sets have been found to be involve α -form crystals. While Set 5 samples include γ' -form, Set 9 samples have γ -form crystals.

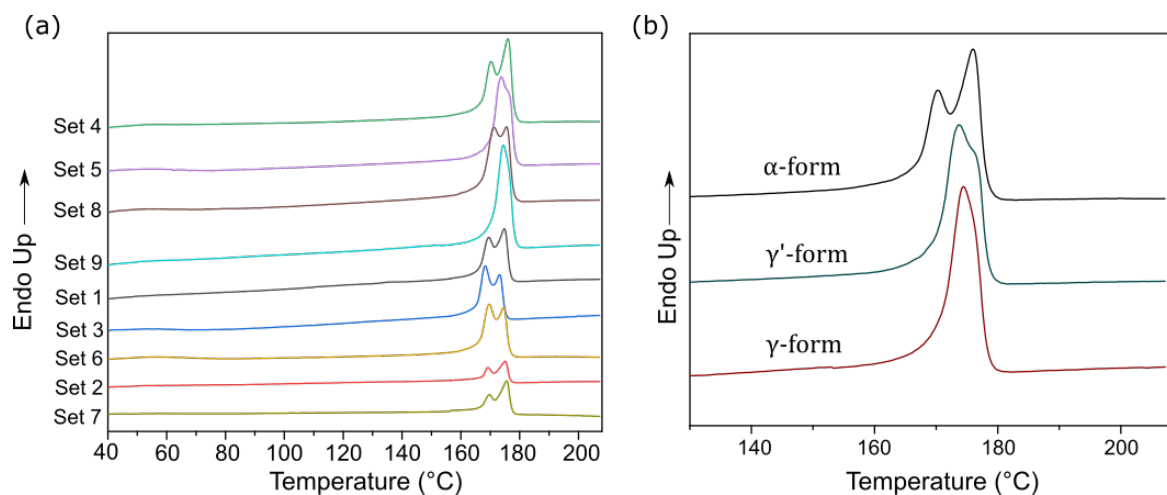


Fig. 5.4 (a) DSC curves of samples from each experimental set (Endo up); (b) Melting behaviour of different crystal forms in polymers

The degree of crystallinity for each experimental condition is shown in Table 5.1. The maximum crystallinity was found as 20.4% in Set 4, which is followed by 20.2% in Set 5. The lowest crystallinity level was 11.7% for Set 3 with 0.3 MPa and 2 hours of compaction time. Table 5.2 shows ANOVA for crystallinity. As p-values are higher than 0.05, the process parameters are not significant. However, the compaction time makes the most contribution with the smallest p-value, even though it was the least significant factor affecting the mechanical and microstructural properties.

Table 5.1 Degree of crystallinity for the samples from each experiment set

Set Number	Pressure (MPa)	Compaction Time (h)	Volume of ink per mm^2 (pl)	Crystallinity (%)
1	0.3	0.5	845 pl	15.4
2	0.3	1	423 pl	18
3	0.3	2	140 pl	11.7
4	0.6	0.5	423 pl	20.4
5	0.6	1	140 pl	16.6
6	0.6	2	845 pl	15.2
7	0.9	0.5	140 pl	16.8
8	0.9	1	845 pl	17
9	0.9	2	423 pl	17.2

Table 5.2 ANOVA for degree of crystallinity

	Degree of Freedom	Sum of Square	Mean Square	F-value	P-value
A=Pressure	2	19.1489	9.5744	7.7144	0.11475
B=Compaction time	2	22.4689	11.2344	9.0519	0.09948
C=Volume of ink per mm^2	2	12.5356	6.2678	5.0501	0.16529
Residuals	2	2.4822	1.2411		

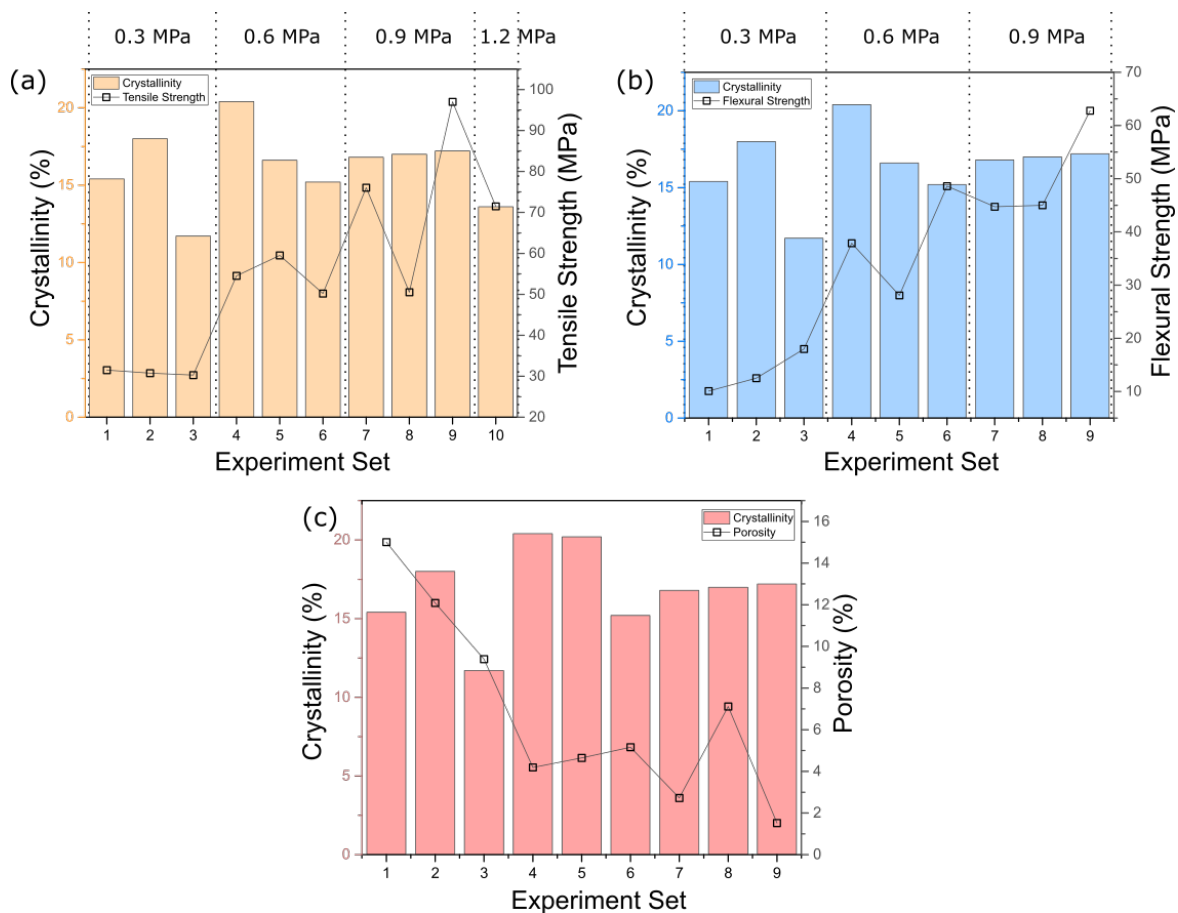


Fig. 5.5 Comparison of final part properties; (a) tensile, (b) flexural and (c) porosity, with degree of crystallinity for each experimental condition

Figure 5.5 presents the relationship between crystallinity and final part properties; tensile strength, flexural strength and porosity respectively. It can be seen that there is no correlation between the results, even though it was expected that higher crystallinity would cause an increase in mechanical properties. A similar observation has been made by Zarringhalam and Majewski et al. on selectively laser sintered Nylon-12 parts [171, 170]. They deduced that the reason for this unusual behaviour is the existence of un-melted cores after sintering. Un-melted polymer crystals generate double phase melting which affects the calculation of crystallinity. Therefore, other DSC analysis elements such as peak height and peak temperatures are investigated to understand the association between polymer morphology and mechanical properties. It was found that the peak heights especially core peak height (un-melted crystal) correlates with the elongation at break.

In the CFAM process, the presence of α -form crystals in the samples is indicated by the presence of the double peak for 7 of the 9 sets presented in Figure 5.1 due to the heat and pressure application. The crystallinity behaviour cannot be compared with polymers that show single phase melting (an indication of absence of α -form and presence of γ -form crystals only).

A new approach for determining the impact of presence of α -form has been used in this study. Since the CFAM process does not include sintering, and un-melted cores were not detected by the X-ray CT or optical microscopy, calculating a DPM based on the double phase melting would not reflect the morphology. For this reason, double peaks at the left and right-hand sides of the DSC graphs were called as alpha and gamma peaks respectively. Since it has been demonstrated in [171] that the core peak height has the most significant element revealing the trends, the connection between alpha peak height and the mechanical properties is shown in Figure 5.6. A clear link can be observed between tensile strength and the alpha peak height (which is correlated with the percentage of α -form in the sample) for the double phase melting. Gamma peak heights in the parts with single phase melting are not aligned with the trend.

It has been demonstrated in [171] that there is a tipping point at the transition from the parts with double melting behaviour to the ones with single melting, where the trend changes to the opposite direction. In agreement with the literature, the CFAM alpha peak height results show the same transition, whereas there is no clear opposite trend in the gamma peak specimens. More data points would be needed to draw a conclusion about the gradient in the mechanical properties of parts with single phase melting behaviour as a function of gamma peak height. The difference between the γ -form and γ' -form has been explained with the differences in the cooling behaviour such as slow cooling and quenching respectively. However, the cooling conditions have been the same for Set 5 and Set 9. For this reason, the difference might have occurred due to the outside conditions. It has been highlighted that the parts with γ -form crystals are strong and tough while the α -forms are brittle [176, 175]. Therefore, the highest tensile strength of Set 9 part can be explained with the high amount of stable γ -form crystals it includes.

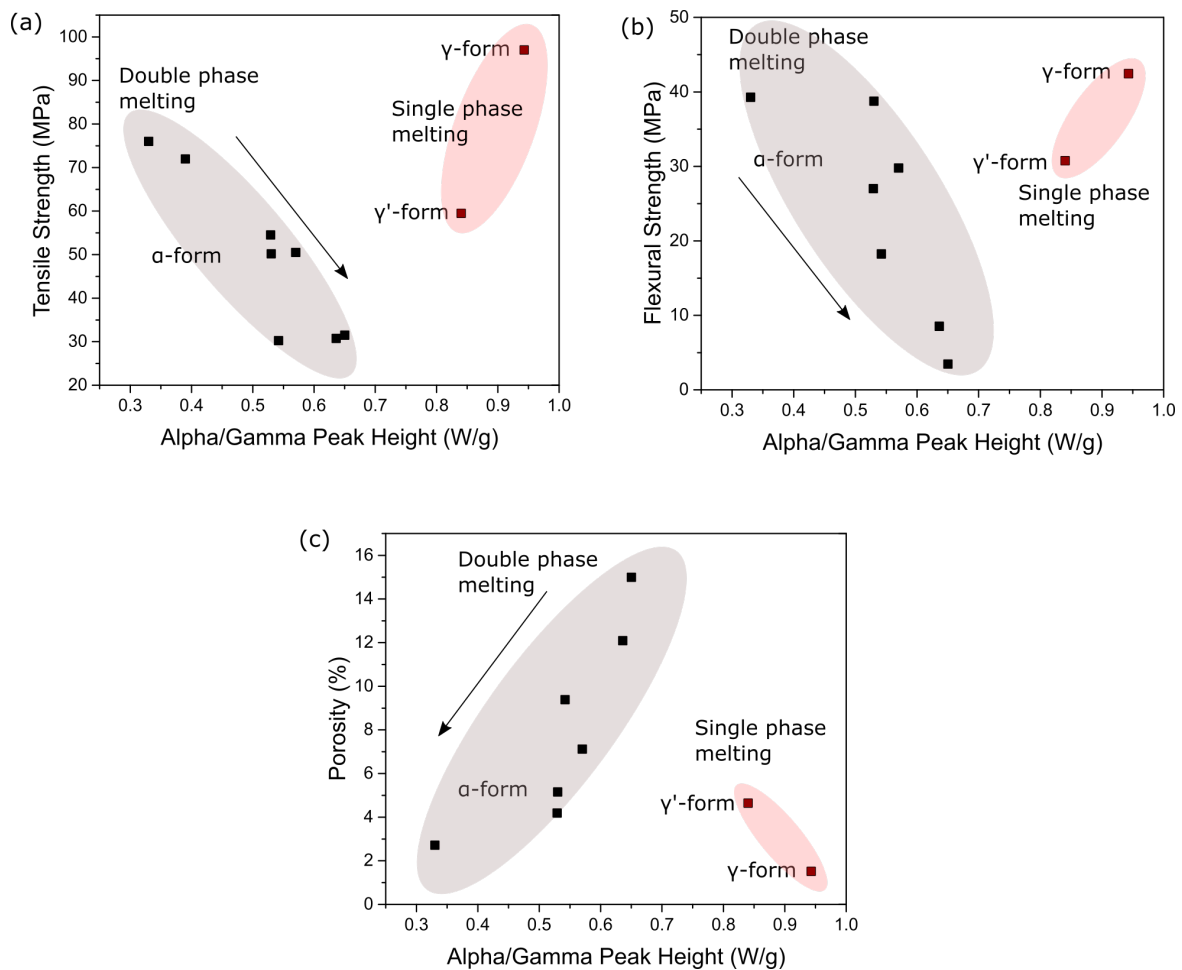


Fig. 5.6 Final part properties; (a) tensile, (b) flexural, (c) porosity, as a function of alpha peak

5.3.2 Effect of cooling rate on crystallinity and interlaminar shear strength (ILSS)

Studies demonstrated that thermal process elements such as dwell time, temperature and cooling rate affect the degree of crystallinity. Since the hydraulic hot press that has been used in this study does not have control over the cooling rate, a furnace compression mould has been designed. However, the control over the cooling temperature in the oven was not successful at higher rates than 5 °C per minute. The compression rig remained at high temperatures even though the furnace heat was reduced. For this reason, only the samples with 5 °C cooling rate were reliable for comparison.

The force-displacement curve from the short beam shear test of hot press samples is given in Figure 5.7. The shear strength of the samples is 42.4 MPa ($\pm 1.4\%$), whereas the furnace compression mould samples with a higher cooling rate have an average of 55.8 MPa ($\pm 9.95\%$). The standard deviation in the shear strength of furnace samples was found to be very high. The DOC of the furnace samples was found as 10.60% on average, which is the lowest crystallinity obtained in this study. Hot press samples produced with the same experimental conditions (0.9 MPa, 2 h, 423 pL) but with 1 °C per minute cooling rate resulted in 17% crystallinity which is higher than the furnace samples. This was expected due to the slow cooling rate, however, the difference between crystallinity levels was not reflected in the interlaminar shear strength of the furnace samples. These results are in agreement with [177] in which the crystallization did not affect the interlaminar shear strength of the samples. It was stated that the reason for no correlation might be the already low level crystallizations in each experimental condition.

The double melting phase observed in both specimens required an investigation of the alpha peak heights. These were found as 0.33 and 0.52 W/g for the hot press and compression rig samples respectively. It is possible to predict that the tensile properties of hot press samples are likely to be higher than the compression rig samples.

The high error level in the furnace samples shows that the distribution of the temperature and cooling times might have been different for each sample depending on their locations under the pressure. Moreover, two samples were discarded due to the compressive failure rather than a shear failure as shown in Figure 5.8. The fracture shows that the fibres are not supported by the matrix, which might be the result of low crystallinity. It has been previously observed that only a high difference between the cooling rates exhibited a significant change in crystallinity. For future studies, quenching can be a reliable solution to see the impact of cooling rate on interlaminar properties.

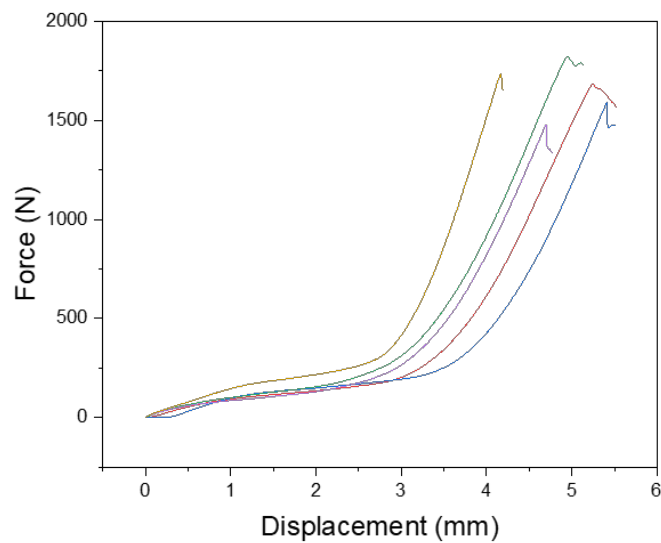


Fig. 5.7 Force-displacement results from shear test of hot press specimens

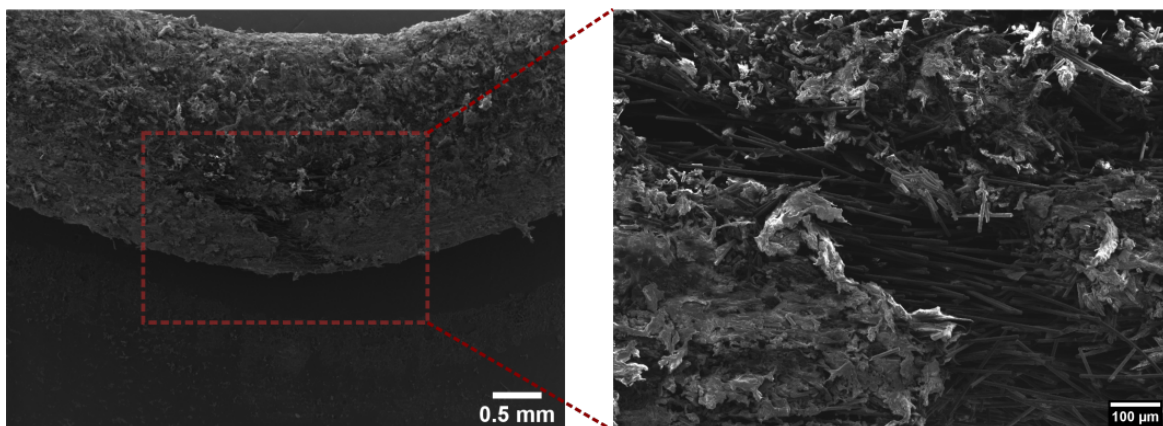


Fig. 5.8 Compressive failure occurred during the short beam shear test in a compression rig sample

5.4 Conclusion

The influence of process parameters such as pressure, compaction time, the volume of ink and cooling rate on the crystallinity of the samples were investigated by DSC analysis. The relationship between the crystallinity and resultant mechanical and microstructural properties was examined. Process parameters were found to be insignificant on the crystallinity, however, the compaction time has the lowest p-value, which shows the importance of thermal

treatment on polymer morphology.

There is supposed to be a parallel relationship between the degree of crystallinity and tensile strength, which does not apply to the polymer parts showing double phase melting. In CFAM, this behaviour is induced by the existence of α -form crystals. Therefore, the heights of the alpha peak representing the alpha form crystals were derived for each experimental condition and were found to correlate well with the resultant properties. A significant link showed that the alpha peak height can be successfully used to understand the effect of polymer morphology on mechanical properties in the case of double melting behaviour. As the gamma form of crystal increased in the material, the tensile and flexural properties were improved, which results in tougher and stronger composite parts.

Finally, the effect of cooling rate on crystallinity level was analysed. The degree of crystallinity was reduced by 50% with the increased cooling rate from 1 °C to 5 °C, however, this did not affect the interlaminar shear strength of the samples significantly. A wide range of cooling rates must be experimented with to observe a reasonable change in interlaminar shear strength in alignment with the literature.

It can be concluded that the crystal formation in thermoplastic matrix materials can be tailored to achieve high-performance composites suitable to specific applications.

Chapter 6

Hybrid Carbon Fibre Reinforced Polymer Composites in CFAM

Summary

In this chapter, the adoption of continuous carbon fibre layers to the CFAM process is proposed as a mean to improve the mechanical properties of the final parts obtained. Preliminary experiments have been performed manufacturing components from a single type of continuous carbon fibre. Three types of continuous carbon fibre have been considered: a twill weave, plain weave and unidirectional (UD) form. The suitability of the fibre types to the compaction and sandblasting processes has experimented.

In the second part of the chapter, parts manufactured using a hybrid composition of continuous and discontinuous fibres are presented. Mechanical and microstructural characterization is performed using tensile testing, short beam shear testing and X-ray CT. Finally, challenges of the hybrid CFAM and potential applications are discussed.

6.1 Introduction

Fibre-reinforced composite materials not only offer lightweight structures with high strength and stiffness but also provide flexibility to tailor the mechanical properties of the final parts to the specific needs for industrial applications. This can be done by integrating various types of matrix and reinforcements, however, one way to even further develop the properties is mixing more than one type of reinforcements into one part. This method is used to avoid catastrophic failure modes associated with the material.

Several researchers investigated hybrid composites and their effects on mechanical properties. It has been observed that the mechanical properties of composites can be further improved by integrating various fibre and matrix types. Hybrid composites can be classified into three groups; interlaminated, intraply and intermingled hybrids [178]. Intraply hybrid composites have two types of fibres laid in the same layer whereas the interlaminated hybrid composites include two types of fibre in different sheets stacked together with a certain proportion [179]. Intermingled composites are composed of hybrid filaments rather than plies. Ideally, similar type of fibres should not be neighbour to each other [180].

The focus of this chapter is interlaminated hybrid composites. Zhang et al. manufactured composite laminates using varying combinations of woven glass and carbon fibre reinforced thermoset layers. The stacking sequence has been optimized and 50% carbon fibre reinforcement has been found to provide the maximum flexural strength when the carbon fibre fabric layers were used as a sandwich for glass fibre layers. An optimal compressive strength has been found to be reached when glass fibre layers are placed in the exterior of the part. The effect of stacking sequence on the tensile properties has found to be insignificant [181]. Alsaadi et al. mixed S-glass fibre and carbon/aramid fibre reinforced layers to investigate the effect of asymmetric and symmetric stacking on the impact behaviour of hybrid parts. The authors found that the hybrid composites have higher impact strength compared to the parts manufactured with only carbon/aramid layers [182]. Hong et al. manufactured hybrid laminates with a combination of continuous and discontinuous fibre layers in order to bring together the advantages of both reinforcements. While discontinuous fibre reinforcement helps to achieve complex configurations, continuous fibre reinforcement gives high strength and stiffness. Brittle failure of the continuous fibre reinforced layers can be achieved by benefiting from the energy absorption competence of the discontinuous fibre layers. The tensile strength of the discontinuous fibre composites was improved from 121 MPa to 333 MPa by adding continuous fibre layers in [183]. In another similar research, Trauth et al. built sheet moulding compounds combining continuous unidirectional carbon fibre and discontinuous

glass fibre via compression moulding. Tensile and compressive elastic properties of the final parts were significantly improved, 171% and 151% respectively, compared to the parts with only discontinuous glass fibre reinforcement. 204% increase in tensile strength was achieved while a decrease was observed in compressive strength. Failure modes of the specimens showed that the fracture occurred first in continuous fibres followed by delamination between layers. Final failure occurred at the discontinuous fibre reinforced phase [184].

CFAM system provides the flexibility to select and mix different types of fibre reinforcement and matrix materials due to layer by layer reinforcement fabrication. In FDM techniques, the filament incorporating fibre and matrix needs to be prepared beforehand, which limits the possible compositions, whereas in sheet lamination it is possible to construct the part by functionally graded materials in a flexible way.

6.2 Preliminary Investigation of Continuous Fibre Layers in CFAM

CFAM process has been developed for discontinuous carbon fibre fabric materials as they are easier to post-process using the sandblasting process. Removal of the excess carbon fibre for continuous layers has not been performed with any of the sheet lamination techniques previously. To be able to understand the challenges, a preliminary investigation has been carried out with trial samples. Section 6.2 presents the results derived from different types of continuous carbon fibre reinforced polymer samples.

6.2.1 Materials and method

Unidirectional, twill and plain weave carbon fibre supplied by Easy Composites have been used. It has been found that HP Deskjet 4130 inkjet printer was not suitable to print on the dry fabrics through since the fibres would become separated during the process, unlike the discontinuous fibres. This led to the fabric being wrinkled and resulted in jams in the printer. Therefore, the JetLab IV inkjet printer has been used to print on the continuous layers. The surface treatment mentioned in Chapter 3 has been applied to avoid the spread of ink. Squares of 10 x 10 mm have been printed onto unidirectional fibre fabric layers with 300 DPI settings to match the HP Deskjet medium printing setting. 16 layers were aligned and stacked together. A hot press was applied using 0.9 MPa pressure for 30 minutes as has been done in Chapter 4. Figure 6.1 shows the printed layers and the final compressed part after an attempt of post-processing with sandblasting.

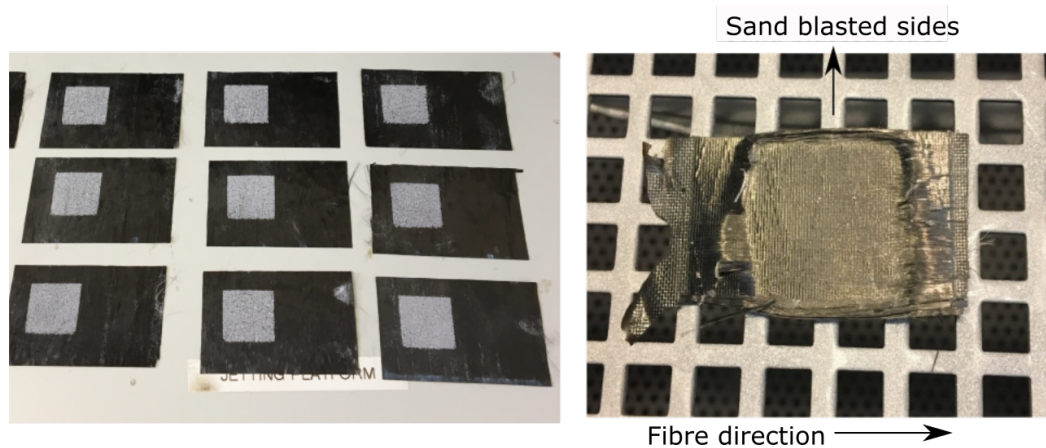


Fig. 6.1 (a) Printed unidirectional carbon fibre layers, (b) final unidirectional part after sandblasting process

As it can be seen in Figure 6.1, the sandblasting process was successful for the edges in the same direction as the fibre. However, the excess material with edges perpendicular to the fibre orientation could not be easily removed. Powder expansion along the fibre direction could also be observed due to the pressure applied. Twill weave carbon fibre reinforced parts were not easily sandblasted either. Therefore, a water jet cutting process has been used instead of sandblasting to extract the specimens from the laminate with the aim of performing characterization of the final parts.

6.2.2 Characterization

Tensile tests have been performed utilising a Tinius Olsen H5K5 force tester with a crosshead speed of 2 mm/min. Tensile samples have been manufactured according to ASTM D3039 standards with the dimension of 13 x 65 mm [185]. 10 layers of fibre substrate have been used for each part. ProtoMAX abrasive waterjet system (Washington, USA) was used to cut the specimens.

Skyscan 1172 Micro-CT Scanner at The University of Sheffield has been used to analyse the microstructural properties of the samples. Specimens have been prepared with the dimension of 5 x 10 mm. They have been mounted on a pillar securely and stabilised in the correct position to get the cross-sectional view of the specimen. After screwing the chuck into the stage of the CT machine, the scanning parameters have been altered. For the specimen with a size of 5x10 mm and pixel size of 4.35 μm , scanning took 9 minutes. Scan results have been reconstructed using the NRecon software. Cross-sectional images are selected and prepared for reconstruction. To measure the porosity, CTAn software is used. After the

selection of the desired area, a binary selection preview is used to change the image to black and white. Raw and binarized images are compared by adjusting 37 the binary threshold value. Once the best match is found, the porosity analysis is performed. Since the binary selection might affect the result significantly, the average of 3 different threshold values has been taken.

6.2.3 Results and discussion

Figure 6.2 shows the cross-sectional section of twill weave and unidirectional fibre reinforced nylon parts as obtained from CT scans. The total porosity was found as 31.7% and 26% from 2 specimens with twill weave carbon fibre. It can be observed that both large and small void formations occurred where the layers are bonded together. Micro size voids inside the thermoplastic powder have also been observed. Since the edges of the part present a significant number of separated fibres, the layers cannot be seen clearly. When the same procedure is repeated for the parts with unidirectional fibre, a more uniform structure is observed. The total porosity was found as 19.5% for the specimen with unidirectional fibre, which is much lower due to the better compaction of UD layers.

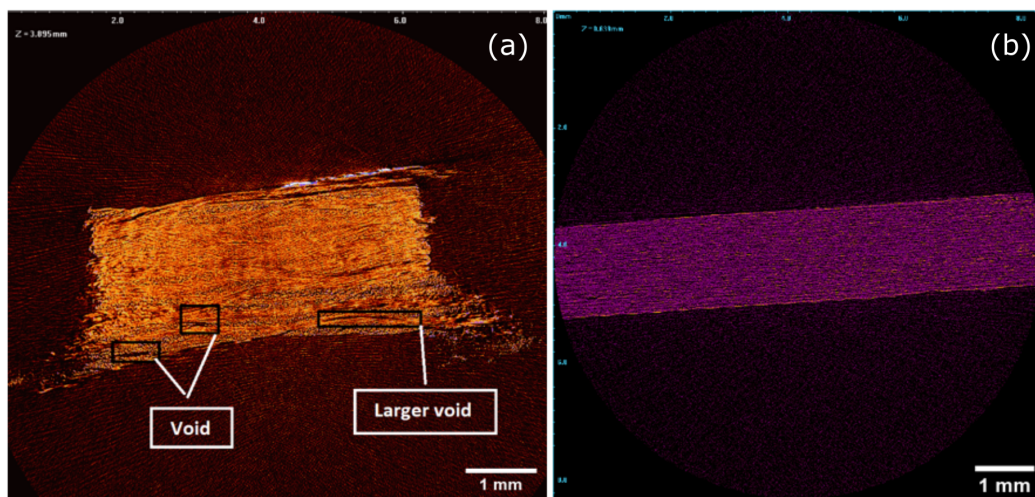


Fig. 6.2 X-ray CT investigation of (a) twill weave and (b) unidirectional carbon fibre parts

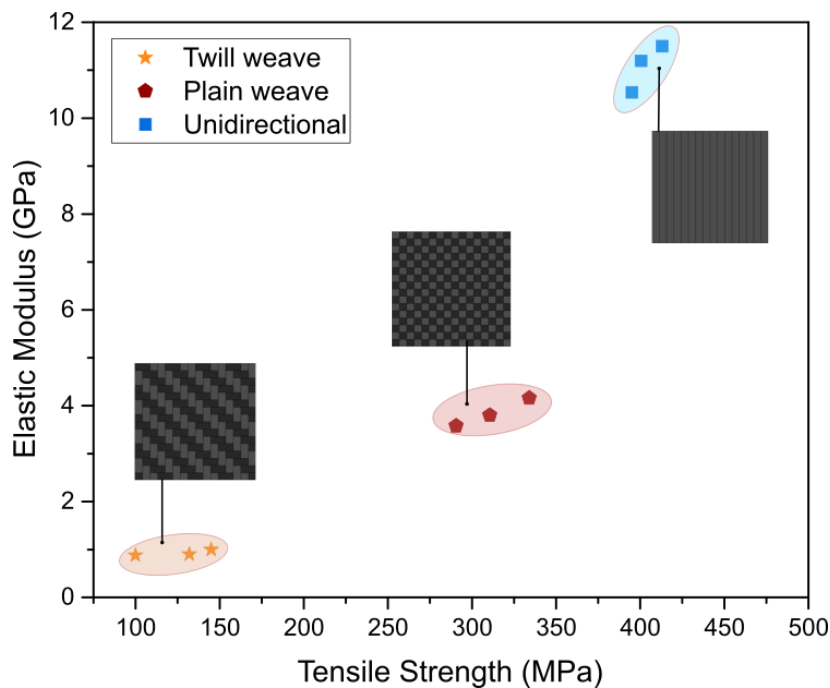


Fig. 6.3 Tensile properties of twill, plain and unidirectional CFRP parts

Figure 6.3 shows the tensile properties of continuous CFRP samples manufactured with different types of fibre fabric. The breakage during tensile testing occurred in the middle of the gauge, which means the stress concentration was accurate. Compared to the tensile properties of discontinuous carbon fibre samples established in Chapter 4 (97 MPa strength and 8.90 stiffness), the use of twill weave improves the tensile strength by only 28% up to 125 MPa while the average stiffness of the samples is reduced to 0.92 GPa, which is a result of insufficient impregnation of the fabric. Plain weave samples have average strength and stiffness of 311 MPa and 3.84 GPa respectively. The improvement in mechanical properties can be attributed to the plain weave sheets having a higher wettability compared to twill weave. Fabric stability makes it harder to shape it under compression, however, the stability also improves the tensile properties by maintaining the fibre orientation and weave angle. Finally, the samples with unidirectional fibre have the highest average of tensile strength and elastic modulus with 402 MPa and 11 GPa, thanks to the fibre orientation in the same direction. The properties are worse than those of traditional unidirectional composites due to the high porosity (19.5%). The drawback of unidirectional fibre is the difficulty of handling during the manufacturing process. The traditionally made UD fibre parts are usually supported with woven fabric sheets at the top and bottom layers to avoid the UD fibre falling apart or pull up. Separation of the fibres during the printing was also one of the problems encountered in the CFAM process. To be able to produce complex shapes, the flexibility and

ease of post-processing of the fibres are important.

Even though the tensile properties are improved significantly, removal of excess fibre is difficult in CFAM continuous fibre reinforced parts. Using a stronger type of blasting media and higher blast pressure might be helpful. However, obtaining a smooth surface finish and a high resolution of the final part geometry would remain as a challenge. Furthermore, a high amount of inner porosity between the layers causes likely low tensile strength and stiffness compared to the conventional carbon fibre manufacturing.

In SLCOM and LOM processes, the continuous CF sheets are cut prior to the bonding, therefore a complex geometry can be achieved. The CFAM system can potentially adopt this approach to create hybrid structures with the composition of discontinuous and previously cut continuous layers. This would be a way of achieving parts with higher strength and stiffness while maintaining the geometric complexity with overhanging structures.

In conclusion, the results show that using pure continuous fibre in the CFAM parts can exhibit and increase in the tensile strength up to 402 MPa, which is similar to the continuous fibre reinforced polymer parts made by Markforged FDM. However, the CFAM process aims to create complex-shaped parts without the need for cutting operations. Using a hybrid approach, previously cut continuous carbon fibre sheets between the discontinuous layers, might be a solution to achieve high-performance complex composites in an efficient way.

6.3 Investigation of Hybrid Carbon Fibre Layers in CFAM

In this section, a combination of carbon fibre fabric sheets, including continuous and discontinuous layers has been used to manufacture hybrid composite parts with the CFAM technique. The sand blasting process was found to be challenging with the pure continuous layers, therefore the aim of the experiments conducted as part of this section is to understand if the hybrid layers have an impact on the ease of post-processing of final parts. Understanding the challenges of adopting hybrid fibre approach may be a way forward to develop an hybrid manufacturing process incorporating LOM and CFAM.

6.3.1 Materials and methods

Discontinuous carbon fibre sheets with 16.95 gsm supplied by ACP Composites and unidirectional carbon fibre dry fabric supplied by Easy Composites have been used to create hybrid

composite parts. Surface treatment with water repellent spray has been applied prior to printing. Droplet imaging has been performed using the jetting station with the micro-syringe dispenser. Droplet behaviour on the unidirectional carbon fibre sheets has been inspected and contact angle has been measured using the ImageJ software as mentioned in Section 3.2.1.

HP Deskjet 4130 thermal inkjet printer has been used to print with 600 DPI settings (423 pL ink per mm) for hybrid sample manufacturing. To avoid the jamming of the printer, sheet wrinkling or fibre separation, the continuous fibre sheets were attached on 100 gsm inkjet paper using masking tape prior to printing at the edges of the sheet.

Figure 6.4 shows the three laminates manufactured with different compositions. The percentages refer to the ratio of the continuous fibre sheets to the total number of sheets. Laminate 1 consists the dog-bone (Type 1B specimen in ISO 527-4) printed layers with the aim of testing the sandblasting process with hybrid approach. However, the hybrid lamination and using little number of continuous fibre sheets did not show any improvement in sandblasting. Since the continuous fibre sheets were very well compressed with the discontinuous ones, it was hard to remove the excess fibres. Therefore, Laminate 2 and 3 were produced to be post-processed with water jet cutter. A 148 x 210 mm rectangular were printed on the sheets, covering the whole surface, followed by stacking the sheets.

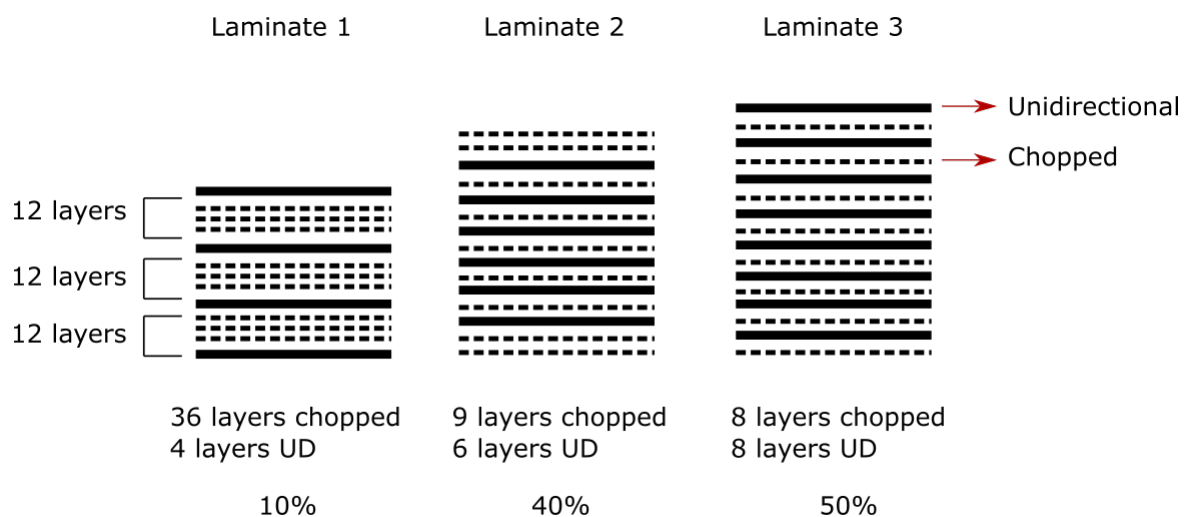


Fig. 6.4 Hybrid laminates manufactured with different compositions and stacking sequences

The hot press process was applied using the optimized parameters for discontinuous fibres; 0.9 MPa pressure and 2 hours of compaction time. Then, the tensile specimens with the dimensions of 150 x 12 mm rectangular coupons were cut and extracted from the compressed

laminate using the ProtoMax abrasive waterjet cutter. ASTM D3039 standard was followed since the standard enables the use of appropriate end-tabs for continuous fibre reinforced parts. End tabs are necessary for the samples in which the continuous fibres are dominant since the friction between the grips and the sample is important to avoid any premature failure. It has been observed in the preliminary experiments that there is a need for end tabs in this experiment even if the continuous layers are not at the outer sides. Therefore, end tabs were manufactured with manual lay-up of continuous prepreg carbon fibre material.

Figure 6.5 shows the specimens and the angled laminate manufactured for end tabs. The angle was obtained by laying up the layers as slightly offset. To improve the bonding between the specimens and end tabs, the contact surfaces between the sample and the tabs were abraded using 120 grit sandpaper. Roughening the surface increases the friction and provides better attachment to the grips. The sanded surfaces were then cleaned with isopropyl alcohol prior to the bonding.

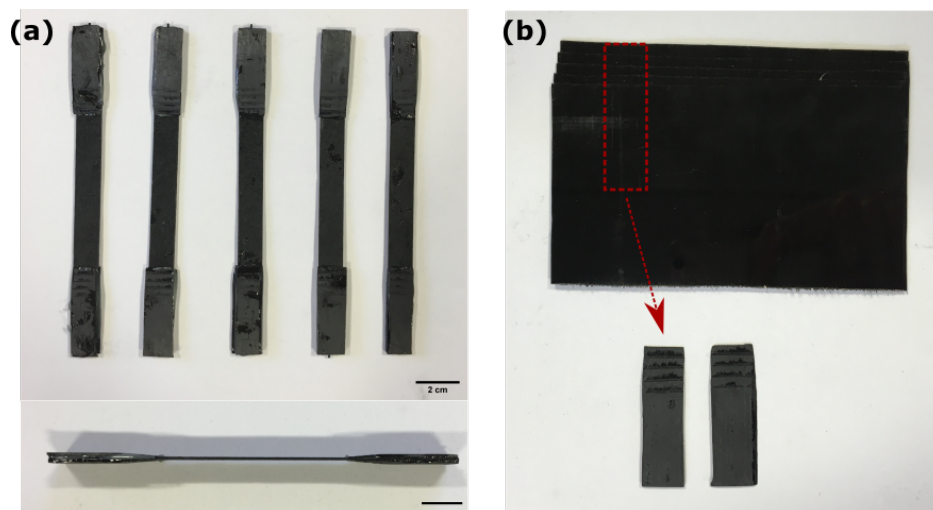


Fig. 6.5 (a) Hybrid tensile test specimens, (b) end tab preparation (scale bar shows 2 mm)

Short beam shear test samples were prepared from Laminate 3 to test the interlaminar bonding of discontinuous and continuous carbon fibre layers. The dimensions were 20x10 mm according to the BS EN ISO 14130:1998 standard. 5 samples cut in different directions were tested. Microstructural analysis was carried out by using X-ray CT and optical microscopy. 10x10 mm rectangular bar with 2 mm thickness was waterjet cut from the Laminate 3 to be cold mounted. Grinding and polishing processes were applied to examine the cross-section of the samples with a Nikon Eclipse ME600 optical microscope. X-ray CT samples were

extracted from the laminate using a 5 mm diameter punch. Scanning parameters and X-ray CT software that were mentioned in Section 3.3.2 were used for hybrid samples as well.

6.3.2 Results and discussion

Contact angle measurements

Fibre-matrix interface is heavily affected by the droplet substrate interaction. The contact angle is a good indication of characterizing the droplet behaviour on the substrate. The surface wettability, spreading of the ink and penetration of the matrix material to the substrate can be analysed by contact angle measurement. It has been observed that the printed ink does not get absorbed on the continuous carbon fibre due to the fibres being densely packed and therefore the material being less porous than the chopped fibre sheets, however, the ink spreads along the direction of the fibre, which affects the resolution of the printing. Hence, the surface treatment has been also applied to continuous fibre sheets to make the substrate a hydrophobic surface, providing stable droplets. Figure 6.6 presents the contact angle analysis of a droplet dispensed on a continuous carbon fibre fabric, which was calculated as 154° . It is 42° higher than the one on a discontinuous carbon fibre sheet. It is known that the droplet evaporation rate on a hydrophobic surface is correlated with the droplet height, which is higher in the droplets that have higher contact angle [186, 187]. Negligible wetting of the substrate causes an increase in the evaporation of droplets, whereas there is less evaporation if the droplet has more surface contact area with the substrate [188]. There is less amount of powder that remained attached to the printed surface as compared to the discontinuous carbon fibre, which can be attributed to the higher contact angle.

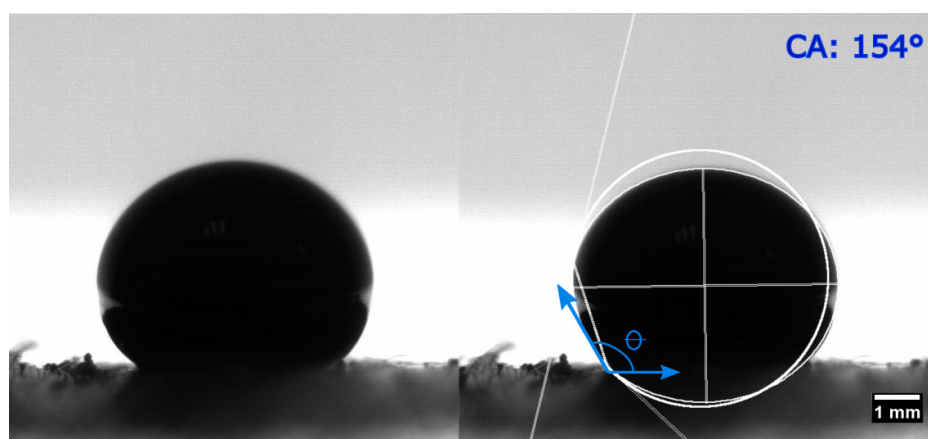


Fig. 6.6 Contact angle measurement for the droplet printed on unidirectional fibre

Microstructural properties of hybrid parts

Figure 6.7 gives X-ray CT scan-obtained images of a hybrid composite specimen manufactured from Laminate 2 with 40% continuous, and 60% discontinuous carbon fibre fabric sheets. Unlike the chopped fibre specimens analysed in Section 4.3.2, the carbon fibre volume fraction has been found to be difficult to be calculated for the hybrid samples. The top view of the specimen presents a transition from a discontinuous layer to a continuous, which is a result of a slope during an X-ray CT scan. The cross-sectional view also shows this angle. Fibre segmentation is not reliable due to the differences in the densities of continuous and discontinuous fibres. However, the percentage of porosity is calculated as 22.4% and pore segmentation is visualised with 3D pore distribution as shown in Figure 6.7(c). The porosity result derived from stitched optical microscopy images is 24.5%. Figure 6.7(d) shows one of the stitched images. The majority of the high volume pores are formed between the continuous and discontinuous fibre layers. This could be a result of negligible wettability of the unidirectional layers themselves. Small pore formation still occurs where the discontinuous carbon fibres interact with the polymer powder.

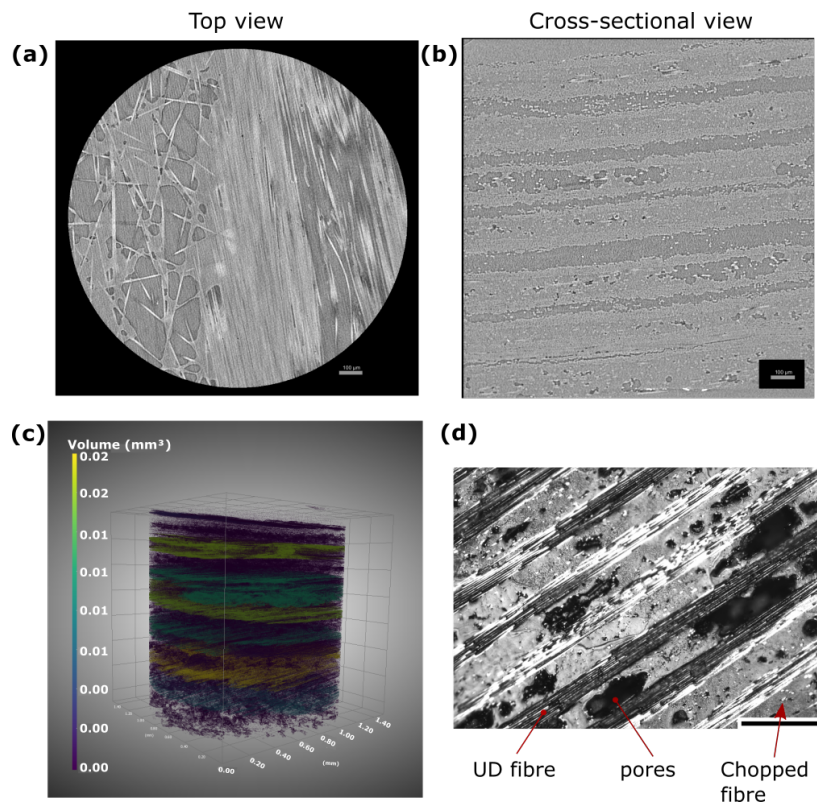


Fig. 6.7 X-ray CT imaging of hybrid specimen with 40% UD (a) Top view , (b) cross-sectional view, (c) 3D pore distribution with segmentation, (d) optical microscopy imaging (scale bar shows 500 micron)

Tensile properties of hybrid parts

Figure 6.8 shows the tensile strength and stiffness of each type of laminate. As expected, tensile properties are improved with the addition of unidirectional carbon fibre in the same direction as the fibre. Hybrid specimens involving 4 layers of UD carbon fibre (10%) provide a 94% increase in tensile properties due to the addition of continuous layers by reaching 188.7 MPa compared with the 97 MPa achieved for the discontinuous CFRP samples examined in Chapter 4. When the UD layers are 40% of the total number of layers, average tensile strength and stiffness are 422 MPa and 22 GPa respectively, which exceeds the properties of pure unidirectional carbon fibre samples made by the CFAM process. However, the properties are reduced to 242 MPa tensile strength and 11 GPa elastic modulus, when the fibre content is increased to 50%. It can be deduced that if the UD fibre content increased beyond 40%, there is a detrimental effect on properties due to high level of delamination.

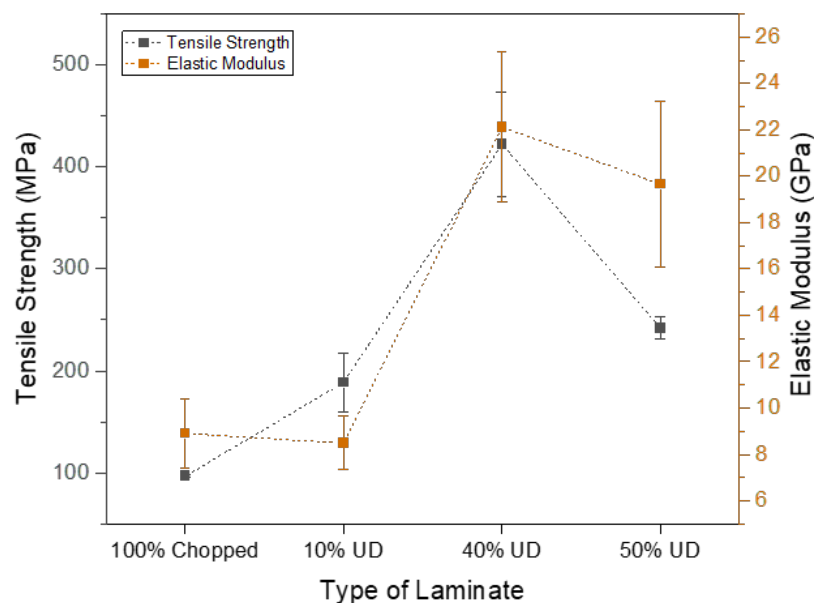


Fig. 6.8 Tensile properties of hybrid laminates

Figure 6.9 shows the stress-strain graphs for each specimen obtained from three types of laminates. Even though the graphs show the breakage of the samples, tensile testing of Laminate 2 (40%) and Laminate 3 (50%) did not result in clearly broken specimens. The interlaminar delamination between the UD and discontinuous fibres due to poor bonding caused a slip, which was reflected as a failed specimen to the tensometer. All the repeats ended up with a similar failure mode around the grip area as GAT (Grip/At grip/Top) and LIT (Lateral/Inside

gip/Top) according to the standards given in Appendix B. However, specimens from Laminate 1 (10%) failed in the middle of the gauge area as XGM (eXplosive/Gage/Middle).

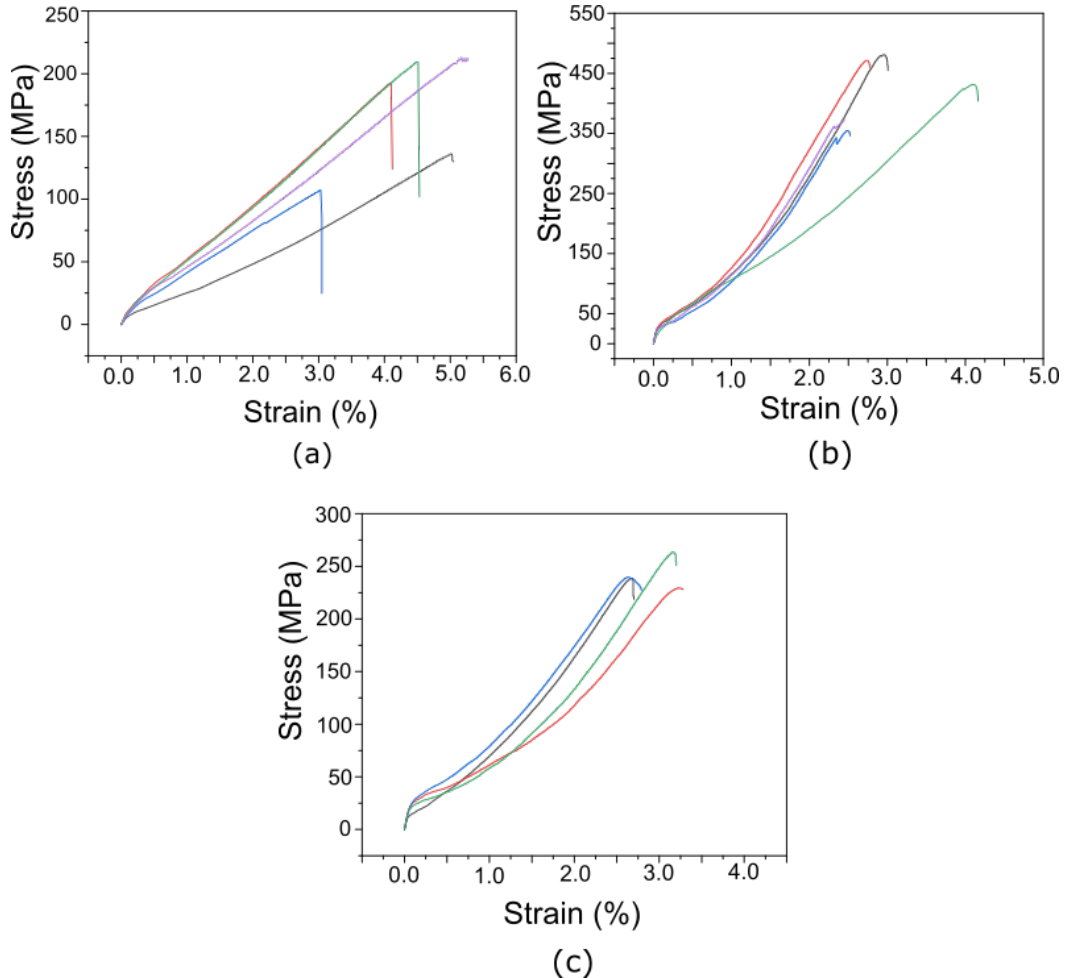


Fig. 6.9 Tensile stress-strain graphs of hybrid specimens; (a) 10% continuous, (b) 40% continuous, (c) 50% continuous

The axial cracks that occurred in the samples from laminate 2 and 3 are the result of relatively low shear strength. In the UD composites, there are many important parameters such as the tab taper angle, tab length, type of adhesive and the specimen thickness to create a stress concentration in the middle of the specimens. Although end tabs were manufactured according to the standards, these factors might have influenced the results as well due to the insufficient friction between the end tabs and the specimen. However, the low tensile strength and stiffness in the specimen with 50% UD compared to the specimens with 40% UD can be explained by the low shear strength between the UD and chopped carbon fibre. The higher level of UD-chopped weak layer interaction in the samples consisting 50% UD fibre reduces the strength.

Interlaminar properties of hybrid parts

Figure 6.10 shows force-displacement curves obtained from short beam shear testing of Laminate 3 samples. It is not feasible to acquire one general shear strength from the test results since the failure behaviour of the hybrid materials is very different from the single material behaviour. Hader-Kregl et al. have also observed a similar behaviour while researching inter-ply of steel/composite hybrid laminates [189]. It is necessary to divide the graph into 2 phases since these phases are representative of different regions of interest during the test. The first phase is where the clear visible delamination occurs between the continuous and discontinuous layers. The force required to generate a displacement plateaus once the layers delaminate during Phase 1. If force is continued to be applied, the discontinuous layers withstand plastic deformation in Phase 2, which is also indicated by an increase in the force required to achieve further displacement. Once the shear or compressive failure occurs in the chopped layers, the test ends. Espadas-Escalante and Isaksson also observed these two characteristic curves and the authors determined that the delamination is likely to occur in the first load drop [190]. The large scale delamination between the UD and chopped layers is shown in Figure 6.11. While the left part of the specimen also delaminates, the middle point stays intact.

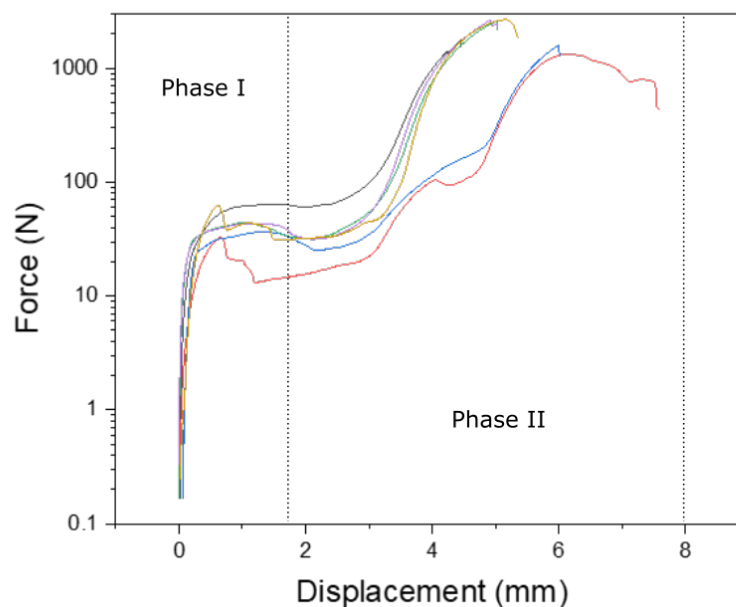


Fig. 6.10 Force-displacement curves from shear test of hybrid samples

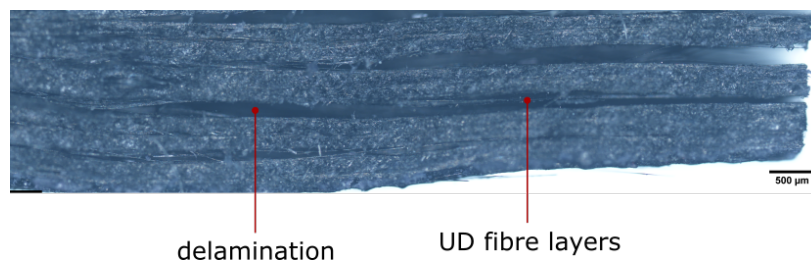


Fig. 6.11 Shear failure in hybrid composite short beam shear test specimen (50% continuous fibre)

6.3.3 Conclusion

In this section, the feasibility of adopting continuous carbon fibre layers into the CFAM process has been investigated. Three types of specimens were manufactured using twill weave, plain weave and unidirectional carbon fibre substrates. The specimens were then characterized using tensile testing and Micro-CT. As expected, the sand blasting process was found to be not suitable for the removal of strong continuous fibre layers. It was easier to separate the fibres with the blast media in the same direction, however it was not possible to cut through across the fibre for partly compressed excess layers. Tensile testing samples were created with the help of a water-jet cutter. Unidirectional carbon fibre reinforced parts showed the highest tensile strength and stiffness, similar to the properties of FDM continuous carbon fibre reinforced parts. The parts have been found to have high porosity content which is again close to the porosity percentage in FDM parts. The difference between FDM and hybrid CFAM is that the cutting operation does not allow to build complex shaped parts.

Therefore, hybrid parts composed of discontinuous and continuous carbon fibre fabric layers were investigated. The suitability of little number of continuous layers in between the discontinuous layers to the sand blasting process was tested. Microstructural characterization showed a high amount of porosity at the interface of UD and chopped layers, which caused poor interlaminar bonding. Contact angle measurements also proved that a relatively low level of wettability in the UD layers is the source of poor impregnation. Mechanical tests results revealed that hybrid samples exhibit different failure mechanisms and it is not possible to make a reliable comparison. However, it can be deduced that the tensile properties of the hybrid specimens increase with the inclusion of a limited number of UD layers. The poor interfacial bonding starts to influence the performance of the parts negatively when the number of UD threshold is exceeded.

To solve the sand blasting process issues with the continuous carbon fibre, the UD fibres

can be cut according to the 2D slice and printed prior to the bonding similar to the LOM and SLCOM processes. The discontinuous carbon fibre reinforced sample created with the CFAM approach, can be wrapped by the previously cut continuous fibre to increase the impact and tensile properties of the final parts. A debulking process can be applied to bond the top/bottom continuous fibre layers and the specimen.

Chapter 7

Quality Inspection of Complex-shaped CFAM Parts

Summary

This chapter presents the final step of benchmarking a novel manufacturing system, which is investigating the dimensional accuracy and quality of final products. First of all, a short literature review on geometric tolerances of additively manufactured parts and the characterization techniques that have been used are given. Then studies focused on the dimensional accuracy of composite AM parts so far are summarized.

Secondly, the experimental section elaborates on the design of a drone frame to create a benchmark specimen. A comparison of tolerances in CFAM, High Speed Sintering (HSS) and FDM parts is presented. Different types of filaments containing carbon fibre or nylon are used to print using an open-source 3D printer. 3D scanning as a characterization method for dimensional tolerances is examined. Small features that are not reliable to be measured by 3D scanning are investigated with linear measurements.

Finally, the maximum force that can be applied to the drone frames is tested using a four-point bending rig with the aim of comparing the deformation behaviour of the final parts produced with different AM techniques.

7.1 Introduction

Although the complexity level of printed net shape components is one of the main advantages of AM techniques over conventional methods, printable geometric features are still limited [191]. The deviation in the dimensions of AM parts is found to be higher than in the traditional manufacturing processes such as injection moulding, casting and forming, due to the varying process parameters [192, 193]. The dimensional accuracy is one of the important characteristics of a part for it to be considered as an end-use product. Therefore, AM needs to develop to overcome these design restrictions for standardized mass production [194]. However, the characterization techniques used for dimensional accuracy are still in progress for new AM processes and little information is currently available in the literature.

Studies mainly focused on FDM and powder bed fusion processes for analysing the effect of process parameters on the physical quality of final parts. The printing parameters in FDM such as build orientation and layer thickness found to be significantly influential on dimensional errors [195, 196]. Overall, the shrinkage and warpage of the specimens due to the material solidification process and polymer composition in FDM were the most observed negative impact on physical properties [197].

Sood et al. analysed the effect of FDM process parameters on the dimensional accuracy of ABS parts by using Taguchi's design of experiments [198]. Shrinkage was observed in the overall length and width of the parts; however, the thickness of the part was higher than the desired value. Mahmood et al. demonstrated that the deviation from nominal dimensions in FDM parts increases as the size of the measured feature is increased [199]. Measurements taken from the features like holes showed higher deviation compared to the other geometric elements. Lieneke et al. determined experimental tolerances using the ISO IT grades standards [194]. These standards have been used in [133] to evaluate the dimensional accuracy of parts printed with three different AM systems; FDM, powder bed fusion and material jetting, in which characterization processes for analysing the geometrical accuracy of AM parts have been reviewed and discussed. Another research compared the performance of different powder bed processes and investigated the effect of machine parameters on the dimensional accuracy and tolerances of parts [191]. CT scan and 3D laser scanning were used to analyse the outer and inner features. Both techniques were found to be successful to determine the tolerances, although the 3D scanning had missing points due to the features standing too close to each other. CT scan was more effective to measure the inner parts.

Previous research has commonly been carried out on unreinforced polymer AM. The characterization of dimensional accuracy of composite parts made with AM processes has been analysed to a lesser extent, as benchmarking of composites in AM has only recently emerged. Chopped carbon fibre reinforced parts printed by Markforged MarkTwo were investigated for the first time in terms of dimensional accuracy by Yasa et al. [200] in 2019. The ability to print thin walls has experimented with different wall thicknesses. It was found that as the wall thickness is decreased, the deviation from the desired value is increased. No comparison study between the nylon and carbon fibre reinforced nylon parts has been carried out. In 2020, unreinforced PLA parts and PLA-graphene nanoparticle composite parts printed by FDM were compared in terms of geometric properties [201]. The variation between the compared parts was not significant. Composite parts provided better mechanical properties without an effect on the geometrical accuracy. A similar result was reported by Reverte et al. confirming that the addition of short carbon fibre to the polymer in fused filament fabrication did not affect the dimensional accuracy of the final parts, in adverse it improved Reverte2020.

In this chapter, complex-shaped composite and polymer drone frames are produced with FDM, SLS, and CFAM to evaluate geometrical accuracy. The drone frames are also tested to investigate the load resistance by applying force on 4-point bending equipment. The aim is to understand the deformation behaviour of end-use composite products in AM under a controlled compression.

7.2 Methodology

7.2.1 Materials and manufacturing

Specimens used in this chapter were built using FDM and HSS to compare their dimensional accuracy with the CFAM parts. A central printed circuit board (PCB) plate of a drone frame was designed in Autodesk Fusion 360 with relatively complex geometrical features, including curves, concentric circles, thin bridges and small holes. Figure 7.1 shows the design and the inspired application with similar geometry. Different types of filaments composed of carbon fibre and nylon were printed using an open-source material extrusion 3D printer. Although the fibre volume fraction information is not available for most of the filaments, the brand names and the material content information is given in Table 7.1. Prototypes 1 to 5 were produced with FDM, while Prototype 6 composed of Nylon 12 was produced with HSS facilitated in The University of Sheffield (TUoS). The last row shows the Prototype 7

produced with CFAM. Detailed information about the bulk properties of materials used for manufacturing and pictures of prototypes 1 to 6 are presented in Appendix C.

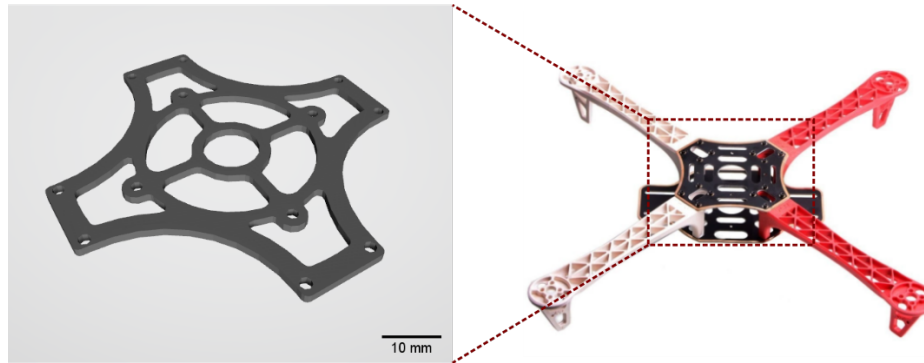


Fig. 7.1 Design of the central PCB plate in drone frame and the inspired application (F450 Quadcopter Frame [202])

Table 7.1 Types of manufacturing techniques and materials for the drone frames

Part Name	Manufacturing Technique	Filament/Material Brand	Material Content
Prototype 1	FDM	AddNorth Adura Cold White	Nylon (copolyamide)
Prototype 2	FDM	AddNorth Adura X Black	Carbon fibre reinforced nylon (Content is not available)
Prototype 3	FDM	Polymaker PolyMide PA6-CF Black	20% carbon fibre reinforced PA6
Prototype 4	FDM	Prusament PC Blend Carbon Fibre	Polycarbonate blend filled with recycled carbon fibre
Prototype 5	FDM	Polymaker PolyMide CoPA Nylon Black	Copolymer blend of Nylon 6 and Nylon 6,6
Prototype 6	HSS at TUoS	EOS Gmbh PA2200	Nylon-12
Prototype 7	CFAM at TUoS	ACP Composites Carbon Fibre Surfacing Veil, EOS Gmbh PA2200	Carbon fibre reinforced Nylon-12

7.2.2 3D scanning and measurements

Einscan 2X, CN, which is a triangulation-based system, was utilised to perform the 3D scanning of the samples only with carbon fibre reinforced polymers. Specimens were placed on a turntable base with a clamp to take a 360° scan as shown in Figure 7.2. The images were post-processed using Shining 3D software, in which the defects were repaired and the geometry was cleaned from the noise. The final performance of the parts and tolerances were investigated with Autodesk PowerInspect Software, in which the original STL file and the prototype scans in STL format were synchronized using cloud points. An upper and lower tolerance of ± 0.2 mm was used as the base level to compare the nominal and scanned dimensions. FDM desktop printing processes have ± 0.5 mm tolerance limit, while industrial FDM printers have ± 0.2 mm due to the shrinkage and warping problem [203]. Markforged determine the free fit tolerance as ± 0.1 to ± 0.2 mm for the carbon fibre reinforced polymer parts [204]. SLS processes allows more deviation in the design for the polymer parts which is ± 0.3 mm due to shrinking. Therefore, ± 0.2 mm tolerance limit was selected to do a performance analysis in this study since it is an average standard for different techniques.



Fig. 7.2 Einscan 3D scanner set-up

In addition to 3D scanning, manual measurements were taken using a standard measurement equipment. Three different measuring points were determined considering the key design parameters as shown in Figure 7.3. The accuracy of the inner and outer diameters of the central circle (M1 and M2) is important for the components to fit properly. Even though the compatibility of small holes to the thread is critical for assembly, they were not considered for measurement. The deviation between the small holes in the same part is very high due to some of them getting blocked during printing, which does not give a reliable result. The

holes are need to be treaded as well, so they would need further post-processing. Instead, the distance between two small holes (M3) was measured. These measurements were then used to classify the manufacturing processes into IT classes according to the BS EN ISO 286-1 standards [205]. Figure 7.2 shows the standard tolerance grades for the ranges that have been measured in this study. The tolerance grades provide a great guidance for determining whether the manufacturing process is suitable for the desired product dimensions. For instance, the injection moulding process parts result in IT13 tolerance grade which is not sufficient for a part that requires IT8.

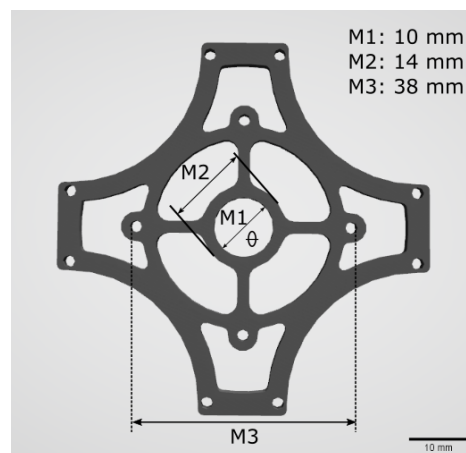


Fig. 7.3 Points of measurements and nominal values for tolerance performance analysis

Table 7.2 Maximum deviation for international standard tolerance grades

Range		Standard tolerance grades							
Above	Up to	IT 9	IT 10	IT 11	IT 12	IT 13	IT 14	IT 15	IT 16
1 mm	3 mm	0.025	0.04	0.06	0.1	0.14	0.25	0.4	0.6
6 mm	10 mm	0.036	0.058	0.09	0.15	0.22	0.36	0.58	0.9
10 mm	18 mm	0.043	0.07	0.11	0.18	0.27	0.43	0.7	1.1
30 mm	50 mm	0.062	0.1	0.16	0.25	0.39	0.62	1	1.6

7.2.3 Load resistance test

A drone frame must be designed to withstanding the weight of components such as motor and batteries [206]. The dynamic characteristics of a Quadcopter drone frame have been

investigated using finite element analysis previously [207]. In this study, a 4-point bending test set-up was used to examine the load resistance of real-scale final parts. Figure 7.4 shows the experimental set-up using H5K Tinius Olsen hydraulic tensometer in which load and support spans were adjusted to 40 mm and 20 mm respectively. A crosshead speed of 1 mm/min was applied.

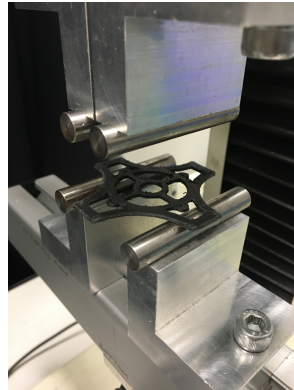


Fig. 7.4 Four point bending test for load resistance

7.3 Results and Discussion

7.3.1 Tolerance performance analysis

Figure 7.5 and 7.6 show the tolerance maps derived from Autodesk PowerInspect software for each prototype. Prototypes 2,3,4,5 and 7 (CFAM) were 3D scanned, since Prototype 1 and 6 are made of only nylon. While the green regions indicate the exact fit to the nominal dimensions, the blue and red regions represent the negative and positive discrepancy from the desired values respectively. Purple regions are the areas that could not be scanned properly due to the laser not being able to penetrate through at the right angle. For some regions, they are also a sign of high deviation or areas out of tolerance. Table 7.3 shows the mean and standard deviations also in absolute values for each prototype.

Table 7.3 Mean and standard deviations of general discrepancy for each scanned prototype

Part Name	Mean	Standard Deviation	Performance
Prototype 2	-0.011	0.161	80%
Prototype 3	-0.071	0.190	70%
Prototype 4	-0.005	0.139	86%
Prototype 5	-0.084	0.195	64%
Prototype 7 (CFAM)	-0.024	0.188	83%

Negative mean values show that the dimensions of the prototypes are generally smaller than the nominal dimensions of the original STL file. This is mainly because polymer shrinkage occurs during the printing process as mentioned in the literature. Prototype 4 with the recycled carbon fibre content has the best tolerance performance with 86% as can be also seen in Figure 7.7(a). CFAM drone frame follows prototype 4 with 83% performance. Prototype 5, which is manufactured from a Nylon 6/ Nylon 6,6 copolymer filament without any reinforcement, showed the worst tolerance performance with 64%. It has been previously found that the addition of carbon fibre to the polymer reduces the shrinkage and warpage at the final parts and affected the dimensional accuracy positively, compared to the pure polymer parts. This can be attributed to the high conductivity of carbon fibres achieving a homogeneous material solidification process and current results are in line with this observation [208, 209]. Similarly, the prototypes reinforced with carbon fibre showed better dimensional accuracy compared to the Nylon 6 and Nylon 6,6 prototype, which is a semi-crystalline polymer that tends to shrink during the cooling period.

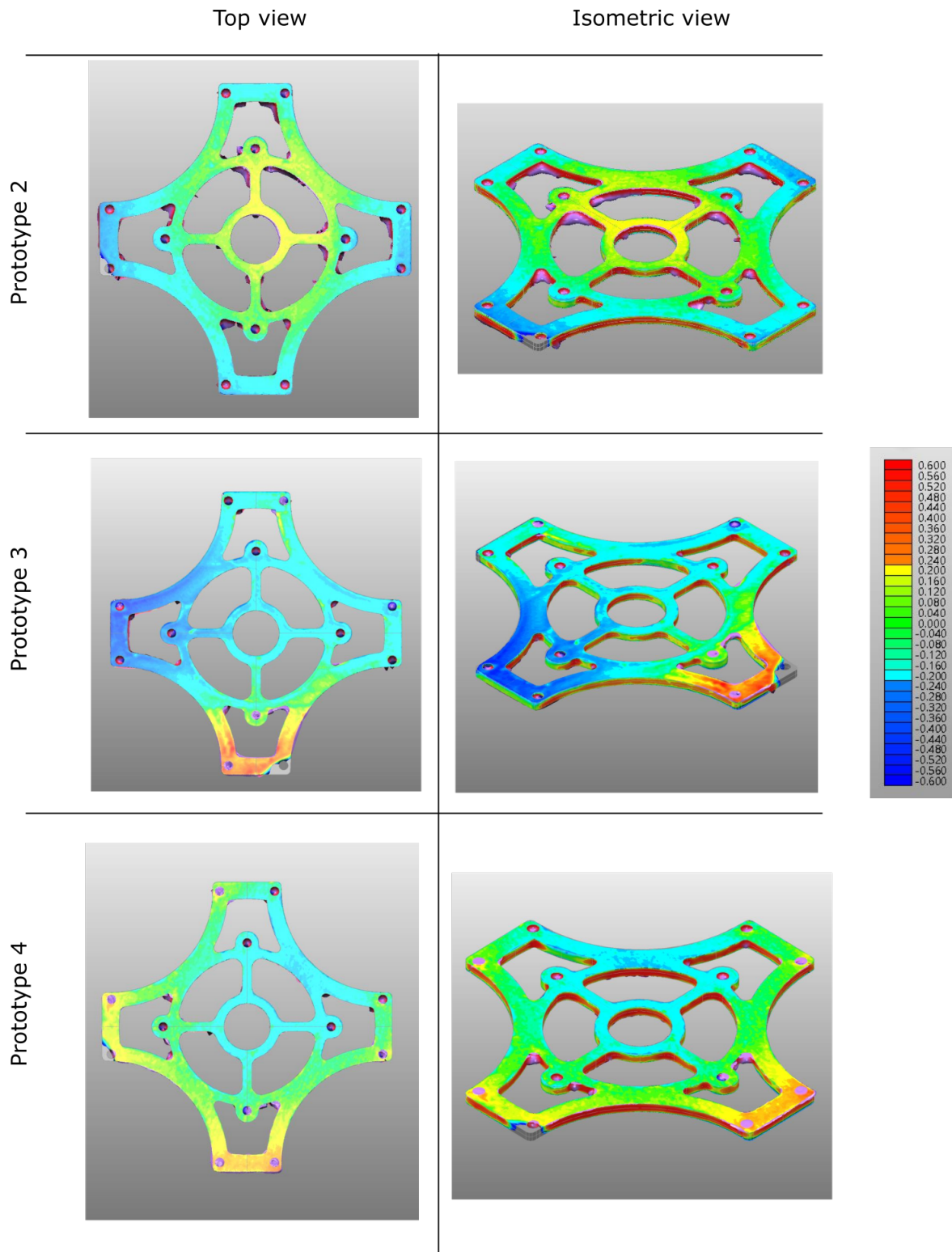


Fig. 7.5 Tolerance map of the prototypes 2, 3 and 4

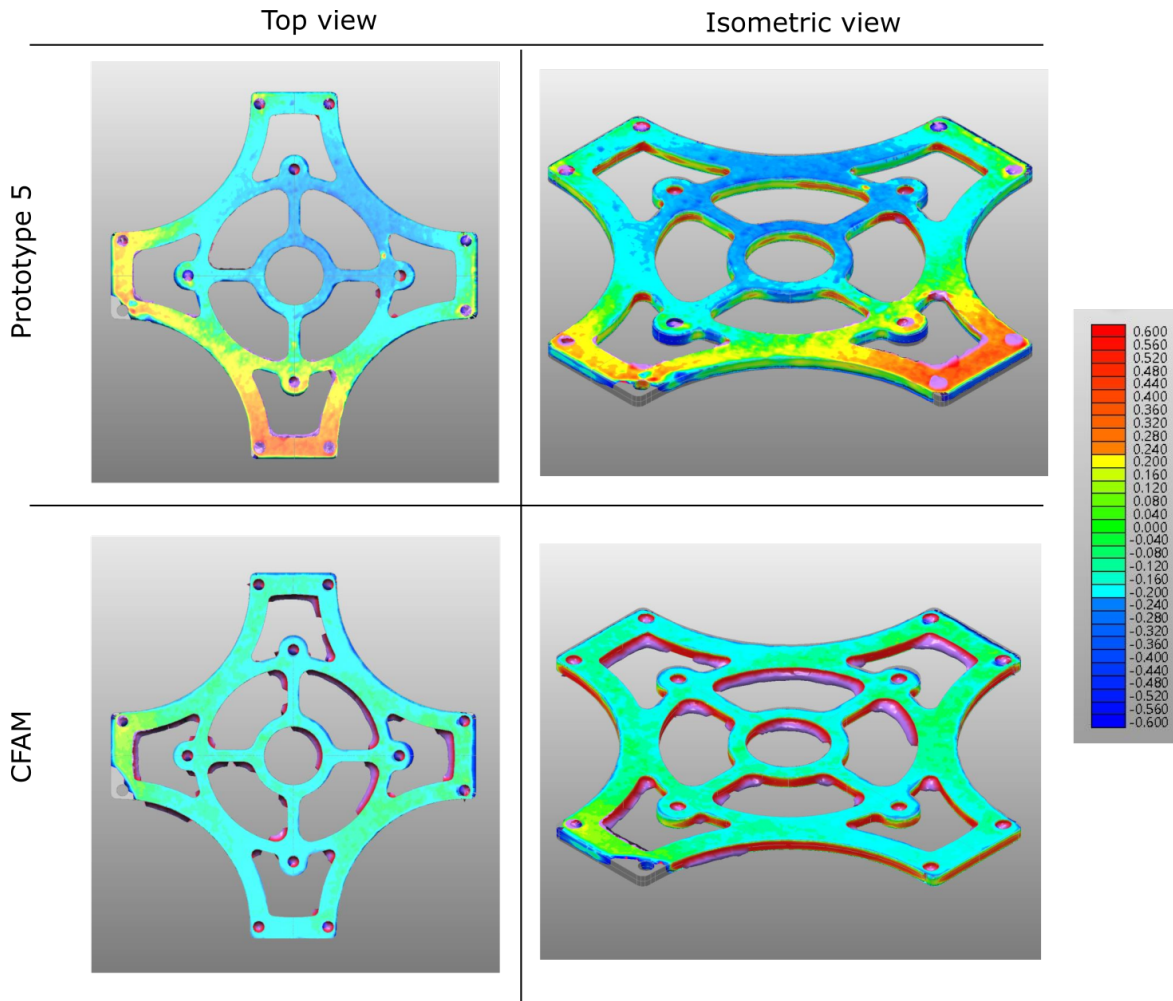


Fig. 7.6 Tolerance map of the prototype 5 and CFAM

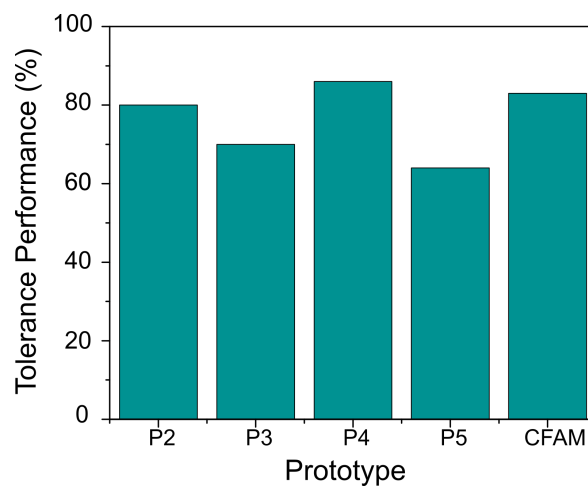


Fig. 7.7 Tolerance performance of scanned samples

The tolerance map of the CFAM prototype shows that the shrinkage occurred relatively consistent all over the part. Hot press process provides more constrained molecular chain formation by applying pressure during the cooling time, compared to the free polymer crystallization process during FDM material solidification. This result is aligned with the traditional thermoforming of thermoplastics in which the shrinkage occurs in a consistent way [210]. FEA models can be used to predict the final geometry and help in the design process. In the CFAM prototype, none of the small holes were blocked, whereas the FDM prototypes had some of them completely filled with the printed filament. The post-processing of parts was not sufficient to provide dimensional accuracy since there is still a high deviation between them. On the other hand, with CFAM, even though the general accuracy is affected by the polymer shrinkage or process parameters, the sand blasting process provides efficient and uniform removal of excess sheets.

As it was mentioned in [191] even though 3D scanning is a useful and straightforward technique to analyse the general tolerance performance for outer dimensions, the small features should also be investigated. Additionally, the amount of purple region existing in the CFAM prototype at the inner walls requires further investigation. Therefore, the linear measurements were taken manually. Three measurements from each feature were taken. Figure 7.8(a) shows the discrepancies of the selected feature dimensions from the nominal values, while Figure 7.8(b) shows the thickness variation for each prototype. The tolerances were mainly on the negative side. As it was also demonstrated in the literature, there was a correlation between the size of the feature and the standard deviation in CFAM part. As the feature size increases, the discrepancy (%) is decreased.

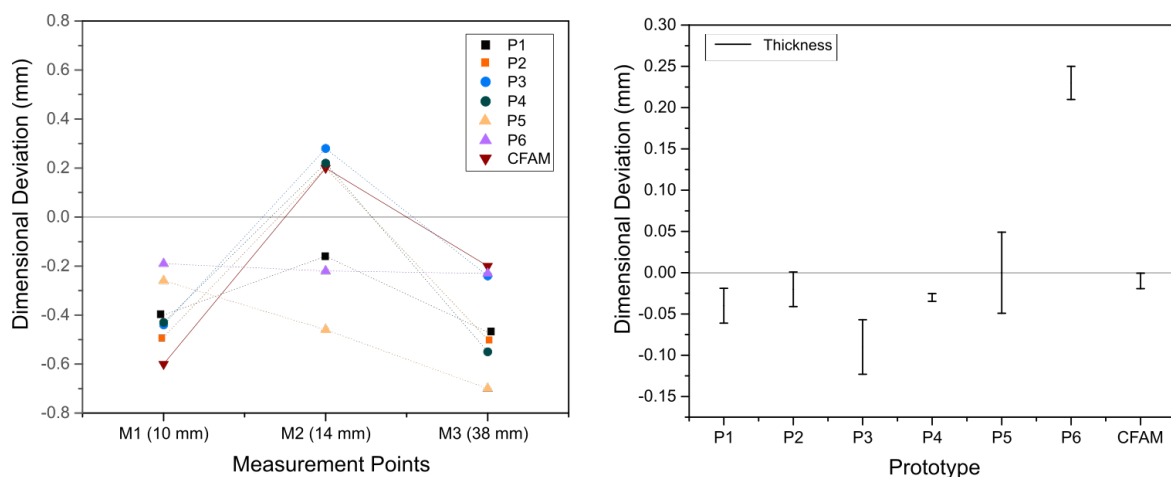


Fig. 7.8 (a) Standard deviations of selected feature dimensions (b) Thickness of each prototype and standard deviations

The thickness of prototype 6 made with a powder bed process has the highest variation, even though the feature dimensions of the part have consistent discrepancies from the nominal values in the x and y directions. CFAM part has relatively uniform thicknesses all around the component due to the hot press process having a significant effect on the thickness uniformity. Prototype 4 shows the lowest error level in the thickness measurements, which is the reason for it to have maximum performance in the 3D scanning. However, the repeatability of these results is an issue since the FDM process parameters vary significantly.

According to the standard IT grades classification, all the prototypes have been in between IT9 and IT16, which is in agreement with the grades obtained for AM parts in the literature [194]. Traditional manufacturing techniques such as casting, cutting and drilling also fall in between the similar grades, except the turning and stripping operations that have higher grade (IT7-IT8).

The tolerances for M1 (10mm) has the highest variation from IT 9 to IT 16. The tolerances for M2 (14mm) resulted in between IT13 and IT14 while the tolerances for M3 (38mm) were in the range of IT12-IT14.

7.3.2 Challenges in Manufacturing of CFAM Prototype

As mentioned in Chapter 4, the CFAM process parameters, especially pressure level, affect the thickness of the samples significantly, therefore the constant pressure must be supplied to reach the desired thickness. In the CFAM drone frame manufacturing, 1.5 mm of nominal thickness was achieved by 0.9 MPa pressure level and 20 layers of carbon fibre sheets. A higher pressure level is not recommended due to not only the low mechanical properties but also the dimensional accuracy as mentioned in Chapter 4. It has been observed that molten polymer is squeezed out of the printed region due to high pressure, which deteriorates the resolution level. Some of the small features are blocked. The pressure level of 0.9 MPa, the optimum pressure level found in Chapter 4, was again sufficient for strong bonding and high-resolution surface finish.

Furthermore, the alignment of the sheets is critical for complex geometries in CFAM. A stairstep effect can be observed in the walls of the samples which were produced without precise alignment. Figure 7.9 shows the attempts of producing the complex shaped drone frame from (a) to (d). Sample (d) was achieved by using a 4 point square alignment rig. During the inkjet printing onto the sheets, four reference circles were printed around the geometry, followed by the deposition of powder to make the circles visible. These circles were then

punctured with a 6 mm diameter single hole punch, and using these reference points, the sheets were inserted into 6 mm diameter dowels to align. Therefore, a better alignment of the printed sheets is achieved, and the sand blasting of the small features can be easily performed.

The benchmark samples showed that the dimensional accuracy of CFAM is in the same range with other AM systems, however, it can be further improved. The printing resolution can be increased by reducing the droplet size in JetLab IV system, while the volume of ink per mm can be kept constant at the optimized level by decreasing the droplet spacing. It is also possible to improve the dimensional tolerances by optimizing the post-processing operations. Blasting media of glass bead was observed to be more suitable for the removal of sheets around intricate geometries since it is not as harsh as the alumina blast media. Consequently, a better surface finish can be achieved in the final products.

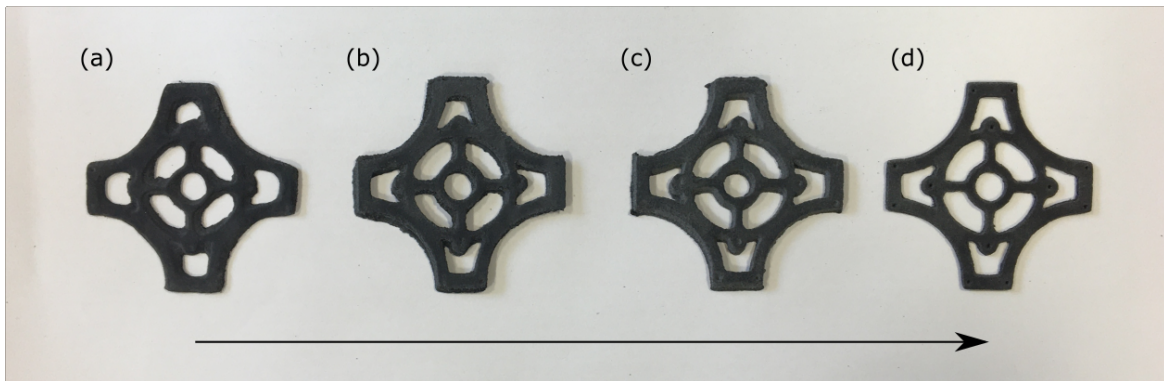


Fig. 7.9 Geometrical accuracy improvement in CFAM part with better sheet alignment from (a) to (d)

7.3.3 Load resistance analysis

The primary aim of a drone design is to achieve excellent flying characteristics. The time period that a drone frame can remain in flight mode should be maximized for a high-quality drone. Frames are made of delicate and fragile structures and it must be ensured that they are not deformed by the stresses that occur due to acceleration and motor vibration. Producing robust frames to overcome these issues causes disadvantages such as less efficient motors and batteries. Therefore, frame design needs to be optimized to have robust and resistant drones to high impact, but at the same time to be lightweight and low-cost [211].

In this section, the load resistance of the prototypes was tested in order to understand the physical responses of real-scale composite structures under compressive force. Figure

7.10 shows the load-displacement curves and the weights of each prototype. CFAM part could withstand 76 MPa maximum force with lower displacement, which was the highest among the prototypes. The maximum load that CFAM part with 15% carbon fibre can carry was higher than Prototype 3 with 20% carbon fibre content (48.6 MPa). This can be attributed to the high mechanical properties and stronger interfacial bonding that a low porosity level brings. It can be also observed that the carbon fibres were not effective to reinforce the nylon in the filament of Prototype 2 which ended up showing the same properties with nylon. On the other hand, recycled carbon fibre contributed the mechanical properties of polycarbonate significantly in Prototype 4.

It can be concluded that the CFAM part has better load carrying capability compared to the FDM parts, while it is also the lightest design.

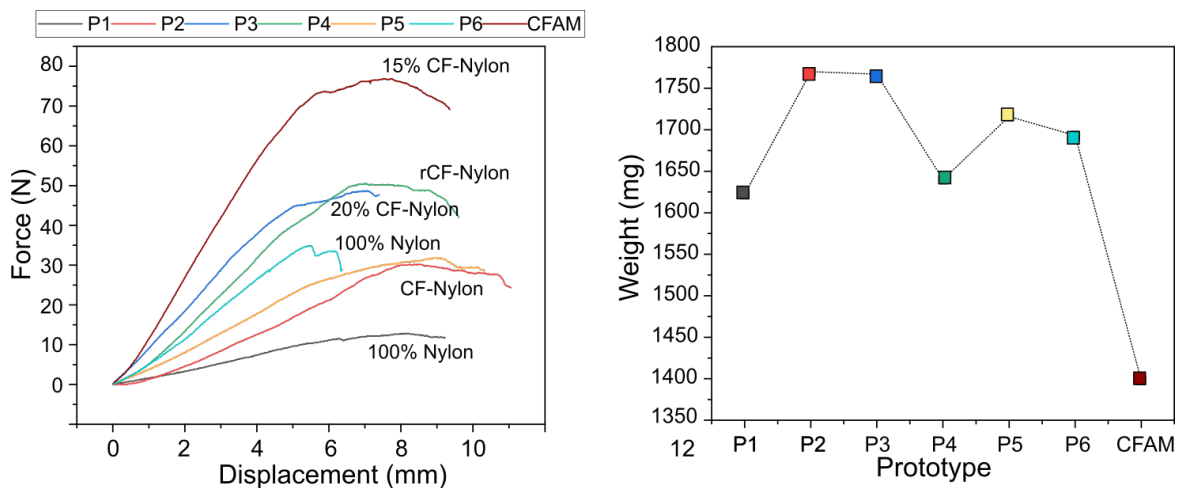


Fig. 7.10 Force-displacement profile and the weights of drone frames

7.4 Conclusion

In this chapter, complex-shaped drone frames were designed and manufactured using FDM, SLS and CFAM as a benchmark to investigate the dimensional tolerances of final AM parts. Tolerance maps were created for the prototypes including multiple material filament using 3D scanning and Autodesk PowerInspect software. The features that are key factors for the design were analysed with linear measurements. It was found that the geometric accuracy highly varies not only depending on the type of AM process and material content, but also on the selected features and their size. SLS was found to be the most accurate for the dimensions in the x and y directions. FDM and CFAM processes were compared and it has

been observed that the fibre reinforcement to the polymer in AM improves the dimensional accuracy. Although the tolerances are within the same range as FDM, the hot press process provides an additional advantage with the improved dimensional stability due to the effect of pressure during the crystallization process in CFAM. However, the alignment of the sheets and post-processing of inner features are important to have reliable end-use products. Further work should investigate the inclining and hanging geometries.

Finally, impact resistance of the drone frames were examined with four-point bending test equipment. CFAM was found to be producing the most resistant drone frame under the load, as well as the most lightweight structure.

Chapter 8

Conclusions and Future Work

8.1 Conclusions

This thesis has documented the development of a new additive manufacturing process to produce discontinuous fibre reinforced polymer composite parts, inspired by sheet lamination techniques. Current composite AM mainly focuses on FDM techniques which results in parts with low mechanical properties and high void content due to the lack of heat and pressure, unlike traditional composite manufacturing such as compression moulding and autoclave processes in which the trapped air between the layers are removed by a high level of consolidation. The presented method aims to bring those traditional composite manufacturing elements into AM, providing better interlayer bonding, therefore obtaining high-density parts with low porosity content.

The development stages of the new additive manufacturing process, described as Composite Fibre Additive Manufacturing (CFAM), have been explained in Chapter 3. The process consists of 6 steps which are inkjet printing the sliced geometry onto the discontinuous carbon fibre sheets with a generic ink solution layer by layer, deposition of polymer in powder form, removal of excess dry powder, consolidation of stacked and aligned printed carbon fibre layers using hot press process which results in bonded sheets with the help of melted and crystallized polymer powder, removal of excess un-bonded carbon fibre sheets using sand blasting process, and finally the post-processing and cleaning of the final part. Each manufacturing step has been examined in detail to create a reliable and consistent process. Complex shaped CFRP benchmark parts were successfully produced for proof of concept.

Chapter 4 presents the optimization process of selected critical process parameters which are the amount of pressure, compaction time and printed volume of ink per mm. An L9 orthogonal array of Taguchi design was used to determine the experimental conditions to be tested. Mechanical and microstructural properties of final parts resulting from designated conditions were investigated using mechanical tests, X-ray CT and optical microscopy. The outcomes were analysed using Taguchi analysis in Minitab and ANOVA in R statistics software to establish the impact of each parameter and their optimal levels. The applied pressure has been found to be the most significant factor with an optimum level of 0.9 MPa to reduce the porosity content from 12% to 1.5% in the final parts. Fibre volume fraction was also increased to 15%. Consequently, tensile and flexural strength were improved to 97 and 42 MPa, which exceeded the current FDM processes producing discontinuous carbon fibre polymer composites. The volume of ink was an important factor after the pressure for tensile strength, whereas it only contributed 2.7% to the flexural results. A medium amount of ink (223 g/m^2) was chosen as the best level for both properties, indicating that there is a threshold for the amount of polymer powder required by the process. The high amount of ink holds more powder on the surface which causes a low fibre volume fraction in the final parts. Compaction time has been found to be influencing flexural strength (13.4%) more than the tensile strength (7%), which shows the impact of thermal treatment on the matrix dominant properties.

In Chapter 5, the effect of process parameters on polymer morphology and crystallization behaviour was investigated using DSC analysis with the aim of understanding the source of porosity. The analysis has resulted in a double phase melting curve for most of the specimens which shows the existence of different crystal forms within the component depending on the manufacturing conditions. The degree of crystallinity did not correlate with any of the mechanical properties, however, a new approach has been established to understand the relationship between polymer morphology and final part properties, focusing on the peak heights of each crystal form given in the DSC analysis. Results show a clear link between the peak height representing alpha form crystals and the resultant properties for the parts which have double phase melting. As alpha peak height increases, the tensile and flexural properties reduced due to the increasing amount of alpha form crystal in the part. High amount of gamma-form crystals provides strong and tough material properties. This approach provides a better understanding of polymer crystallization and its effect on the final parts.

Following the matrix characteristics, this study elaborated on fibre characteristics and the potential hybrid approach, consisting of continuous and discontinuous carbon fibre layers.

Preliminary investigation showed that the pure continuous carbon fibre layers with different types of fabric can increase the tensile strength up to 400 MPa. However, the use of continuous layers has been found to be incompatible with the post-processing application. The hybrid approach demonstrated similar results, therefore the extraction of the test samples was performed with water jet cutting. The short beam shear test revealed that the interlaminar bonding between the different types of carbon fibre fabric is not strong. Premature tensile failure occurs due to the delamination, and high porosity. Therefore, discontinuous carbon fibre is concluded to be the best type of fabric for CFAM due to its easy processability.

Finally, Chapter 7 investigated the dimensional tolerances of complex-shaped drone frames produced with CFAM, FDM and SLS. 3D Scanning has been successfully used to measure the tolerance performance of fibre reinforced polymer parts. Additionally, linear measurements were taken from the selected critical design regions. CFAM part achieved the general tolerances of AM processes. The polymer shrinkage that occurred during the crystallization was the most consistent in the CFAM part compared to the other fibre reinforced FDM parts, which is an advantage in terms of the reliability of the dimensions. The final product can be processed with the consideration of specific tolerances, and the desired dimensions can be achieved.

The CFAM process has been proven to be improving the mechanical and microstructural properties of additively manufactured discontinuous carbon fibre reinforced parts by integrating thermal inkjet printing with the heat and pressure application. Rapid prototyping of dimensionally accurate complex-shaped parts with 1.5% porosity and 15% fibre volume fraction can be achieved with flexible chopped fibre and matrix composition.

8.2 Future Work

The research on additive manufacturing of composites has been significantly growing since the composite AM enables the production of lightweight complex-shaped components with high strength and stiffness in an efficient way. There are many challenges in this field that need to be addressed in order to carry composite AM through industrial standards.

The development of characterization standards for additive manufacturing is important to keep pace with rapid technological progression and implementation of composite AM in the high-performance industry. ASTM International launched a technical committee called F42 to develop standards for AM. The ASTM International Additive Manufacturing Centre

of Excellence is currently working on 14 projects to address the gaps in the standards for composite AM. Non-destructive techniques such as X-ray CT are useful tools to advance.

The relationship between the process parameters and the mechanical performance of the final parts must be established to further improve the quality of the parts. In the CFAM technique, inkjet printing parameters and droplet behaviour can be further elaborated to improve the resolution and binder properties. Different types of ink solutions can be developed and experimented. Hot press process has been found to be significantly influential on the microstructural properties. However, there is a need for a hot press machine which has more sensitive control over the pressure level to understand the impact of a wide range of pressure levels. The effect of post-processing applications on surface properties is another topic that needs to be further investigated.

The tensile properties are usually measured in the x or y direction in additively manufactured parts. The properties parallel to the build direction (z-direction) need to be tested to investigate the weakness in the bonding of printed layers. Lack of understanding in this area limits the applications.

Matrix characteristics contribute to the impact and flexural properties of the composites, therefore it is important to pay attention to the polymer morphology and its effect on fibre matrix interaction. It was proven in CFAM that the crystallization process has an impact on the final properties. For further work, a wide range of thermal treatment conditions can be experimented with to produce different crystal forms in the material. Since CFAM is very flexible to include different types of matrix and discontinuous fibre materials, a thermoplastic matrix such as PEEK can be easily implemented to obtain parts that can withstand high temperatures and the parts with high creep resistance. Moreover, there is recent progress in printable thermosetting resins. CFAM can adopt these innovative matrix materials and potentially produce higher performance parts.

Fibre characteristics are crucial for improving the mechanical performance of composites. Higher volume fractions and longer fibres are needed to reach the standards of industrial composites, without losing the ease of processability. Therefore, highly aligned discontinuous fibres can help to further improve the mechanical properties as was already proven in [52]. The post-processing of these fibres should be tested to understand whether they are suitable for CFAM or they can be used in hybrid applications. Furthermore, not only carbon fibre but also chopped glass fibre and Kevlar can be used in CFAM to produce parts with different com-

positions. In this manner, it is important to note that CFAM might be a good application area for recycled fibres that have a low environmental impact since they are made in chopped form.

The incorporation of continuous fibre decreased the design flexibility in the CFAM system, however a new approach combining two different sheet lamination techniques, LOM and CFAM, can be developed to further improve the mechanical properties. Continuous fibres can be previously cut according to the design to be included as top and bottom layers for the final part with debulking technique for composites. In this way, the design flexibility can be still maintained.

Finally, the dimensional accuracy of the additively manufactured parts can differ depending on the design features. In future studies, the effect of process parameters on dimensional accuracy should be investigated in detail. Ink droplet behaviour, the particle size of the polymer powder and their effect on the printing resolution can be a good start. Moreover, the surface roughness and quality must be investigated to ensure a high-quality finish in end-use products.

References

- [1] P. K. Mallick, *Fiber-Reinforced Composites*, CRC Press, 1946. CRC Press, 1946.
- [2] B. Jang, *Advanced Polymer Composites Principles and Applications*. ASM International, 1994.
- [3] K. K. Chawla, *Ceramic Matrix Composites*. Chapman and Hall, 1993.
- [4] J. Frketic, T. Dickens, and S. Ramakrishnan, “Automated manufacturing and processing of fiber-reinforced polymer (FRP) composites: An additive review of contemporary and modern techniques for advanced materials manufacturing,” 2017.
- [5] S. Babu and R. Goodridge, “Additive manufacturing,” *Materials Science and Technology (United Kingdom)*, vol. 32, no. 7, pp. 615–616, 2016.
- [6] N. van de Werken, H. Tekinalp, P. Khanbolouki, S. Ozcan, A. Williams, and M. Tehrani, “Additively manufactured carbon fiber-reinforced composites: State of the art and perspective,” *Additive Manufacturing*, vol. 31, no. July 2019, p. 100962, 2020.
- [7] H. A. Hegab, “Design for additive manufacturing of composite materials and potential alloys: a review,” *Manufacturing Review*, 2016.
- [8] P. Parandoush, C. Zhou, and D. Lin, “3D Printing of Ultrahigh Strength Continuous Carbon Fiber Composites,” *Advanced Engineering Materials*, vol. 21, no. 2, pp. 1–8, 2019.
- [9] D. Hull and T. W. Clyne, *An Introduction to Composite Materials*. Cambridge University Press, aug 1996.
- [10] Y. Anand and V. Dutta, “Testing of Composites: A Review,” *Advanced Materials Manufacturing & Characterization*, vol. 3, p. 1, 2013.
- [11] L. A. Pilato and M. J. Michno, *Advanced Composite Materials*. Springer Berlin Heidelberg, 1994.
- [12] W. Cantwell and J. Morton, “The impact resistance of composite materials — a review,” *Composites*, vol. 22, pp. 347–362, sep 1991.
- [13] J. Summerscales and D. Short, “Carbon fibre and glass fibre hybrid reinforced plastics,” *Composites*, vol. 9, pp. 157–166, jul 1978.

- [14] C. Zweben, "Composites: Overview," in *Encyclopedia of Condensed Matter Physics*, pp. 192–208, Elsevier, 2005.
- [15] Y. Abdin, A. Jain, S. Lomov, and V. Carvelli, "Fatigue analysis of carbon, glass and other fibres," in *Fatigue of Textile Composites*, pp. 85–104, Elsevier, 2015.
- [16] H. M. Yang, "1.8 aramid fibers," in *Comprehensive Composite Materials II*, pp. 187–217, Elsevier, 2018.
- [17] V. Mahesh, S. Joladarashi, and S. M. Kulkarni, "A comprehensive review on material selection for polymer matrix composites subjected to impact load," *Defence Technology*, vol. 17, pp. 257–277, feb 2021.
- [18] R. Hsissou, R. Seghiri, Z. Benzekri, M. Hilali, M. Rafik, and A. Elharfi, "Polymer composite materials: A comprehensive review," *Composite Structures*, vol. 262, p. 113640, apr 2021.
- [19] E. J. Barbero, *Introduction to Composite Materials Design, Third Edition*. CRC Press, oct 2017.
- [20] R. F. Gibson, *Principles of Composite Material Mechanics*. Mc-Graw Hill, Inc., 1994.
- [21] A. B. Strong, *Fundamentals of composites manufacturing : materials, methods and applications*. Dearborn, Mich. : Society of Manufacturing Engineers, 2nd ed. ed., 2008.
- [22] A. Cartledge, *The Fatigue of Carbon Fibre Composites Containing Interlaminar Inkjet Printed Polymer Droplets*. PhD thesis, The University of Sheffield, 2017.
- [23] P. K. Gupta and R. K. Srivastava, "Fabrication of ceramic reinforcement aluminium and its alloys metal matrix composite materials: A review," in *Materials Today: Proceedings*, 2018.
- [24] S. Sikarwar and B. Yadav, "Nanocomposite Material For Packaging of Electronic Goods," *International Journal of Scientific and Innovative Research*, vol. 1, no. 2, pp. 93–108, 2013.
- [25] F. Matthews and R. D. Rawlings, *Composite Materials: engineering and science*. Boca Raton, Fla.: CRC., 2006.
- [26] E. Barocio, B. Brenken, A. Favaloro, and R. B. Pipes, "Interlayer fusion bonding of semi-crystalline polymer composites in extrusion deposition additive manufacturing," *Composites Science and Technology*, p. 109334, feb 2022.
- [27] S.-J. Park and M. K. Seo, *Polymer Composites, Macro- and Microcomposites : Macro- and Microcomposites*, ch. Advances in Polymer Composites: Macro- and Microcomposites – State of the Art, New Challenges, and Opportunities, pp. 137–185. John Wiley and Sons, Incorporated, 2012.
- [28] N. Nash, T. Young, P. McGrail, and W. Stanley, "Inclusion of a thermoplastic phase to improve impact and post-impact performances of carbon fibre reinforced thermosetting composites — a review," *Materials & Design*, vol. 85, pp. 582–597, nov 2015.

- [29] C. Sonnenfeld, H. Mendil-Jakani, R. Agogu , P. Nunez, and P. Beauch ne, “Thermoplastic/thermoset multilayer composites: A way to improve the impact damage tolerance of thermosetting resin matrix composites,” *Composite Structures*, vol. 171, pp. 298–305, jul 2017.
- [30] B. Vieille, V. M. Casado, and C. Bouvet, “About the impact behavior of woven-ply carbon fiber-reinforcedthermoplastic- and thermosetting-composites: A comparative study,” *Composite Structures*, 2013.
- [31] D. Hull and T. W. Clyne, ch. Fibres and Matrices, pp. 9–38. Cambridge University Press, 1996.
- [32] T. Lee, F. Boey, and K. Khor, “On the determination of polymer crystallinity for a thermoplastic PPS composite by thermal analysis,” *Composites Science and Technology*, vol. 53, pp. 259–274, jan 1995.
- [33] R. F. Boyer, “Glassy transitions in semicrystalline polymers,” *Journal of Polymer Science: Polymer Symposia*, vol. 50, no. 1, pp. 189–242, 1975.
- [34] A. Pramanik, A. K. Basak, Y. Dong, P. K. Sarker, M. S. Uddin, G. Littlefair, A. R. Dixit, and S. Chattopadhyaya, “Joining of carbon fibre reinforced polymer (CFRP) composites and aluminium alloys – A review,” *Composites Part A: Applied Science and Manufacturing*, vol. 101, pp. 1–29, 2017.
- [35] E. Soliman, U. Kandil, and M. R. Taha, “Improved strength and toughness of carbon woven fabriccomposites with functionalized mwcnts,” *Materials*, vol. 7, pp. 4640–4657, 2014.
- [36] *Rudd H.C., Long A., Kendall K., Mangin C. Liquid Moulding Technologies : Resin Transfer Moulding, Structural Reaction Injection Moulding and Related Processing Techniques*, 1997.
- [37] P. Parandoush and D. Lin, “A review on additive manufacturing of polymer-fiber composites,” *Composite Structures*, vol. 182, pp. 36–53, dec 2017.
- [38] Z. Qureshi, T. Swait, R. Scaife, and H. El-Dessouky, “In situ consolidation of thermoplastic prepreg tape using automated tape placement technology: Potential and possibilities,” *Composites Part B: Engineering*, vol. 66, pp. 255–267, nov 2014.
- [39] N. Minsch, F. H. Herrmann, T. Gereke, A. Nocke, and C. Cherif, “Analysis of Filament Winding Processes and Potential Equipment Technologies,” *Procedia CIRP*, vol. 66, pp. 125–130, 2017.
- [40] F. Abdalla, S. Mutasher, Y. Khalid, S. Sapuan, A. Hamouda, B. Sahari, and M. Hamdan, “Design and fabrication of low cost filament winding machine,” *Materials & Design*, vol. 28, pp. 234–239, jan 2007.
- [41] B. Williams, E. Shehata, and S. H. Rizkalla, “Filament-Wound Glass Fiber Reinforced Polymer Bridge Deck Modules,” *Journal of Composites for Construction*, vol. 7, no. 3, pp. 266–273, 2003.

- [42] W. Polini and L. Sorrentino, "Influence of winding speed and winding trajectory on tension in robotized filament winding of full section parts," *Composites Science and Technology*, vol. 65, pp. 1574–1581, aug 2005.
- [43] A. Beakou, M. Cano, J.-B. Le Cam, and V. Verney, "Modelling slit tape buckling during automated prepreg manufacturing: A local approach," *Composite Structures*, vol. 93, pp. 2628–2635, sep 2011.
- [44] H. B. Olsen and J. J. Craig, "Automated composite tape lay-up using robotic devices," *IEEE International Conference on Robotics and Automation*, 1993.
- [45] G. Marsh, "Automating aerospace composites production with fibre placement," *Reinforced Plastics*, vol. 55, pp. 32–37, may 2011.
- [46] I. Gibson, D. Rosen, and B. Stucker, *Additive Manufacturing Technologies: Rapid Prototyping to Direct Digital Manufacturing*. Springer, 2010.
- [47] S. Mellor, L. Hao, and D. Zhang, "Additive manufacturing: A framework for implementation," *International Journal of Production Economics*, vol. 149, pp. 194–201, mar 2014.
- [48] M. Vaezi, S. Chianrabutra, B. Mellor, and S. Yang, "Multiple material additive manufacturing—Part 1: A review," *Virtual and Physical Prototyping*, 2013.
- [49] C. Zhou, Y. Chen, Z. Yang, and B. Khoshnevis, "Digital material fabrication using mask-image-projection-based stereolithography," *Rapid Prototyping Journal*, vol. 19, no. 3, pp. 153–165, 2013.
- [50] F. Ning, W. Cong, Y. Hu, and H. Wang, "Additive manufacturing of carbon fiber-reinforced plastic composites using fused deposition modeling: Effects of process parameters on tensile properties," *Journal of Composite Materials*, 2017.
- [51] S. Singh and R. K. Bhushan, "Additive manufacturing of carbon fiber reinforced composites for medical application: Issues and challenges," *International Journal of Engineering Research and Technology (IJERT) AMDMM*, 2019.
- [52] H. Yu, K. Potter, and M. Wisnom, "A novel manufacturing method for aligned discontinuous fibre composites (high performance-discontinuous fibre method)," *Composites Part A: Applied Science and Manufacturing*, vol. 65, pp. 175–185, oct 2014.
- [53] M. Hashimoto, T. Okabe, T. Sasayama, H. Matsutani, and M. Nishikawa, "Prediction of tensile strength of discontinuous carbon fiber/polypropylene composite with fiber orientation distribution," *Composites Part A: Applied Science and Manufacturing*, vol. 43, pp. 1791–1799, oct 2012.
- [54] L. G. Blok, M. L. Longana, H. Yu, and B. K. S. Woods, "An investigation into 3D printing of fibre reinforced thermoplastic composites," *Additive Manufacturing*, vol. 22, pp. 176–186, 2018.
- [55] D. Zindani and K. Kumar, "An insight into additive manufacturing of fiber reinforced polymer composite," *International Journal of Lightweight Materials and Manufacture*, vol. 2, pp. 267–278, dec 2019.

- [56] A. Zocca, C. Gomez, T. Mühler, and J. Günster, "Powder-Bed Stabilization for Powder-Based Additive Manufacturing," *Advances in Mechanical Engineering*, vol. 6, 2014.
- [57] P. A. Lykov, S. B. Sapozhnikov, I. S. Shulev, D. A. Zherebtsov, and R. R. Abdrakhimov, "Composite Micropowders for Selective Laser Sintering," *Metallurgist*, vol. 59, no. 9-10, pp. 851–855, 2016.
- [58] A. N. Chen, J. M. Wu, K. Liu, J. Y. Chen, H. Xiao, P. Chen, C. H. Li, and Y. S. Shi, "High-performance ceramic parts with complex shape prepared by selective laser sintering: a review," *Advances in Applied Ceramics*, vol. 117, no. 2, pp. 100–117, 2018.
- [59] S. Kumar and J.-P. Kruth, "Composites by rapid prototyping technology," *Materials and Design*, vol. 31, 2009.
- [60] A. Slocombe and L. Li, "Selective laser sintering of TiC–al₂o₃ composite with self-propagating high-temperature synthesis," *Journal of Materials Processing Technology*, vol. 118, pp. 173–178, dec 2001.
- [61] Z. Zhu, S. Lou, and C. Majewski, "Characterisation and correlation of areal surface texture with processing parameters and porosity of high speed sintered parts," *Additive Manufacturing*, vol. 36, p. 101402, dec 2020.
- [62] A. Salazar, A. Rico, J. Rodríguez, J. S. Escudero, R. Seltzer, and F. M. de la Escalera Cutillas, "Fatigue crack growth of SLS polyamide 12: Effect of reinforcement and temperature," *Composites Part B: Engineering*, vol. 59, pp. 285–292, mar 2014.
- [63] W. Jing, C. Hui, W. Qiong, L. Hongbo, and L. Zhanjun, "Surface modification of carbon fibers and the selective laser sintering of modified carbon fiber/nylon 12 composite powder," *Materials & Design*, vol. 116, pp. 253–260, feb 2017.
- [64] G. D. Goh, Y. L. Yap, S. Agarwala, and W. Y. Yeong, "Recent Progress in Additive Manufacturing of Fiber Reinforced Polymer Composite," *Advanced Materials Technologies*, vol. 4, no. 1, pp. 1–22, 2019.
- [65] D. Karalekas and K. Antoniou, "Composite rapid prototyping: Overcoming the drawback of poor mechanical properties," *Journal of Materials Processing Technology*, 2004.
- [66] D. Karalekas, "Study of the mechanical properties of nonwoven fibre mat reinforced photopolymers used in rapid prototyping," *Materials & Design*, vol. 24, pp. 665–670, dec 2003.
- [67] C. M. Cheah, J. Y. H. Fuh, A. Y. C. Nee, and L. Lu, "Mechanical characteristics of fiber-filled photo-polymer used in stereolithography," *Rapid Prototyping Journal*, vol. 5, pp. 112–119, 1999.
- [68] R. Singh, "Process capability analysis of fused deposition modelling for plastic components," *Rapid Prototyping Journal*, vol. 20, pp. 69–76, 2014.

- [69] N. Mohan, P. Senthil, S. Vinodh, and N. Jayanth, "A review on composite materials and process parameters optimisation for the fused deposition modelling process," *Virtual and Physical Prototyping*, 2017.
- [70] H. Pruss and T. Vietor, "Design for Fiber-Reinforced Additive Manufacturing," *Journal of Mechanical Design*, 2015.
- [71] F. Baumann, J. Scholz, and J. Fleischer, "Investigation of a New Approach for Additively Manufactured Continuous Fiber-reinforced Polymers," in *Procedia CIRP*, 2017.
- [72] A. N. Dickson, J. N. Barry, K. A. McDonnell, and D. P. Dowling, "Fabrication of continuous carbon, glass and Kevlar fibre reinforced polymer composites using additive manufacturing," *Additive Manufacturing*, 2017.
- [73] A. S. Gozdz and G. T. Mark, *Three dimensional printer for fiber reinforced composite filament fabrication, US9126367B1*, 2014.
- [74] F. V. Der Klift, M. Ueda, A. Todoroki, Y. Hirano, R. Matsuzaki, and Y. Koga, "3D Printing of Continuous Carbon Fibre Reinforced Thermo-Plastic (CFRTP) Tensile Test Specimens," *Open Journal of Composite Materials*, vol. 06, pp. 18–27, 2016.
- [75] M. Handwerker, J. Wellnitz, and H. Marzbani, "Review of mechanical properties of and optimisation methods for continuous fibre-reinforced thermoplastic parts manufactured by fused deposition modelling," *Progress in Additive Manufacturing*, vol. 6, pp. 663–677, may 2021.
- [76] J. Justo, L. Távara, L. García-Guzmán, and F. París, "Characterization of 3D printed long fibre reinforced composites," *Composite Structures*, 2018.
- [77] H. L. Tekinalp, V. Kunc, G. M. Velez-Garcia, C. E. Duty, L. J. Love, A. K. Naskar, C. A. Blue, and S. Ozcan, "Highly oriented carbon fiber-polymer composites via additive manufacturing," *Composites Science and Technology*, 2014.
- [78] Y. Zhang, J. Stringer, A. Hodzic, and P. J. Smith, "Toughening mechanism of carbonfibre-reinforced polymer laminatescontaining inkjet-printedpoly(methyl methacrylate) microphases," *Journal of Composite Materials*, 2018.
- [79] M. Ueda, S. Kishimoto, M. Yamawaki, R. Matsuzaki, A. Todoroki, Y. Hirano, and A. L. Duigou, "3d compaction printing of a continuous carbon fiber reinforced thermo-plastic," *Composites Part A: Applied Science and Manufacturing*, vol. 137, p. 105985, oct 2020.
- [80] H. Mei, Z. Ali, Y. Yan, I. Ali, and L. Cheng, "Influence of mixed isotropic fiber angles and hot press on the mechanical properties of 3d printed composites," *Additive Manufacturing*, vol. 27, pp. 150–158, may 2019.
- [81] Y. Ming, Y. Duan, B. Wang, H. Xiao, and X. Zhang, "A novel route to fabricate high-performance 3d printed continuous fiber-reinforced thermosetting polymer composites," *Materials*, vol. 12, p. 1369, apr 2019.

- [82] J. Sloan, "Arevo labs launches 3d printing platform for composite parts fabrication,," *CompositesWorld*, 2015.
- [83] J. Knabel, "Stratasys presents new 8-axis fdm production machine,," *3PRINTR*, 2016.
- [84] G. W. Melenka, B. K. Cheung, J. S. Schofield, M. R. Dawson, and J. P. Carey, "Evaluation and prediction of the tensile properties of continuous fiber-reinforced 3d printed structures," *Composite Structures*, vol. 153, pp. 866–875, oct 2016.
- [85] R. Matsuzaki, M. Ueda, M. Namiki, T. K. Jeong, H. Asahara, K. Horiguchi, T. Nakamura, A. Todoroki, and Y. Hirano, "Three-dimensional printing of continuous-fiber composites by in-nozzle impregnation," *Scientific Reports*, 2016.
- [86] H. Dou, Y. Cheng, W. Ye, D. Zhang, J. Li, Z. Miao, and S. Rudykh, "Effect of process parameters on tensile mechanical properties of 3d printing continuous carbon fiber-reinforced PLA composites," *Materials*, vol. 13, p. 3850, aug 2020.
- [87] M. L. Shofner, K. Lozano, F. J. Rodríguez-Macías, and E. V. Barrera, "Nanofiber-reinforced polymers prepared by fused deposition modeling," *Journal of Applied Polymer Science*, vol. 89, pp. 3081–3090, jun 2003.
- [88] F. Ning, W. Cong, J. Qiu, J. Wei, and S. Wang, "Additive manufacturing of carbon fiber reinforced thermoplastic composites using fused deposition modeling," *Composites Part B: Engineering*, vol. 80, pp. 369–378, oct 2015.
- [89] W. Zhang, C. Cotton, J. Sun, D. Heider, B. Gu, B. Sun, and T.-W. Chou, "Interfacial bonding strength of short carbon fiber/acrylonitrile-butadiene-styrene composites fabricated by fused deposition modeling," *Composites Part B: Engineering*, vol. 137, pp. 51–59, mar 2018.
- [90] G. Liao, Z. Li, Y. Cheng, D. Xu, D. Zhu, S. Jiang, J. Guo, X. Chen, G. Xu, and Y. Zhu, "Properties of oriented carbon fiber/polyamide 12 composite parts fabricated by fused deposition modeling," *Materials and Design*, vol. 139, pp. 283–292, 2018.
- [91] R. T. L. Ferreira, I. C. Amatte, T. A. Dutra, and D. Bürger, "Experimental characterization and micrography of 3d printed PLA and PLA reinforced with short carbon fibers," *Composites Part B: Engineering*, vol. 124, pp. 88–100, sep 2017.
- [92] C. Mahajan and D. Cormier, "3D Printing of Carbon Fiber Composites With Preferentially Aligned Fibers," *Materials Science and Engineering*, 2015.
- [93] D. Jiang and D. E. Smith, "Anisotropic mechanical properties of oriented carbon fiber filled polymer composites produced with fused filament fabrication," *Additive Manufacturing*, vol. 18, pp. 84–94, dec 2017.
- [94] L. J. Love, V. Kunc, O. Rios, C. E. Duty, A. M. Elliott, B. K. Post, R. J. Smith, and C. A. Blue, "The importance of carbon fiber to polymer additive manufacturing," *Journal of Materials Research*, 2014.
- [95] SLCOM, "Selective lamination composites object manufacturing," *Envision Tec*, <https://envisiontec.com/wp-content/uploads/2016/09/2017-SLCOM1.pdf>, 2016.

- [96] L. Kaplan, “CBAM: Composite Based Additive Manufacturing,” 2017.
- [97] R. Swartz., E. Gore, B. Crist, J. Bayldon, C. Wagner, N. Tarzian, and E. Su, “W02017139766—method and apparatus for automated composite-based additive manufacturing,” *U.S. Patent 10,046,552*, 2017.
- [98] “Method and apparatus for automated composite-based additive manufacturing,” 2017.
- [99] Impossible Objects, *Impossible Objects Presents CBAM Technology*, 2016.
- [100] V. Beedasy and P. J. Smith, “Printed electronics as prepared by inkjet printing,” *Materials*, vol. 13, p. 704, feb 2020.
- [101] G. D. Martin, S. D. Hoath, and I. M. Hutchings, “Inkjet printing - the physics of manipulating liquid jets and drops,” *Journal of Physics: Conference Series*, vol. 105, p. 012001, mar 2008.
- [102] E. Tekin, P. J. Smith, S. Hoeppener, and A. M. J. van den Berg et al., “Inkjet printing of luminescent CdTe nanocrystal–polymer composites,” *Advanced Functional Materials*, vol. 17, pp. 23–28, jan 2007.
- [103] H. Meier, U. Löffelmann, D. Mager, P. J. Smith, and J. G. Korvink, “Inkjet printed, conductive, 25 um wide silver tracks on unstructured polyimide,” *physica status solidi (a)*, vol. 206, pp. 1626–1630, mar 2009.
- [104] B. Karaş, V. Beedasy, Z. Leong, N. A. Morley, K. Mumtaz, and P. J. Smith, “Integrated fabrication of novel inkjet-printed silver nanoparticle sensors on carbon fiber reinforced nylon composites,” *Micromachines*, vol. 12, p. 1185, sep 2021.
- [105] T. Boland, T. Xu, B. Damon, and X. Cui, “Application of inkjet printing to tissue engineering,” *Biotechnology Journal*, vol. 1, pp. 910–917, sep 2006.
- [106] Y. Zhang, C. Tse, D. Rouholamin, and P. Smith, “Scaffolds for tissue engineering produced by inkjet printing,” *Open Engineering*, vol. 2, jan 2012.
- [107] S. F. S. Shirazi, S. Gharekhani, M. Mehrali, H. Yarmand, H. S. C. Metselaar, N. A. Kadri, and N. A. A. Osman, “A review on powder-based additive manufacturing for tissue engineering: selective laser sintering and inkjet 3d printing,” *Science and Technology of Advanced Materials*, vol. 16, p. 033502, jun 2015.
- [108] Y. Zhang, J. Stringer, R. Grainger, P. J. Smith, and A. Hodzic, “Fabrication of patterned thermoplastic microphases between composite plies by inkjet printing,” *Journal of Composite Materials*, 2015.
- [109] E. J. Fleet, Y. Zhang, S. A. Hayes, and P. J. Smith, “Inkjet printing of self-healing polymers for enhanced composite interlaminar properties,” *Journal of Materials Chemistry A*, 2015.
- [110] H. P. Le, “Progress and trends in ink-jet printing technology,” *Journal of Imaging Science and Technology*, vol. 42, no. 1, pp. 49–62, 1998.
- [111] P. J. Smith and A. Morrin, “Reactive inkjet printing,” *Journal of Materials Chemistry*, 2012.

- [112] A. Hudd, *The Chemistry of Inkjet Inks*, ch. Inkjet Printing Technologies, pp. 3–18. World Scientific Publishing Co Pte Ltd, 2009.
- [113] I. M. Hutchings, G. D. Martin, and S. D. Hoath, *Fundamentals of Inkjet Printing : The Science of Inkjet and Droplets*, ch. Introductory Remarks, pp. 1–11. John Wiley and Sons, 2016.
- [114] H. Gudapati, M. Dey, and I. Ozbolat, “A comprehensive review on droplet-based bioprinting: Past, present and future,” *Biomaterials*, vol. 102, pp. 20–42, sep 2016.
- [115] J. Plog, Y. Jiang, Y. Pan, and A. Yarin, “Electrostatic charging and deflection of droplets for drop-on-demand 3d printing within confinements,” *Additive Manufacturing*, vol. 36, p. 101400, dec 2020.
- [116] M. Ezzeldin, P. van den Bosch, A. Jokic, and R. Waarsing, “Model-free optimization based feedforward control for an inkjet printhead,” in *2010 IEEE International Conference on Control Applications*, IEEE, sep 2010.
- [117] J. Li, F. Rossignol, and J. Macdonald, “Inkjet printing for biosensor fabrication: combining chemistry and technology for advanced manufacturing,” *Lab on a Chip*, vol. 15, no. 12, pp. 2538–2558, 2015.
- [118] F. P. Brishty, R. Urner, and G. Grau, “Machine learning based data driven inkjet printed electronics: jetting prediction for novel inks,” *Flexible and Printed Electronics*, vol. 7, p. 015009, mar 2022.
- [119] D. H.-J. Lukaszewicz, C. Ward, and K. D. Potter, “The engineering aspects of automated prepreg layup: History, present and future,” *Composites Part B: Engineering*, vol. 43, pp. 997–1009, apr 2012.
- [120] Sudarisman and I. J. Davies, “Influence of compressive pressure, vacuum pressure, and holding temperature applied during autoclave curing on the microstructure of unidirectional CFRP composites,” *Advanced Materials Research*, vol. 41-42, pp. 323–328, apr 2008.
- [121] Y. Li, Q. Li, and H. Ma, “The voids formation mechanisms and their effects on the mechanical properties of flax fiber reinforced epoxy composites,” *Composites Part A: Applied Science and Manufacturing*, vol. 72, pp. 40–48, may 2015.
- [122] V. M. Drakonakis, J. C. Seferis, and C. C. Doumanidis, “Curing pressure influence of out-of-autoclave processing on structural composites for commercial aviation,” *Advances in Materials Science and Engineering*, vol. 2013, pp. 1–14, 2013.
- [123] H. Zhu, B. Wu, D. Li, D. Zhang, and Y. Chen, “Influence of voids on the tensile performance of carbon/epoxy fabric laminates,” *Journal of Materials Science Technology*, vol. 27, pp. 69–73, jan 2011.
- [124] Q. He, H. Wang, K. Fu, and L. Ye, “3D printed continuous CF/PA6 composites: Effect of microscopic voids on mechanical performance,” *Composites Science and Technology*, vol. 191, no. December 2019, p. 108077, 2020.

- [125] C. Pascual-González, P. S. Martín, I. Lizarralde, A. Fernández, A. León, C. Lopes, and J. Fernández-Blázquez, “Post-processing effects on microstructure, interlaminar and thermal properties of 3d printed continuous carbon fibre composites,” *Composites Part B: Engineering*, vol. 210, p. 108652, apr 2021.
- [126] *PA 2200, MSDS No. 9012-0014 [Online]; EOS Gmbh, Germany, May 16, 2012. https://www.sculpteo.com/media/imagecontent/PA2200_Safety_data_sheet_2-0-0_05-12_us.pdf.*
- [127] *HP Instant Ink 67/305; MSDS No. 3JB27Series; HP Japan Inc., December 10, 2019.*
- [128] *Microfab, InkJet Microdispenser.*
- [129] T. Xu, J. Jin, C. Gregory, J. J. Hickman, and T. Boland, “Inkjet printing of viable mammalian cells,” *Biomaterials*, vol. 26, pp. 93–99, jan 2005.
- [130] R. P. Tortorich, E. Song, and J.-W. Choi, “Inkjet-printed carbon nanotube electrodes with low sheet resistance for electrochemical sensor applications,” *Journal of The Electrochemical Society*, vol. 161, pp. B3044–B3048, nov 2013.
- [131] *Scotchgard Fabric Water Shield, MSDS No. UU-0110-0917-0 [Online]. 3M United Kingdom, March 23 2020, https://static.viking-direct.co.uk/is/content/odeu13/PDF/MSDS_1073193_EN_23-03-2020.pdf.*
- [132] M. Mele, G. Campana, and G. L. Monti, “A decision method to improve the sustainability of post processing in multi jet fusion additive manufacturing,” *Procedia Manufacturing*, vol. 43, pp. 2–9, 2020.
- [133] P. Minetola, F. Calignano, and M. Galati, “Comparing geometric tolerance capabilities of additive manufacturing systems for polymers,” *Additive Manufacturing*, vol. 32, p. 101103, mar 2020.
- [134] N. Otsu, “A threshold selection method from gray-level histograms,” *IEEE Transactions on Systems, Man, and Cybernetics*, vol. 9, pp. 62–66, jan 1979.
- [135] A. Spierings, M. Schneider, and R. Eggenberger, “Comparison of density measurement techniques for additive manufactured metallic parts,” *Rapid Prototyping Journal*, vol. 17, pp. 380–386, aug 2011.
- [136] A. du Plessis, P. Sperling, A. Beerlink, L. Tshabalala, S. Hoosain, N. Mathe, and S. G. le Roux, “Standard method for microCT-based additive manufacturing quality control 2: Density measurement,” *MethodsX*, vol. 5, pp. 1117–1123, 2018.
- [137] British Standards Institutions, “BSI Standards Plastics–Determination of tensile properties,” 1997.
- [138] “Astm d7264/d7264m-07 standard test method for flexural properties of polymer matrix composite materials,”
- [139] Standard, “Fibre-reinforced plastic composites. determination of apparent interlaminar shear strength by short-beam method,” ed: *BS EN ISO 14130:1998*.

- [140] D. C. Montgomery, *Design and Analysis of Experiments*. New York ; Chichester : Wiley, 1991.
- [141] I. Baturynska, O. Semeniuta, and K. Martinsen, "Optimization of process parameters for powder bed fusion additive manufacturing by combination of machine learning and finite element method: A conceptual framework," *Procedia CIRP*, vol. 67, pp. 227–232, 2018.
- [142] S. Maghsoodloo, G. Ozdemir, V. Jordan, and C.-H. Huang, "Strengths and limitations of taguchi's contributions to quality, manufacturing, and process engineering," *Journal of Manufacturing Systems*, vol. 23, pp. 73–126, jan 2004.
- [143] R. K. Roy, *A primer on the Taguchi method*. Society of Manufacturing Engineers, 2010.
- [144] G. Dong, G. Wijaya, Y. Tang, and Y. F. Zhao, "Optimizing process parameters of fused deposition modeling by taguchi method for the fabrication of lattice structures," *Additive Manufacturing*, vol. 19, pp. 62–72, jan 2018.
- [145] A. M. Aboutaleb, L. Bian, N. Shamsaei, and S. M. Thompson, "Multi-objective process optimization of additive manufacturing: A case study on geometry accuracy optimization," *Solid Freeform Fabrication Symposium*, 2016.
- [146] C. Camposeco-Negrete, "Optimization of FDM parameters for improving part quality, productivity and sustainability of the process using taguchi methodology and desirability approach," *Progress in Additive Manufacturing*, vol. 5, pp. 59–65, feb 2020.
- [147] V. Wankhede, D. Jagetiya, A. Joshi, and R. Chaudhari, "Experimental investigation of (fdm) process parameters using taguchi analysis," *Materials Today: Proceedings*, vol. 27, pp. 2117–2120, 2020.
- [148] H. Koushyar, S. Alavi-Soltani, B. Minaie, and M. Violette, "Effects of variation in autoclave pressure, temperature, and vacuum-application time on porosity and mechanical properties of a carbon fiber/epoxy composite," *Journal of Composite Materials*, vol. 46, pp. 1985–2004, dec 2011.
- [149] B. S. Kumar and S. Balachandar, "A study on the influence of hot press forming process parameters on flexural property of glass/PP based thermoplastic composites using box-behnken experimental design," *ISRN Materials Science*, vol. 2014, pp. 1–6, mar 2014.
- [150] S. H. Hong and K. H. Chung, "Effects of vacuum hot pressing parameters on the tensile properties and microstructures of SiC-2124 al composites," *Materials Science and Engineering: A*, vol. 194, pp. 165–170, may 1995.
- [151] S. Rahul, K. Balasubramanian, and S. Venkatesh, "Optimizing inkjet printing process to fabricate thick ceramic coatings," *Ceramics International*, vol. 43, pp. 4513–4519, apr 2017.
- [152] H. Kang, D. Soltman, and V. Subramanian, "Hydrostatic optimization of inkjet-printed films," *Langmuir*, vol. 26, pp. 11568–11573, apr 2010.

- [153] A. Lystrup and T. L. Andersen, "Autoclave consolidation of fibre composites with a high temperature thermoplastic matrix," *Journal of Materials Processing Technology*, vol. 77, pp. 80–85, may 1998.
- [154] X.-W. Yu, H. Wang, and Z.-W. Wang, "Analysis of yarn fiber volume fraction in textile composites using scanning electron microscopy and x-ray micro-computed tomography," *Journal of Reinforced Plastics and Composites*, vol. 38, pp. 199–210, nov 2018.
- [155] A. M. Rodriguez, P. Reynaud, G. Fantozzi, J. Adrien, and E. Maire, "Porosity analysis of long-fiber-reinforced ceramic matrix composites using x-ray tomography," *Scripta Materialia*, vol. 60, pp. 388–390, mar 2009.
- [156] M. J. Emerson, K. M. Jespersen, A. B. Dahl, K. Conradsen, and L. P. Mikkelsen, "Individual fibre segmentation from 3d x-ray computed tomography for characterising the fibre orientation in unidirectional composite materials," *Composites Part A: Applied Science and Manufacturing*, vol. 97, pp. 83–92, jun 2017.
- [157] P. A. Hessman, T. Riedel, F. Welschinger, K. Hornberger, and T. Böhlke, "Microstructural analysis of short glass fiber reinforced thermoplastics based on x-ray micro-computed tomography," *Composites Science and Technology*, vol. 183, p. 107752, oct 2019.
- [158] C. Toscano and C. Vitiello, "Influence of the stacking sequence on the porosity in carbon fiber composites," *Journal of Applied Polymer Science*, vol. 122, pp. 3583–3589, aug 2011.
- [159] S. R. Athreya, K. Kalaitzidou, and S. Das, "Mechanical and microstructural properties of Nylon-12/carbon black composites: Selective laser sintering versus melt compounding and injection molding," *Composites Science and Technology*, vol. 71, no. 4, pp. 506–510, 2011.
- [160] N. van de Werken, *Additively Manufactured Continuous Carbon Fiber Thermoplastic Composites for High-Performance Applications*. PhD thesis, University of New Mexico, 2019.
- [161] D. Hull, "Matrix-dominated properties of polymer matrix composite materials," *Materials Science and Engineering: A*, vol. 184, pp. 173–183, aug 1994.
- [162] S. Y. Hobbs, "Row nucleation of isotactic polypropylene on graphite fibres," *Nature Physical Science*, vol. 234, pp. 12–13, nov 1971.
- [163] P. K. Sengupta, D. Mukhopadhyay, and S. F. Xavier, "Transcrystallinity in unidirectional carbon fiber reinforced composites., proceedings of conference on interfacial phenomena in composite materials," in *Proceedings of conference on interfacial phenomena in composite materials*, 1989.
- [164] S.-L. Gao and J.-K. Kim, "Cooling rate influences in carbon fibre/PEEK composites. part 1. crystallinity and interface adhesion," *Composites Part A: Applied Science and Manufacturing*, vol. 31, pp. 517–530, jun 2000.

- [165] N. L. Batista, K. Anagnostopoulos, E. C. Botelho, and H. Kim, "Influence of crystallinity on interlaminar fracture toughness and impact properties of polyphenylene sulfide/carbon fiber laminates," *Engineering Failure Analysis*, vol. 119, p. 104976, jan 2021.
- [166] L. Ye, A. Beehag, and K. Friedrich, "Mesostructural aspects of interlaminar fracture in thermoplastic composites: Is crystallinity a key?," *Composites Science and Technology*, vol. 53, pp. 167–173, jan 1995.
- [167] B. P. Heller, D. E. Smith, and D. A. Jack, "Effects of extrudate swell and nozzle geometry on fiber orientation in fused filament fabrication nozzle flow," *Additive Manufacturing*, vol. 12, pp. 252–264, oct 2016.
- [168] B. Brenken, E. Barocio, A. Favaloro, V. Kunc, and R. B. Pipes, "Fused Filament Fabrication of Fiber-Reinforced Polymers: A Review," *Additive Manufacturing*, 2018.
- [169] A. E. Moumen, M. Tarfaoui, and K. Lafdi, "Modelling of the temperature and residual stress fields during 3d printing of polymer composites," *The International Journal of Advanced Manufacturing Technology*, vol. 104, pp. 1661–1676, jun 2019.
- [170] C. E. Majewski, H. Zarringhalam, and N. Hopkinson, "Effects of degree of particle melt and crystallinity in sls nylon-12 parts," 2008.
- [171] H. Zarringhalam, *Investigation into crystallinity and degree of particle melt in selective laser sintering*. PhD thesis, Loughborough University, 2007.
- [172] M. Ivey, G. W. Melenka, J. P. Carey, and C. Ayranci, "Characterizing short-fiber-reinforced composites produced using additive manufacturing," *Advanced Manufacturing: Polymer Composites Science*, vol. 3, pp. 81–91, jun 2017.
- [173] S. Bhandari, R. A. Lopez-Anido, and D. J. Gardner, "Enhancing the interlayer tensile strength of 3d printed short carbon fiber reinforced PETG and PLA composites via annealing," *Additive Manufacturing*, vol. 30, p. 100922, dec 2019.
- [174] S. Gogolewski, K. Czerntawska, and M. Gastorek, "Effect of annealing on thermal properties and crystalline structure of polyamides. nylon 12 (polylauro lactam)," *Colloid and Polymer Science*, vol. 258, pp. 1130–1136, oct 1980.
- [175] N. Ma, W. Liu, L. Ma, S. He, H. Liu, Z. Zhang, A. Sun, M. Huang, and C. Zhu, "Crystal transition and thermal behavior of nylon 12," *e-Polymers*, vol. 20, pp. 346–352, jun 2020.
- [176] M. Ito, K. Mizuochi, and T. Kanamoto, "Effects of crystalline forms on the deformation behaviour of nylon-6," *Polymer*, vol. 39, pp. 4593–4598, sep 1998.
- [177] C. Zopp, D. Nestler, N. Buschner, C. Mende, S. Mauersberger, J. Tröltzsch, S. Nendel, W. Nendel, L. Kroll, and M. Gehde, "Influence of the cooling behaviour on mechanical properties of carbon fibre-reinforced thermoplastic/metal laminates," *Technologies for Lightweight Structures (TLS)*, vol. 1, feb 2018.

- [178] H. Yu, M. L. Longana, M. Jalalvand, M. R. Wisnom, and K. D. Potter, “Hierarchical pseudo-ductile hybrid composites combining continuous and highly aligned discontinuous fibres,” *Composites Part A: Applied Science and Manufacturing*, vol. 105, pp. 40–56, feb 2018.
- [179] Y. Rui, L. Ye-yao, W. Gong-xi, and W. Zhuo-qi, “Effects of hybrid structure on properties of glass-carbon hybrid fibers composite,” *Advances in Engineering Research*, vol. 120, 2017.
- [180] H. Diao, A. Bismarck, P. Robinson, and M. Wisnom, “Production of continuous intermingled cf/gf hybrid composite via fibre tow spreading technology,” *ECCM16 - 16th European Conference on Composite Materials*, 2014.
- [181] J. Zhang, K. Chaisombat, S. He, and C. H. Wang, “Hybrid composite laminates reinforced with glass/carbon woven fabrics for lightweight load bearing structures,” *Materials & Design (1980-2015)*, vol. 36, pp. 75–80, apr 2012.
- [182] M. Alsaadi, “Hybridization effects of s-glass fiber on charpy impact resistance of carbon/aramid fiber reinforced epoxy composite laminates,” *Materials Research Express*, vol. 6, p. 125342, dec 2019.
- [183] C. Hong, J. Kim, G. Kim, and W. Ji, “Effect of stacking sequence on impact resistance performance of hybrid composites laminated with continuous and discontinuous fiber-reinforced layers,” *Functional Composites and Structures*, vol. 3, p. 02LT01, jun 2021.
- [184] A. Trauth and K. A. Weidenmann, “Continuous-discontinuous sheet moulding compounds – effect of hybridisation on mechanical material properties,” *Composite Structures*, vol. 202, pp. 1087–1098, oct 2018.
- [185] A. International and Indexed, “Designation: D 3039/D 3039M – 00 Standard Test Method for Tensile Properties of Polymer Matrix Composite Materials 1,” vol. 15, 2002.
- [186] S. Dash and S. V. Garimella, “Droplet evaporation dynamics on a superhydrophobic surface with negligible hysteresis,” *Langmuir*, vol. 29, pp. 10785–10795, aug 2013.
- [187] Y.-S. Yu, Z. Wang, and Y.-P. Zhao, “Experimental and theoretical investigations of evaporation of sessile water droplet on hydrophobic surfaces,” *Journal of Colloid and Interface Science*, vol. 365, pp. 254–259, jan 2012.
- [188] G. McHale, S. M. Rowan, M. I. Newton, and M. K. Banerjee, “Evaporation and the wetting of a low-energy solid surface,” *The Journal of Physical Chemistry B*, vol. 102, pp. 1964–1967, feb 1998.
- [189] L. Hader-Kregl, G. M. Wallner, C. Kralovec, and C. Eyßell, “Effect of inter-ply on the short beam shear delamination of steel/composite hybrid laminates,” *The Journal of Adhesion*, vol. 95, pp. 1088–1100, jun 2018.
- [190] J. Espadas-Escalante and P. Isaksson, “A study of induced delamination and failure in woven composite laminates subject to short-beam shear testing,” *Engineering Fracture Mechanics*, vol. 205, pp. 359–369, jan 2019.

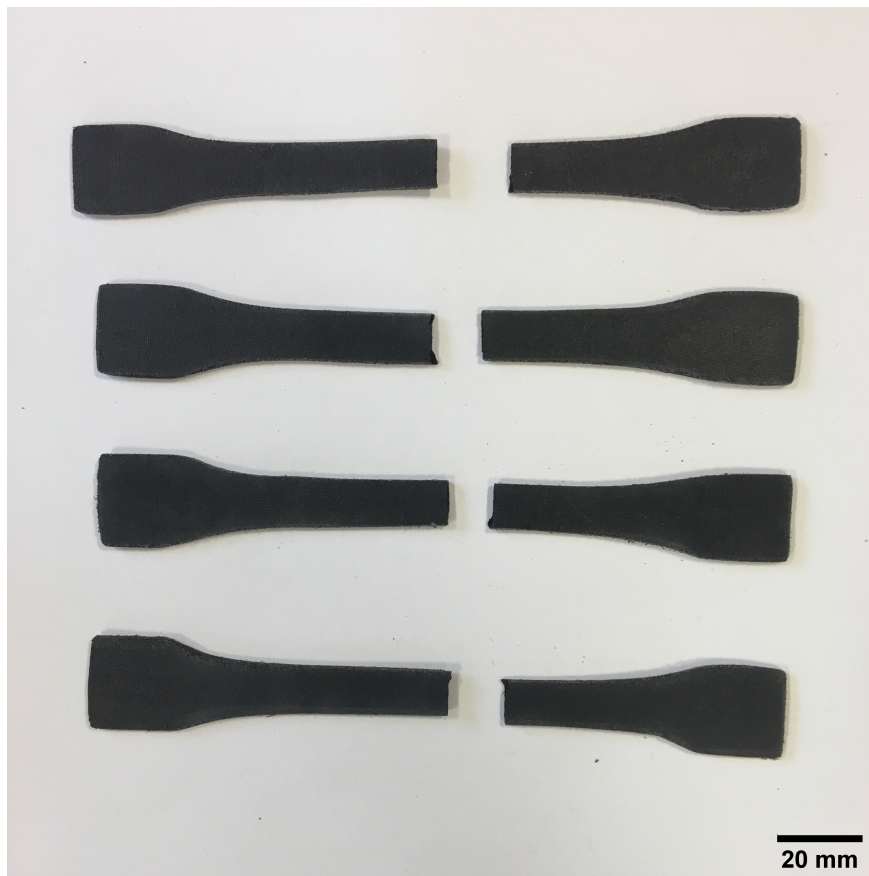
- [191] S. Gruber, C. Grunert, M. Riede, E. López, A. Marquardt, F. Brueckner, and C. Leyens, "Comparison of dimensional accuracy and tolerances of powder bed based and nozzle based additive manufacturing processes," *Journal of Laser Applications*, vol. 32, p. 032016, aug 2020.
- [192] M. Lay, N. L. N. Thajudin, Z. A. A. Hamid, A. Rusli, M. K. Abdullah, and R. K. Shuib, "Comparison of physical and mechanical properties of pla, abs and nylon 6 fabricated using fused deposition modeling and injection molding," *Composites Part B: Engineering*, vol. 176, p. 107341, 2019.
- [193] V. T. Le, H. Paris, and G. Mandil, "Process planning for combined additive and subtractive manufacturing technologies in a remanufacturing context," *Journal of Manufacturing Systems*, vol. 44, pp. 243–254, jul 2017.
- [194] T. Lieneke, V. Denzer, G. A. Adam, and D. Zimmer, "Dimensional tolerances for additive manufacturing: Experimental investigation for fused deposition modeling," *Procedia CIRP*, vol. 43, pp. 286–291, 2016.
- [195] R. K. Sahu, S. Mahapatra, and A. K. Sood, "A study on dimensional accuracy of fused deposition modeling (FDM) processed parts using fuzzy logic," *Journal for Manufacturing Science and Production*, vol. 13, pp. 183–197, oct 2013.
- [196] O. A. Mohamed, S. H. Masood, and J. L. Bhowmik, "Optimization of fused deposition modeling process parameters for dimensional accuracy using i-optimality criterion," *Measurement*, vol. 81, pp. 174–196, mar 2016.
- [197] M. Spoerk, C. Holzer, and J. Gonzalez-Gutierrez, "Material extrusion-based additive manufacturing of polypropylene: A review on how to improve dimensional inaccuracy and warpage," *Journal of Applied Polymer Science*, vol. 137, p. 48545, oct 2019.
- [198] A. K. Sood, R. Ohdar, and S. Mahapatra, "Improving dimensional accuracy of fused deposition modelling processed part using grey taguchi method," *Materials and Design*, vol. 30, pp. 4243–4252, dec 2009.
- [199] S. Mahmood, A. Qureshi, and D. Talamona, "Taguchi based process optimization for dimension and tolerance control for fused deposition modelling," *Additive Manufacturing*, vol. 21, pp. 183–190, may 2018.
- [200] E. Yasa and K. Ersoy, "Dimensional accuracy and mechanical properties of chopped carbon reinforced polymers produced by material extrusion additive manufacturing," *Materials*, vol. 12, p. 3885, nov 2019.
- [201] E. García, P. Núñez, J. Chacón, M. Caminero, and S. Kamarthi, "Comparative study of geometric properties of unreinforced PLA and PLA-graphene composite materials applied to additive manufacturing using FFF technology," *Polymer Testing*, vol. 91, p. 106860, nov 2020.
- [202] *F450 Quadcopter Frame with integrated PDB.* [Online] <https://www.unmannedtechshop.co.uk/product/f450-quadcopter-frame-with-integrated-pdb/>.

- [203] O. Bodur, V. Stepanek, E. M. Walcher, and N. Durakbasa, "Precision in additive manufacturing, optimization and evaluation of the accuracy of 3d printer based on GPS system," in *DAAAM Proceedings*, pp. 0963–0972, DAAAM International Vienna, 2020.
- [204] Markforged, *3D Printing Design Tips*.
- [205] "Bs en iso 286-1:2010 - geometrical product specification (gps) - iso code system for tolerances on linear sizes. basis of tolerances, deviations and fits," 2010.
- [206] J. Bright, R. Suryaprakash, S. Akash, and A. Giridharan, "Optimization of quadcopter frame using generative design and comparison with DJI f450 drone frame," *IOP Conference Series: Materials Science and Engineering*, vol. 1012, p. 012019, jan 2021.
- [207] R. Singh, R. Kumar, A. Mishra, and A. Agarwal, "Structural analysis of quadcopter frame," *Materials Today: Proceedings*, vol. 22, pp. 3320–3329, 2020.
- [208] M. Spoerk, F. Arbeiter, I. Raguž, G. Weingrill, T. Fischinger, G. Traxler, S. Schuschnigg, L. Cardon, and C. Holzer, "Polypropylene filled with glass spheres in extrusion-based additive manufacturing: Effect of filler size and printing chamber temperature," *Macromolecular Materials and Engineering*, vol. 303, p. 1800179, may 2018.
- [209] M. Spoerk, C. Savandaiah, F. Arbeiter, G. Traxler, L. Cardon, C. Holzer, and J. Sapkota, "Anisotropic properties of oriented short carbon fibre filled polypropylene parts fabricated by extrusion-based additive manufacturing," *Composites Part A: Applied Science and Manufacturing*, vol. 113, pp. 95–104, oct 2018.
- [210] M. Mülle, H. Wafai, A. Yudhanto, G. Lubineau, R. Yaldiz, W. Schijve, and N. Verghese, "Influence of process-induced shrinkage and annealing on the thermomechanical behavior of glass fiber-reinforced polypropylene," *Composites Science and Technology*, vol. 170, pp. 183–189, jan 2019.
- [211] T. L. de Oliveira and J. de Carvalho, "Design and numerical evaluation of quadrotor drone frame suitable for fabrication using fused filament fabrication with consumer-grade ABS," *Journal of the Brazilian Society of Mechanical Sciences and Engineering*, vol. 43, aug 2021.

Appendix A

Chapter 4 Supporting Information

A.1 Tensile test failure in discontinuous CFRP samples



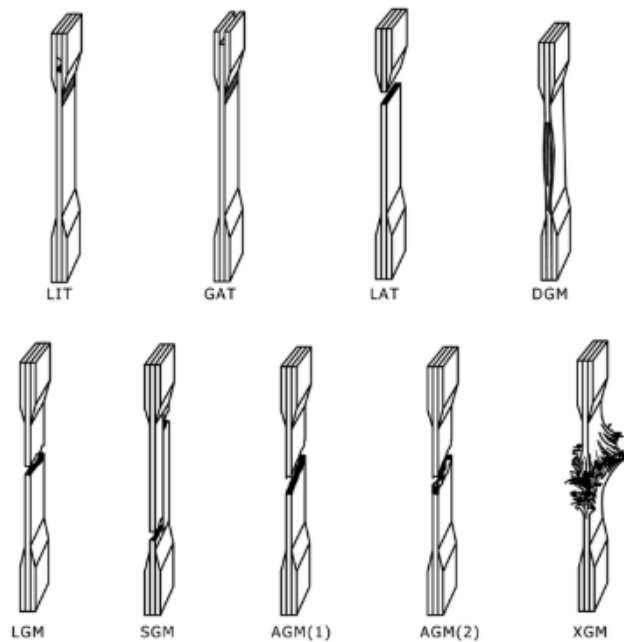
A.2 Flexural test failure for three different pressure level in discontinuous CFRP samples



Appendix B

Chapter 6 Supporting Information

B.1 Tensile test failure modes according to ASTM D3039 Standards

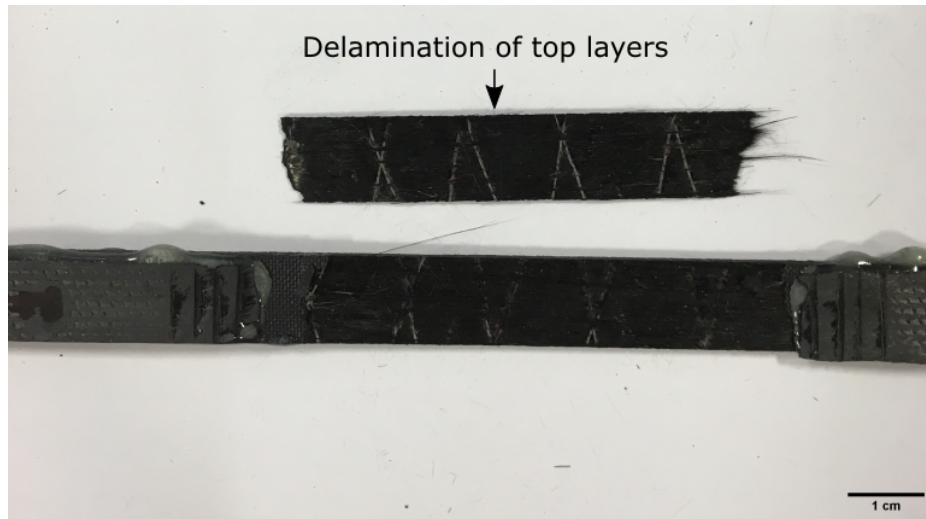


First Character	
Failure Type	Code
Angled	A
edge Delamination	D
Grip/tab	G
Lateral	L
Multi-mode	M(xyz)
long. Splitting	S
explosive	X
Other	O

Second Character	
Failure Area	Code
Inside grip/tab	I
At grip/tab	A
<1W from grip/tab	W
Gage	G
Multiple areas	M
Various	V
Unknown	U

Third Character	
Failure Location	Code
Bottom	B
Top	T
Left	L
Right	R
Middle	M
Various	V
Unknown	U

B.2 Tensile test failure in hybrid samples



Appendix C

Chapter 7 Supporting Information

C.1 Properties of materials used in production of prototypes

Prototype 1

AddNorth Adura Cold White

Nylon filament made from co-polyamide



Property	Method	Value
Density	ISO 527	1.1 g/cm ³
Tensile strength	ISO 527	50 MPa
Tensile Modulus	ISO 527	1720 MPa
Elongation at break	ISO 527	46 %
Flexural strength	ISO 178	52 MPa
Flexural Modulus	ISO 178	1425 MPa

Prototype 2

AddNorth Adura X Black

Carbon fibre reinforced nylon filament



Property	Method	Value
Density	ISO 527	1.2 g/cm ³
Tensile strength	ISO 527	58 MPa
Tensile Modulus	ISO 527	1460 MPa
Elongation at break	ISO 527	25 %
Flexural strength	ISO 178	81 MPa
Flexural Modulus	ISO 178	3650 MPa



Prototype 3

Polymaker PolyMide PA6-CF Black
Carbon fibre reinforced PA6 (Nylon 6) filament

Property	Method	Value
Density	ISO 527	1.2 g/cm ³
Tensile strength	ISO 527	105 MPa
Tensile Modulus	ISO 527	7453 MPa
Elongation at break	ISO 527	3 %
Flexural strength	ISO 178	169 MPa
Flexural Modulus	ISO 178	8339 MPa



Prototype 4

Prusament PC Blend Carbon Fibre
Polycarbonate blend filled with carbon fibre filament

Property	Method	Value
Density	ISO 527	1.2 g/cm ³
Tensile strength	ISO 527	55 MPa
Tensile Modulus	ISO 527	2300 MPa
Elongation at break	ISO 527	3.5 %
Flexural strength	ISO 178	85 MPa
Flexural Modulus	ISO 178	3000 MPa



Prototype 5

Polymaker PolyMide CoPA Nylon Black
Copolymer blend of Nylon 6 and Nylon 6,6 filament

Property	Method	Value
Density	ISO 527	1.1 g/cm ³
Tensile strength	ISO 527	66.2 MPa
Tensile Modulus	ISO 527	2223 MPa
Elongation at break	ISO 527	9.9 %
Flexural strength	ISO 178	97 MPa
Flexural Modulus	ISO 178	1667 MPa

Prototype 6

EOS PA2200 (Nylon-12)

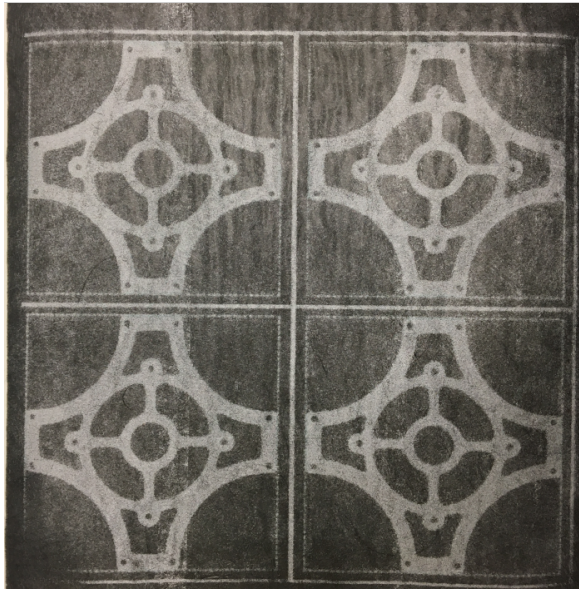
High Speed Sintered Nylon-12



Property	Method	Value
Density	ISO 527	0.93 g/cm ³
Tensile strength	ISO 527	48 MPa
Tensile Modulus	ISO 527	1700 MPa
Elongation at break	ISO 527	24 %
Flexural strength	ISO 178	58 MPa
Flexural Modulus	ISO 178	1500 MPa

C.2 Manufacturing of the central plate in drone frame by CFAM

(a) Printed and powder deposited layer



(b) Sand blasting of the complex part

